CHEMISTRY JOURNAL OF MOLDOVA. General, Industrial and Ecological Chemistry. 2018, 13(2), 8-23
ISSN (p) 1857-1727 ISSN (e) 2345-1688
http://cjm.asm.md
http://dx.doi.org/10.19261/cjm.2018.506

CHEMICAL COMPOSITION AND BIOLOGICAL ACTIVITIES OF SOME *MARRUBIUM* SPECIES ESSENTIAL OIL: A REVIEW

Benalia Yabrir

Faculty of Nature Sciences and Life, Ziane Achour University of Djelfa, PB 3117, Djelfa 17000, Algeria
e-mail: byabrir@yahoo.fr; phone: +(213) 7 77 44 13 83

Abstract. Due to their efficiency and safety, synthetic products raise several questions as for their use; thus, medicinal plants regain interest as potential source of bioactive natural compounds. *Marrubium* species are recognized to possess many beneficial effects on the human body. They are widely used in folk medicine all over the world to treat a variety of ailments. This paper reviews information on the essential oil of *Marrubium* species (except *M. vulgare*) described until now regarding extraction, chemical composition and biological activities. *Marrubium* essential oils, although quantitatively poor, are rich in chemical composition. This composition consists especially of sesquiterpenoids and a little amount of monoterpenes. *Marrubium* essential oils exhibit antioxidant and antimicrobial activities. However, because of the lack of literature concerning essential oil of these species, further studies are necessary, particularly regarding their activities.

Keywords: *Marrubium* specie, essential oil, chemical composition, antioxidant activity, antimicrobial activity.

Received: 05 July 2018/ Revised final: 24 September 2018/ Accepted: 28 September 2018

List of abbreviations:

ABTS	2,2'-azino-bis-3-ethylbenzthiazoline-6-sulphonic acid
AchE	acethylcholinesterase
ATCC	American Type Culture Collection
BchE	butyrylcholinesterase
BHA	butylatedhydroxyaanisole
BHT	butylated hydroxytoluene
CNCTC	Czech National Collection of Type Cultures
CUPRAC	cupric reducing antioxidant capacity
DPPH	1,1-diphenyl-2-picrylhydrazyl
EC50	half maximal effective concentration
EO	essential oil
HD	hydrodistillation
HS-SPME	head space solid-phase micro extraction
IC50	half maximal inhibitory concentration
IPP	isopentenyldiphosphate
ISO	International Organization for Standardization
MAE	microwave-assisted extraction
MAHD	microwave assisted hydro-distillation
MH	monoterpene hydrocarbon
MIC	minimum inhibitory concentration
MMC	minimum microbiocidal concentration
NCIMB	National Collection of Industrial, Food and Marine Bacteria
NRRL	Northern Regional Research Laboratory Culture Collection
OM	oxygenated monoterpene
OS	oxygenated sesquiterpene
PSE	pressurized solvent extraction
RSKK	Refik Saydam National Type Culture Collection
SD	steam-distillation
SFE	supercritical fluid extraction
SFME	solvent-free microwave extraction
SH	sesquiterpene hydrocarbon
XOD	xanthine-oxidase activity

Introduction

Essential oils (EOs) are obtained from a variety of aromatic plant materials including flowers, buds, seeds, leaves, twigs, bark, herbs, wood, fruits, and roots. These aromatic compounds are formed by plants as by-products or final metabolic products [1] and stored in one or several plant organs [2]. They are contained in leaves and/or reproductive structures and sometimes in the stem and roots of plants [3]. According to Chemat, F. and Cravotto, G., the EOs extracted from different organs in the same plants are variable for their names and uses because of their odours [1]. It consists of a mixture of many volatile compounds, and it can be classified into two main groups: hydrocarbons, which consist of terpenes, such as monoterpenes, sesquiterpenes, and diterpenes; and oxygenated compounds, such as esters, aldehydes, ketones, alcohols, phenols, oxides, acids, and lactones [4]. Nitrogen and sulphur compounds also occasionally exist [1]. This composition varies very much due to many factors including genetic and environmental conditions [3,5,6]. The experimental (methods of isolation) can affect as well [7]. The chemical composition of essential oil is in strict direct relation with biological activities and this relation may be attributed both to their major components and to the minor ones [8]. As reported by the same author, the essential oil, in its totality, acted less than the major constituents. The biological activity of essential oils and their constituents was reviewed by Nakatsu, T. *et al.* [9].

According to El-Gazzar, A. and Watson, L., *Labiatae* family have for centuries been acknowledged as a group of considerable pharmaceutical and culinary interest [10]. This family does not contain any dangerous plants; all are aromatic, stimulating or bitter and tonic [11]. The *Labiatea* family contains 236 genera and about 7173 species, almost cosmopolitan, but absent from the coldest regions of high latitude or altitude [12]. This family is well known with two major series of genera: oil-rich and oil-poor species [10]. *Marrubium* genera belong to this family which consists of annual or perennial herbs, and is an oil-poor one. Species of this genus are characterized by grains with tricolpate pollen [13,14] and so oil-poor, according to Lawrence hypothesis [15]. The essential oil yield is an irrefutable evidence.

The exact number of species of the genus *Marrubium* is not well known. Generally, about forty species are mentioned, mainly distributed throughout Asia, North Africa and Europe [12,14]. In Turkey, *Marrubium* genus comprises twenty two species [16-18]; eleven species occur in Iran [19-26]; five to ten species exist in Tunisia [27]; it includes six species and one hybrid in Algeria [28,29] and five species in Greece [30]. Some of *Marrubium* species are described or known as endemic as well as *M. aschersonii* to Tunisia [27]; *M. duabense*, *M. crassidense*, *M. procerum* and nine other species to Iran [24,25,31]; *M. thessalum*, *M. velutinum* and *M. cylleneum* to Greece [30,32,33]; *M. deserti* to Algeria [34]; *M. persicum* to Armenia, Turkey and Iran [35]; *M. bourgaei*, *M. trachyticum*, *M. cephalanthum*, *M. globosum* and thirteen other species to Turkey [16-18].

There are a few studies concerning the essential oil isolated from *Marrubium* species, seventeen of which are elucidated. Those that exist are much more related to chemical characterization and identification of essential oils components [16-43]. The literature regarding the biological activity of EO from *Marrubium* genus is scarce and includes only few studies concerning *M. duabense* [31], *M. globosum* [36,37], *M. cuneatum* [36], *M. peregrinum* [38], *M. deserti* [28, 29], *M. cylleneum* [32] and *M. incanum* [39]. The biological activity is essentially related to antimicrobial [28,29,31,36,39] or antioxidant [28,29,37,38] properties. Anticholinesterase [29] and ocular allergy [32] of *Marrubium* EOs are also investigated.

Because is the most representative among the genus *Marrubium*, more widespread and introduced elsewhere [12], *M. vulgare* will be discussed in a separate paper. Its chemical composition and biological activity are well documented overall the world and widely studied by several researchers.

This paper is not intended to be an exhaustive review, but rather to present an overview of scientific knowledge on chemical composition and biological activities of *Marrubium* essential oils (except *M. vulgare*) described until now. Because methods of extraction of essential oils from medicinal plants affect substantially both chemical compounds and composition of the essential oil, the extraction procedures applied for their isolation will be discussed as well as conventional methods and innovative techniques; followed by the quantification of oil separated from various species of *Marrubium* in term of yields, this constitutes the first section of the review. The second section discusses the chemical composition focusing on the main constituents. Generally, these components are grouped in five

groups namely monoterpene hydrocarbon, oxygenated monoterpene, sesquiterpene hydrocarbon, oxygenated sesquiterpene, the other constituents are combined in a single class. The last section deals with biological activities, including *(i)* antioxidant activity by considering assays used, *(ii)* antimicrobial activity with particular attention to microorganism testing and antimicrobial testing methods, and *(iii)* other activities were also presented according to available data such as allergic conjunctivitis and anticholinesterase activity. In addition, further investigations and studies are suggested.

Progress on the extraction methods of essential oils

Isolation of essential oils

Essential oils isolation is performed in accordance with International Organization for Standardization (ISO 9235) that defines them as "Product obtained from vegetable raw material-either by distillation with water or steam, or from the epicarp of citrus fruits by a mechanical process, or by dry distillation" [44]. Also, according to ISO 9235 "Essential oils may undergo physical treatments (*e.g.*, re-distillation, aeration) that do not involve significant changes in their composition".

The amount of essential oil produced depends on four main criteria: the length of distillation time, temperature, operating pressure, and, most importantly, the type and quality of the plant material [1]. Due to the cost of energy and time and environmental impact of essential oils extraction by conventional methods, new technologies were developed with more efficient extraction processes (reduction of extraction time and energy consumption, increase of extraction yield, improvement of essential oils quality [1]). Thus, many microwave methods were proposed and patented. Supercritical fluid extraction (SFE), microwave-assisted extraction (MAE) and pressurized solvent extraction (PSE) are fast and efficient unconventional extraction methods developed for extracting analytes from solid matrixes, summarize Kaufmann, B. and Christen, P. [45]. Advantages and disadvantages of some of conventional methods and innovative techniques were discussed by Scheffer, J.J.C. [7].

Since the description of Clevenger apparatus for the determination of volatile oil, all *Marrubium* species studied were subjected for the distillation method (Table 1). In this way, dried areal parts of plants were water (hydrodistillation (HD)) or steam (steam distillation (SD)) distilled for 1 to 5 hours.

Extraction yield

The very low yield (0.01%) was obtained from *M. parviflorum* Fisch. and Mey. Subsp. *Oligodon* (Boiss.) Seybold in Turkey [41] and *M. aschersonii* in Tunisia [27]; the highest (0.91%) from *M. astracanicum* Jacq. in Iran [20] (Table1).

Table 1

Extraction of *Marrubium* EOs.

Marrubium specie	*Plant part*	*Extraction method*	*Yield (%)*	*Country*	*Ref.*
M. bourgaei ssp. *caricum* P.H. Davis	Air-dried aerial parts	Hydrodistillation Clevenger type (3h)	-	Turkey	[16]
M. bourgaei Boiss. ssp. *bourgaei*	Powdered aerial parts	Water distillation Clevenger type (3h)	0.4	Turkey	[17]
M. anisodon C. Koch	Air-dried Aerial parts	Hydrodistillation Clevenger type (3h)	-	Turkey	[18]
M. cuneatum Russel	Air-dried aerial parts flowering stage	Water steam distillation All-glass apparatus	0.15	Iran	[19]
M. astracanicum Jacq.	Dried aerial parts flowering stage	Hydrodistillation Clevenger type (5h)	0.91	Iran	[20]
M. parviflorum Fisch. and C. A. Mey.	Air-dried aerial parts flowering stage	Hydrodistillation Clevenger type (3h)	0.08	Iran	[21]
M. astracanicum Jacq.	Air-dried aerial parts	Hydrodistillation Clevenger type (4h)	0.33	Iran	[22]
M. anisodon C. Koch	Dried aerial parts	Hydrodistillation Clevenger type (3-4h)	0.7	Iran	[23]
M. propinquum Fisch. and C.A. Mey.	Dried aerial parts	Hydrodistillation Clevenger type (3-4h)	0.8	Iran	[23]

Continuation of Table 1

Marrubium specie	*Plant part*	*Extraction method*	*Yield (%)*	*Country*	*Ref.*
M. crassidens Bioos.	Air-dried aerial parts flowering stage	Hydrodistillation Clevenger type modified (4h)	0.26	Iran	[24]
M. astracanicum Jacq.	Air-dried aerial parts flowering stage	Hydrodistillation Clevenger type modified (4h)	0.19	Iran	[24]
M. crassidens Boiss.	Air-dried aerial parts flowering stage	Hydrodistillation Clevenger type (3h)	0.2	Iran	[25]
M. persicum C.A. Mey. (HD)	Air-dried aerial parts flowering stage	Hydrodistillation Clevenger type (4h)	0.23	Iran	[26]
M. persicum C.A. Mey. (HS-SPME)	Powdered aerial parts flowering stage	Headspace Solid-Phase Microextraction	-	Iran	[26]
M. persicum C.A. Mey. (SFME)	Dried ground aerial parts	Solvent-Free Microwave Extraction	0.23	Iran	[26]
M. persicum C.A. Mey. (MAHD)	Dried aerial parts	Microwave Assisted Hydrodistillation Microwave oven	0.30	Iran	[26]
M. aschersonii Magnus	Dried aerial parts	Hydrodistillation Clevenger type (2h)	0.01	Tunisia	[27]
M. deserti	Dried aerial parts	Hydrodistillation Clevenger type (4h)	0.02	Algeria	[28]
M. deserti de Noé	Dried aerial parts flowering stage	Hydrodistillation Clevenger type (4h)	0.15	Algeria	[29]
M. thessalum Boiss. and Heldr.	Air-dried aerial parts flowering stage	Hydrodistillation Clevenger type modified (4h)	0.03	Greece	[30]
M. duabense Murata	Air-drying floral and leaves	Hydrodistillation Clevenger type (4h)	0.1	Iran	[31]
M. cylleneum Boiss. and Heldr.	Aerial parts	Steam distillation (3h)	0.16	Greece	[32]
M. velutinum Sm.	Air-dried whole flowering stems	Steam distillation (3h)	0.03	Greece	[33]
M. peregrinum L. (1)	Air-dried whole flowering stems	Steam distillation (3h)	0.07	Greece	[33]
M. peregrinum L. (2)	Air-dried whole flowering stems	Steam distillation (3h)	0.07	Greece	[33]
M. deserti	Floral and leaves	Steam distillation Laboratory apparatus (4h)	-	Algeria	[34]
M. persicum C. A. Mey.	Air-dried aerial parts flowering stage	Hydrodistillation Clevenger type (5h)	-	Iran	[35]
M. cuneatum Banks and Solander	Air-dried aerial parts	Hydrodistillation European pharmac (3h)	0.19	Lebanon	[36]
M. globosum Montbr. and Auch.	Air-dried aerial parts	Hydrodistillation European pharmacopoeia (3h)	0.13	Lebanon	[36]
M. globosum subsp. *globosum*	Air-dried ground plant	Water distillation British-type Clevenger (3h)	0.02	Turkey	[37]
M. peregrinum L. (no. 1)	Air-dried plant	Hydrodistillation European pharmacopoeia (3h)	0.11	Serbia	[38]
M. peregrinum L. (no. 2)	Air-dried plant	Hydrodistillation European pharmacopoeia (3h)	0.09	Serbia	[38]

Continuation of Table 1

Marrubium specie	*Plant part*	*Extraction method*	*Yield (%)*	*Country*	*Ref.*
M. peregrinum L. (no. 3)	Air-dried plant	Hydrodistillation European pharmacopoeia (3h)	0.14	Serbia	[38]
M. incanum Desr.	Air-dried flowering stage	Hydrodistillation European pharmacopoeia	0.05	Serbia	[39]
M. parviflorum Fisch. and Mey. *subsp. oligodon* (Boiss.) Seybold	Dried aerial parts	Water distillation Clevenger type (3h)	0.01	Turkey	[41]
M. astracanicum Jacq	Air-dried leaves flowering stage	Steam distillation Glass apparatus (1h)	0.25	Iran	[42]
M. incanum Desr.	Dried in oven (30°C) aerial parts flowering stage	Steam distillation (3h) Deryng apparatus	0.04	Poland	[43]

Hamedeyazdan, S. *et al.* [35] obtained a very small quantity of essential oil from the aerial parts of *M. persicum* by hydrodistillation which made the authors increase the distillation time until 5h and use xylene as an absorbing medium. Also, Demirci, B. *et al.* [16] and Kirimer, K. *et al.* [18] resort to the use of n-hexane to recover the essential oil by trapping, due to the poor yield of oil from air-dried aerial parts of *M. bourgaei* ssp. *carcicum* P.H. Davis and *M. anisodon* respectively, were all subjected to hydrodistillation for 3 h.

These values confirm the hypothesis of Lawrence, according to which *Labiatae* genera with tricolpate pollen grains are oil-poor [15]. First of all, there are two main pollen types in *Labiatae*: tri- and hexacolpate [46], secondly, the pollen grains of subfamily *Lamioideae* are inoperculate and usually tricolpate [13], and then most species of *Marrubium* genera belonging to *Lamiaceae* (*Labiatae*) family are tricolpate pollen [13,14]. Mohammadhosseini, F. did not found any difference between the EO's yield extracted from *M. persicum* by using classical or advanced methods [26]. In a review of Kaufmann, B. and Christen, P., it is demonstrated that extraction yields of the analytes by using techniques involving microwave assisted extraction and pressurized are equivalent to or even higher than those obtained with conventional methods [45]. On the other hand, Chemat, F. and Cravotto, G. stated that, the yield of EOs from plants is between 0.005% and 10% [1].

Chemical composition

Essential oils are considered as secondary metabolites, which occur in some species but not others. Like all substances, they are characterized by an analytic and highly variable chemical composition. Most components isolated within essential oils are poly-molecular (*i.e.* composed of a wide variety of compounds). In addition to the major compounds (generally between 2 and 6), there are minor compounds and a certain number of constituents in the form of traces. These constituents belong, almost exclusively, to two groups characterized by distinct biogenetic origins: the terpenoids group (terpenic compounds) and the group of aromatic compounds (phenylpropanoids) derived from phenylpropene, much less common [3]. They may also contain various products derived from degradative processes involving non-volatile constituents [4].

The structure of terpenoid compounds consists of several "isoprene" units, the universal five-carbon building block, on which is often present one or more similar or different functional groups, mostly being oxygenated sites with one or more oxygen atoms (O), and some nitrogen (N) or sulphur (S) functional groups . This isoprene is the basis of the concept of the "isoprene rule" enunciated in 1953 by Ruzicka, L. [47]. This rule considers isopentenyl diphosphate (IPP), referred to as active isoprene, as the true precursor of the terpene molecule.

Essential oil phenylpropanoids are derived from phenylalanine; the phenylpropane skeletal compounds are derived from the latter, synthesized *via* the shikimate pathway [3]. According to the same authors, this group provides indispensable and significant flavour and odour to the oil, when present.

Chemical composition related to the main constituents

Between fourteen (*M. crassidens* [25]) and one hundred thirty nine (*M. parvoflorum* [41]) components of the essential oil of *Marrubium* species were identified and those identified account for about 99.81% (*M. incanum* [43]) to 86.33% (*M. cylleneum* [32]) of total oil contents. Some of them (germacrene D, *β*-caryophyllene, caryophyllene oxide, bicyclo-germacrene and spathulenol) are generally considered as either

main or minor constituents in EO of *Marrubium* species (Table 2). A major constituent of one species may not be for another species.

Germacrene D is one of the most common sesquiterpenes found in the oils of *Marrubium* genus except for some species as well as *M. bourgaei* [17], *M. duabense* [31], *M. velutinum* Sm and *M. peregrinum* [33], *M. astracanicum* Jacq [42] and *M. astracanicum* [22]. It is considered as the main component of *M. deserti* [28], *M. anisodon* [23], *M. incanum* [43], *M. cuneatum* [36], and one of the main constituents of *M. incanum* [39], *M. peregrinum* [38,40], *M. parviflorum* [21,41], *M. propinquum* [23], *M. astracanicum* [24], *M. crassidens* [24,25], *M. thessalum* [30], *M. persicum* [26,35], *M. cuneatum* Russel [19] and *M. deserti* [29,34]. In other species, the amount of this compound is small and/or in the form of trace. A very low percentage (0.1%) was found in the EO of *M. persicum* C.A. Mey. obtained by headspace solid-phase microextraction method (HS-SPME) [26] and in *M. globosum* Montbr. and Auch. (0.3%) [36]. Low quantities were found in *M. persicum* C.A. Mey. obtained by microwave assisted hydrodistillation technique (MAHD) (6.1%) [26], *M. peregrinum* (2) (4.81%) [33], *M. cylleneum* (3.68%) [32], *M. astracanicum* (1.4%) [20] and *M. anisodon* (1%) [18].

Table 2

Main constituents (in %) of *Marrubium* species EO.

Marrubium specie	*Germacrene D*	*Caryophyllene oxide*	*β-caryophyllene*	*Bicyclo-germacrene*	*Spathulenol*	*Other major constituents*	*Ref.*
M. bourgaei ssp. *caricum* P.H. Davis	10.3	3.6	23.2	7.4	1.3	(Z)-*β*- Farnesene (13.5) Carvacrol (12.5)	[16]
M. bourgaei Boiss. ssp. *bourgaei*	-	3.8	-	-	-	Hexadecanoic acid (33.3) Hexahydrofarnesyl acetone (6.4) Heptacosane (4.8)	[17]
M. anisodon C. Koch	1.0	1.5	13.3	-	-	(Z)-*β*-Farnesene (20.2) Nonacosane (18.5)	[18]
M. cuneatum Russel	24.1	-	2.2	37.9	4.8	Limonene (3.7)	[19]
M. astracanicum Jacq.	1.4	1.6	0.7	-	2.5	Methylcyclopentane (15.5) Thymol (10.6) *n*-Heptane (7.4)	[20]
M. parviflorum Fisch. and C.A. Mey.	21.5	1.8	15.6	26.3	2.2	-	[21]
M. astracanicum Jacq.	-	2.4	21.2	4.8	3.2	Valeranone (5.4) 6,10,14-Trimethyl-2-pentadecanone (4.2)	[22]
M. anisodon C. Koch	44.2	6.6	10.4	0.4	-	*α*-Pinene (15) Limonene (5)	[23]
M. propinquum Fisch. and C.A. Mey.	15.8	-	20.1	0.9	-	(E)-*β*-Farnesene (43.8)	[23]
M. crassidens	14.2	4.6	29.0	14.2	5.6	-	[24]
M. astracanicum Jacq.	23.4	-	0.9	11.9	6.8	*α*-Humulene (33.7)	[24]
M. crassidens Boiss.	12.9	11.1	20.3	7.5	5.6	Cubenol (11.0) Hexadecanoic acid (8.1)	[25]
M. persicum C.A. Mey. (HD)	0.7	2.8	7.4	-	19.5	*α*-Thujene (17.4) *α*-Pinene (21.5) *δ*-Elemene (7.5)	[26]
M. persicum C.A. Mey. (HS-SPME)	0.1	8.4	14.0	-	2.1	*δ*-Elemene (16.9) Eugenol (11.2) Methyl eugenol (10.2)	[26]

Continuation of Table 2

Marrubium specie	*Germacrene D*	*Caryophyllene oxide*	*β-caryophyllene*	*Bicyclo-germacrene*	*Spathulenol*	*Other major constituents*	*Ref.*
M. persicum C.A. Mey. (SFME)	9.5	3.4	6.1	-	25.4	*α*-Pinene (17.4) *δ*-Elemene (6.8) Methyl eugenol (6.4)	[26]
M. persicum C.A. Mey. (MAHD)	6.1	13.1	8.0	-	8.1	*δ*-Elemene (12.4) Camphene (8.5) *α*-Selinene (7.2)	[26]
M. aschersonii magnus	0.5	-	2.4	-	0.4	*β*-Bisabolene (22.0) *α*-Thujene (10.3) Eugenol (10.1) *α*-Humulene (6.2)	[27]
M. deserti	45.7	1.6	-	1.2	-	*β*-Bourbonene (4.0) *α*-Terpinolene (3.9) *Δ*-Cadinene (3.8)	[28]
M. deserti de Noé	7.91	0.90	1.32	2.84	0.96	Tetracosane (31.11) *Δ*-Cadinene (6.52) *α*-Cadinol (6.26) *t*-Cadinol (5.81)	[29]
M. thessalum Boiss. and Heldr.	15.3	21.7	17.6	2.0	-	*β*-Bisabolene (12.6) trans- *β*-Farnesene (8.1)	[30]
M. duabense Murata	-	1	-	6.01	1.08	Limonene (33.53) *α*-Terpineol (10.78) trans-Caryophyllene (8.25) *β*-Elemene (6.37)	[31]
M. cylleneum Boiss. and Heldr.	3.68	36.54	10.85	-	9.44	2-Pentadecanone-6, 10, 14-trimethyl (5.36) Viridiflorol (4.20)	[32]
M. velutinum Sm	-	-	24.25	3.28	0.79	*γ*-Muurolene (27.78) *β*-Caryophyllene oxide (6.03) (E)-*β*- Farnesene (4.42)	[33]
M. peregrinum L. (1)	-	-	-	11.03	3.05	(E)-*β*- Farnesene (24.16) (Z)-*β*- Farnesene (16.47) epi-Bicyclosesquiphellandrene (12.31)	[33]
M. peregrinum L. (2)	4.81	-	-	4.81	1.52	(E)-*β*- Farnesene (21.49) (Z)-*β*- Farnesene (12.04) *γ*-Muurolene (9.68)	[33]
M. deserti	7.02	-	-	-	-	*Δ*-Cadinene (17.63) 6,10,14-Trimethylpentadeca-2-one (4.61) 9-Methyl-undec-1-ene (4.17)	[34]
M. persicum C.A. Mey.	10.5	2.1	7.4	1.3	0.5	*m*-Tolualdehyde (19.2) Acetophenone (14.6) *β*-Farnesene (6.2)	[35]
M. globosum Montbr. and Auch.	0.3	4.5	12.4	-	5.2	Hexadecanoic acid (7.4) (E)-*β*-Farnesene (5.8)	[36]
M. cuneatum Banks and Solander	15.6	6.2	5.2	5.2	6.5	Hexadecanoic acid (6.5) *p*-Methoxyacetophenone (5.4)	[36]
M. globosum subsp. *globosum*	6.5	7.9	9.0	3.1	15.8	-	[37]
M. peregrinum L. (no. 1)	6.79	4.23	13.20	7.63	5.18	1-Octen-3-ol (4.88) *γ*-Muurolene (5.59)	[38]

Continuation of Table 2

Marrubium specie	*Germacrene D*	*Caryophyllene oxide*	*β-caryophyllene*	*Bicyclo-germacrene*	*Spathulenol*	*Other major constituents*	*Ref.*
M. peregrinum L. (no. 2)	8.56	3.73	14.34	6.42	5.68	γ-Muurolene (5.56) 1-Octen-3-ol (5.08)	[38]
M. peregrinum L. (no. 3)	9.05	4.98	17.99	9.80	3.76	(E)-β- Farnesene (5.08) (Z)-β-Farnesene (5.12) γ-Muurolene (6.26)	[38]
M. incanum Desr.	26.2	3.5	-	11.5	2.0	(E)-Caryophyllene (27.0) α- Humulene (4.4) α-Copaene (4.2)	[39]
M. peregrinum L.	28.1	-	31.3	15.3	1.2	Hexadecanoic acid (10.4)	[40]
M. parviflorum Fisch. and Mey. subsp. *oligodon* (Boiss.) *Seybold*	11.1	1.0	10.0	-	1.4	Hexadecanoic acid (15.4) (E)-β-Farnesene (7.3)	[41]
M. astracanicum Jacq.	-	35.8	13.1	-	-	Citronellal (16.9) Geranyl acetate (4.9)	[42]
M. incanum Desr.	30.44	0.73	-	1.06	t	E-Caryophyllene (26.37) α-Cadinol (17.21) α-Humulene (10.78)	[43]

β-Caryophyllene is the second important sesquiterpenes component in the *Marrubium* EO's. It is considered as the major constituent in *M. peregrinum* [38,40], *M. crassidens* [24,25], *M. bourgaei* [16], *M. astracanicum* [22], *M. globosum* [36]. Highest content was also found in *M. velutinum* [33], *M. propinquum* [23], *M. thessalum* [30], *M. parviflorum* [21,41], *M. persicum* [26,35], *M. anisodon* [18,23], *M. astracanicum* [42], *M. cylleneum* [32], *M. globosum* [37]. A smaller content was found in *M. astracanicum* [20,24]. However, it is absent in some species as well as *M. bourgaei* [17], *M. duabense* [31], *M. incanum* [39,43], *M. peregrinum* [33], *M. deserti* [28,34].

The third representative component found in EO of *Marrubium* was spathulenol, an oxygenated sesquiterpene which arises from the C5-C10 cyclization of the aromadendrane skeleton. The largest amounts of this compound were found in *M. globosum* [37], *M. persicum* C.A. Mey. (by HD and solvent-free microwave extraction (SFME)) [26], *M. cylleneum* [32], *M. astracanicum* [24], while the weakest percentages were found in *M. incanum* [43], *M. aschersonii* [27], *M. persicum* [35], *M. velutinum* [33], *M. deserti* [29]. This compound was not found in other studied species [17,18,23,28,30,34,42].

Caryophyllene oxide and bicyclo-germacrene were other main constituents of some *Marrubium* EOs. Caryophyllene oxide was identified as the major compound of *M. cylleneum* [32], *M. astracanicum* [42], *M. thessalum* [30], *M. persicum* C.A. Mey. (MAHD) [26], while bicyclo-germacrene in *M. cuneatum* [19], *M. parviflorum* [21]. These compounds were all absent in *M. aschersonii* [27] and *M. deserti* [34].

The rule of Lawrence [15], of which *β*-caryophyllene and germacrene D are the main constituent of oils isolated from *Labiatea* genera with tricolpate pollen grains is not confirmed in some *Marrubium* genera. Kurkcuoglu, M. *et al.* reported that the major compounds of the essential oil of *M. bourgaei* were hexadecanoic acid (33.3%), hexahydrofarnesyl acetone (6.4%) and heptacosane (4.8%) [17]. The study performed by Hamdaoui, B. *et al.* revealed that *β*-bisabolene (22.0%), *α*-thujene (10.3%) and eugenol (10.1%) were the main constituents of the EO isolated from *M. aschersonii* [27]. In the oil of *M. duabense*, limonene (33.53%), *α*-terpineol (10.78%), *trans*-caryophyllene (8.25%) and *β*-elemene (6.37%) dominated [31]. Kirimer, K. *et al.* showed that the important compounds of the EO of *M. anisodon* were (Z)-*β*-farnesene (20.2%), nonacosane (18.5%) and *β*-caryophyllene (13.3%)

[18]. According to Lazari, D.M. *et al*., the essential oil of two different populations of *M. peregrinum* contained (E)-*β*-farnesene (21.49-24.16%) and (Z)-*β*-farnesene (12.04-16.47%) as main compounds [33]. The GC-MS analysis of the EO of *M. deserti* revealed the presence of tetracosane (31.11%), germacrene D (7.91), *Δ*-cadinene (6.52%), *α*-cadinol (6.26%), *t*-cadinol (5.81%) as the main constituents [29]. Methylcyclopentane (15.5%), thymol (10.6%), *n*-heptane (7.4%) were the most representative components in the EO of *M. astracanicum* [20]. In *M. propinquum*, (E)-*β*-farnesene (43.8%) is by far the most common component [23]. Thus, the main components vary from oil to oil and the variation in occurrence of certain compounds in a plant is a function of any one of, or a combination of, three factors: genetically determined properties, the age of the plant, and the environment [5]. Sarikurkcu, C. *et al*. indicates that the composition of any plant essential oil studied is influenced by the presence of several factors, such as local, climatic, seasonal and experimental conditions [37]. But, according to Franz, K.H.C. and Novak, G., the dissimilarities due to genetically differences are much bigger than by different environmental conditions [6]. Iranian authors attribute the variation of oil components of *Marrubium* species (*M. astracanicum*, *M. crassidens*, *M. persicum*) growing in different provinces of Iran to the collection time, drying conditions, extraction methods, chemotypes, geographic and edaphic and climatic factors [20,24,35]. In Algeria, Chebrouk, F. *et al*. assign the absence of monoterpene in the extracted oil from *M. deserti* from septentrional east Sahara to the abiotic factors such as specific climate of the region and the geographic factors as altitude and soil [34]. According to Hamedeyazdan, S. *et al*., these factors could influence the biosynthetic pathways of plants, the relative proportion of the main characteristic compounds of the EO as the secondary metabolites would be variable [35].

On the other hand, Mohammadhosseini, F. studied the chemical composition of the essential oils and volatile fractions from *M. persicum* by using classical (hydrodistillation) and advanced (headspace solid-phase microextraction, microwave assisted hydrodistillation and solvent-free microwave extraction) methods [26]. In this study, sesquiterpene hydrocarbons were recognized as the most frequent groups of natural compounds in the profiles of the advanced approaches, whereas in the traditional one monoterpene hydrocarbons were found to be the dominant constituting group. Scheffer, J.J.C. argued that methods used to isolate essential oils may give rise to varying compositions; thus, for example, a long lasting distillation may influence the composition of the oil isolated, because isomerization, saponification and other reactions may occur under distillation conditions [7].

Some of major compounds of EO of *Marrubium* species are presented (Figure 1). These structures vary according to: number of isoprene units present in the molecule (hemiterpenes “C5”, monoterpenes “C10”, sesquiterpenes “C15”), rarely diterpenes “C20”; saturated or unsaturated nature of the bonds; their arrangement, linear or cyclic; spatial configuration (chair form, boat form) and nature of the functional groups, terpene alcohols (R - OH), ketones (R1 - CO - R2), phenols (C_6H_6 - OH), aldehydes (R - CHO), esters (R1 - COO - R2), ethers (R1 - O) [4].

Grouped constituents of essential oils

As shown in Table 3, sesquiterpenoids were the dominant fraction in *Marrubium* EOs, which is in accordance with Lawrence hypothesis [15], except for *M. duabese* [31] and *M. persicum* (HD) [26]. Monoterpenes were present in appreciable [26] or in trace amounts [39]; in some species (*M. thessalum* [30], *M. crassidens* [25] and *M. deserti* [34]) they were totally absent. Both types of terpenoids were characterized by the predominance of hydrocarbon fractions with some differences according to plant species. *Marrubium* genus seems to produce oils that are rich in hydrocarbon compounds, with sesquiterpenes forming the major part [28]. In sesquiterpenoids group components, hydrocarbons related to oxygenated functional groups predominated. Their content varies from 92.8% (*M. propinquum*) [23] to 20.9% (*M. persicum* C.A. Mey. (HD)) [26], while oxygenated forms varies from 32.4% (*M. crassidens*) [25] to 0.8% (*M. aschersonii*) [27]. In monoterpenoids, hydrocarbons form the totality in *M. crassidens* [24], *M. astracanicum* [24] and *M.deserti* [28]; it ranges from 43.7% (*M. persicum* C.A. Mey. (HD)) [26] to 0.8% (*M. incanum*) [43], when oxygenates range from 14.0% (*M. aschersonii*) [27] to 0.5% (*M. parviflorum*) [21] or trace amount (*M. incanum*) [39].

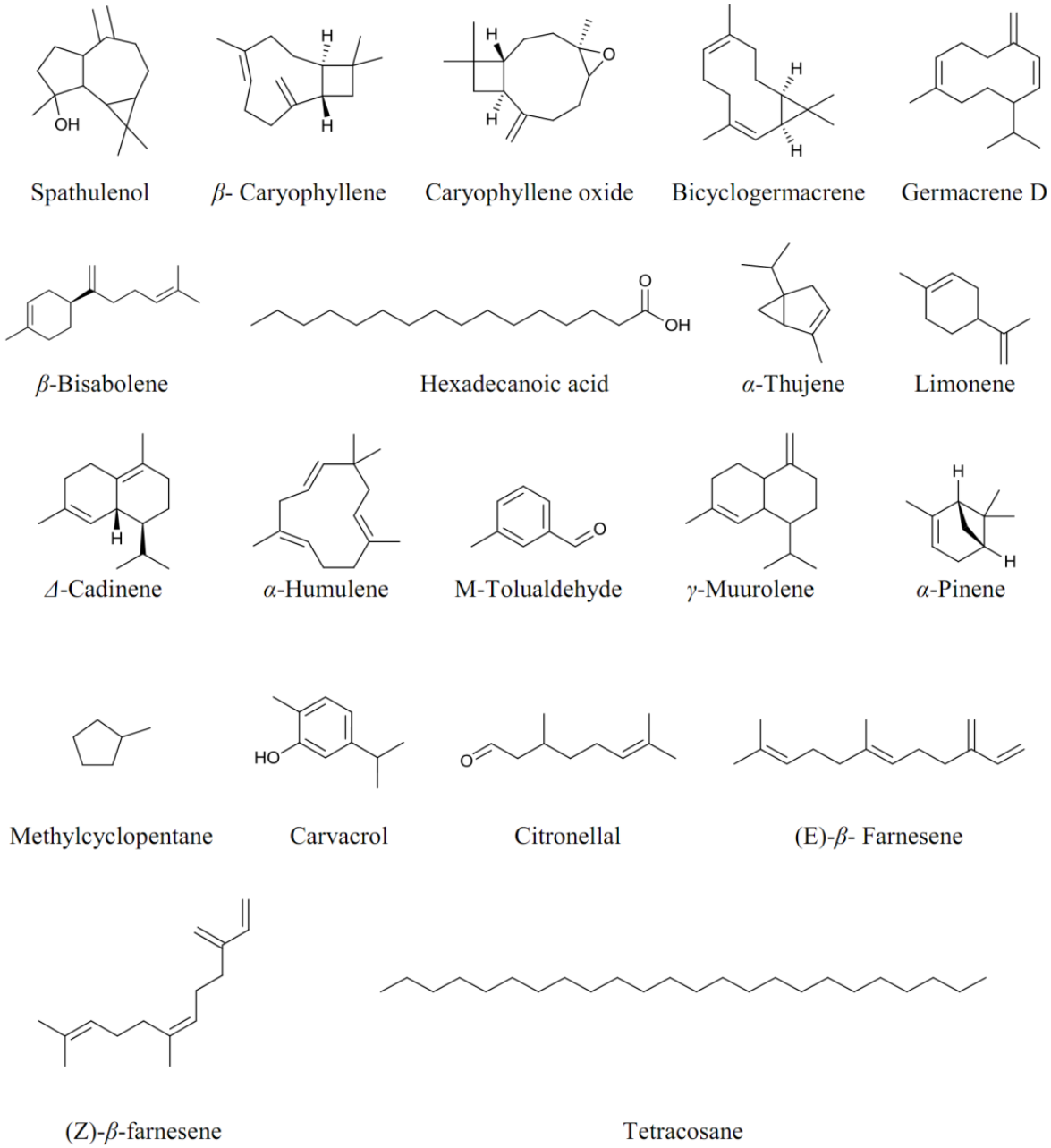

Figure1. Structure of some major compounds of EO of *Marrubium* species.

Table 3

Grouped components of EO of *Marrubium* species (%).

Marrubium species	*MH*[a]	*OM*[b]	*SH*[c]	*OS*[d]	*Other*	*Ref.*
M. cuneatum Russel	7.8	-	78.9	-	-	[19]
M. parviflorum Fisch. and C.A. Mey.	11.4	0.5	72	5.8	-	[21]
M. astracanicum Jacq	-	-	54.3	-	-	[22]
M. anisodon C. Koch	21.3	3.5	62.2	6.6	-	[23]
M. propinquum Fisch. and C.A. Mey.	2.6	0.6	92.8	-	-	[23]
M. crassidens Bioos.	2.8	0	74.0	13.4	-	[24]
M. astracanicum Jacq.	3	0	72.3	13.4	-	[24]

Continuation of Table 3

Marrubium species	*MH*[a]	*OM*[b]	*SH*[c]	*OS*[d]	*Other*	*Ref.*
M. crassidens Boiss.	0	0	44.5	32.4	14.8	[25]
M. persicum C.A. Mey. (HD)	43.7	2.2	20.9	26.7	1.1	[26]
M. persicum C.A. Mey. (HS-SPME)	13.7	12.8	41.3	10.5	21.4	[26]
M. persicum C.A. Mey. (SFME)	22.0	6.8	33.2	29.6	7.2	[26]
M. persicum C.A. Mey. (MAHD)	24.1	4.1	45.1	22.1	3.8	[26]
M. aschersonii Magnus	12.3	14.0	37.3	0.8	15.1	[27]
M. deserti	5.1	0	67.5	0	-	[28]
M. deserti de Noé	4.32	9.26	33.85	16.45	35.84	[29]
M. thessalum Boiss. and Heldr.	0	0	60	29.6	10.4 (miscellaneous)	[30]
M. duabense Murata	33.53	7.9	25.24	2.08	-	[31]
M. velutinum Sm	-	1.06	71.73	10.74	-	[33]
M. peregrinum L. (1)	-	5.58	73.05	6.95	-	[33]
M. peregrinum L. (2)	-	5.34	65.63	6.23	-	[33]
M. deserti	0	0	57.75	0	42.25	[34]
M. persicum C.A. Mey.	9	1.2	27.9	4.8	-	[35]
M. peregrinum L. (1)	3.20	6.68	49.10	11.84	12.84	[38]
M. peregrinum L. (2)	3.37	6.88	52.28	10.94	14.13	[38]
M. peregrinum L. (3)	3.63	7.93	62.71	11.00	10.88	[38]
M. incanum Desr.	-	traces	84.1	9.3	2.9	[39]
M. incanum Desr.	0.8	4.77	76.35	21.16	-	[43]

[a] *Monoterpene hydrocarbon;* [b] *Oxygenated monoterpene;*
[c] *Sesquiterpene hydrocarbon;* [d] *Oxygenated sesquiterpene.*

Biological activities

Synthetic products widely used, both in medication and in the food industry, raise currently several questions as to their efficiency and safety. If in the first case the development of resistance of microorganisms to various antibiotics is of concern to medical specialists, the use of additives such as antioxidants is suspected to have adverse effects on the health of consumers. EOs are beginning to raise a lot of interest as a potential source of bioactive natural molecules. They are being studied for their possible use as an alternative to synthetic products. The effectiveness of EO has been attributed mainly to the presence of bioactive compounds in their composition. According to Nagy, M. and Svajdlenska, E., the difference in chemical composition of EOs of *Marrubium* species may cause an important change in the biological activities of oils [40].

Antioxidant activity

Only three species of *Marrubium* were investigated for their EO's antioxidant activities. The first study on the antioxidant activity of the members of *Marrubium* was conducted on *M. globosum* [37]. The two other species were carried out on *M. deserti* [28,29] and on *M. peregrinum* [38].

The antioxidant effect of EOs of *M. globosum* was determined by three different *in vitro* assays namely 1,1-diphenyl-2-picrylhydrazyl (DPPH), *β*-carotene/linoleic acid and reducing power [37]. In this study, the antiradical dose required to reduce 50% of the free radical (EC50 of DPPH) was 1203.38±7.18 µg/mL, which was considered very weak compared to the positive control butylated hydroxytoluene (BHT) (55.48±0.87 µg/mL), also, the EC50 value of reducing power assay, 4315.80±2.54 µg/mL, was very weak compared to BHT (171.26±1.11 µg/mL). In *β*-carotene/linoleic acid this EOs showed the weakest activity potential, too. In this test system, the % inhibition capacity of the EOs (79.26±1.46%) was found inferior to the inhibition capacity of the positive control BHT (97.44±0.74%). According to this study, the polar sub-fraction of the methanol extract exerted the strongest antioxidant activity,

when compared with the EO one, which is almost equal to BHT and could be used in the food industry and other fields which are processing natural products [37].

The antioxidant activity of *M. deserti* EOs from Algerian species were evaluated using three *in vitro* assays: scavenging effect on DPPH, the 2,2'-azino-bis-3-ethylbenzthiazoline-6-sulphonic acid (ABTS) test and the phosphomolybdenum method [28] and *β*-carotene-linoleic acid, DPPH free radical scavenging, and CUPRAC (cupric reducing antioxidant capacity) assays [29]. The results of these studies showed that the essential oils of *M. deserti* exhibited a remarkable antioxidant activity and significant reducing power compared with the standard antioxidants such as butylated hydroxyanisole (BHA), BHT, *α*-tocopherol and ascorbic acid. The concentration of *M. deserti* oil resulting in a 50% inhibition of the DPPH free radical scavenging activity (IC50) was 22.3 µg/mL. In the ABTS assay, the antioxidant activity was 8.93 mM expressed as Trolox equivalents and in the phosphomolybdenum method, the total antioxidant activity of the essential oil was 0.70 mM expressed as *α*-tocopherol equivalents [28]. In the *β*-carotene-linoleic acid assay, the oil exhibited good lipid peroxidation inhibition activity, demonstrating 76.81±0.59% at 200 µg/mL concentration. In DPPH and CUPRAC assays, however, the essential oil showed weak activity [29]. Authors stipulate that this oil may be suggested for furthe use as a natural additive in food and pharmaceutical industries.

M. peregrinum EOs from three different localities (Rimski sanac - no. 1, Novi Knezevac - no. 2 and Senta - no. 3) of Serbia were evaluated for their antioxidant properties by Kaurinovic, B. *et al.* [38]. The free radical scavenging capacity (RSC) was assessed measuring the scavenging activity of EOs on DPPH, O_2•⁻, NO• and OH• radicals; the xanthine-oxidase activity (XOD) was determined by the nitric method and effects on lipid peroxidation (LP) were evaluated by following the activities of EOs in the Fe^{2+}/ascorbate induction system. Results showed that all samples expressed strong antioxidant effects, with the best effect on DPPH radical from that of Senta locality, with IC50 values as follows: 13.48; 13.41 and 11.69 µg/mL for *M. Peregrinum* no. 1, no. 2 and no. 3, respectively. That of BHT (positive control) was 14.31 µg/mL. Regarding the O_2•⁻ assay, the greatest ability was from EO from the Senta (no. 1) locality (IC50= 10.82 µg/mL), which is a bit weaker compared to BHT (10.46 µg/mL). Similar results were obtained from the same locality in the NO• method, where the EO exhibited the strongest inhibitory effect (IC50= 8.81 µg/mL compared to BHT, IC50= 8.63 µg/mL). Concerning the deoxyribose assay, all the examined EOs from all three locations, except those at the lowest concentration (0.213 µg/mL), inhibited the degradation of deoxyribose greater than BHT (24.12%). The highest activity was shown by the EO of *M. peregrinum* from Senta (no. 3) again, especially at the concentration of 2.130 µg/mL (67.12%) and 1.598 µg/mL (55.18%). The antioxidant activities of all three EOs were dose dependent. Results of activities of XOD with *M. peregrinum* EO showed that only the EO from Senta (no. 3) expressed a stronger protective effect than BHT (17.63 *vs.* 19.23 µg/mL). The examined EOs expressed strong antioxidant capacity in the LP technique. The largest inhibitory activity was exhibited by EO from plants collected at Senta locality, too (from 37.02 to 71.32% of inhibition of LP), greater than BHT (26.15%). In conclusion, the authors of this study state that EOs of this specie could serve as safe antioxidant and antiseptic supplements in preventing deterioration of foodstuffs and beverages and pharmaceuticals.

Antimicrobial activity

Some *Marrubium* EOs have been shown to have moderate antimicrobial activity [29,36,39] or negligible [31,36] while other were ineffective [28,31]. This difference in microbial activity might be attributed to the change of chemical composition of EO [31,36,40] and concentrations used in tests [29,31,39]. Thus, when comparing published data, attention should be drawn to methodological differences: selection of plant extracts, microorganism testing and antimicrobial testing methods. In general, it is the G+ bacteria that are most affected by the *Marrubium* EOs especially at high concentrations [31,36,39].

The EO of *M. deserti* collected from Algerian area steppe had no activity on pathogenic bacteria tested (from the American Type Culture Collection (ATCC) and consists of (*Staphylococcus aureus* (ATCC 25923), *Escherichia coli* (ATCC 25922), *Pseudomonas aeruginosa* (ATCC 27853)) and yeasts and molds (*Candida albicans* and *Aspergillus flavus*), at each of the three concentration used (EO dilutions in ethanol 1/2, 1/5, and 1/10 v/v) [28]. However, EO of *M. deserti* from south Algeria inhibit the growth of microorganisms, but at highest concentrations; the minimum inhibitory concentration was 25 µL/mL for bacteria,

Staphylococcus epidermidis MU 30, *Bacillus cereus* RSKK 863 (Refik Saydam National Type Culture Collection), *Micrococcus luteus* NRRL B-4375 (Northern Regional Research Laboratory Culture Collection), *Streptococcus mutans* CNCTC 8/77 (Czech National Collection of Type Cultures) and for yeasts, *Candida albicans* ATCC 10239; it was 50 µL/mL for *Staphylococcus aureus* ATCC 25923 and *Bacillus subtilus* ATCC 6633, and it was 80 for *Staphylococcus aureus* ATCC6538P [29].

According to the study conducted by Golmakani, H. *et al*. in North Khorassan Province (Iran), the antibacterial bioassay of *M. duabense* Murata EO shows that only *Clostridium perfringens* was affected by a higher concentration while *Staphylococcus aureus*, *Salmonella pullorum* and *Escherichia coli* displayed no significant growth inhibition [31]. This is suspected to be associated with the high contents of oxygenated compounds. Authors suggest introducing *M. duabense* as a medicinal plant against anaerobic bacteria after larger and controlled clinical trials.

Grassia, A. *et al.* demonstrated that EO of *M. cuneatum* collected from Lebanon exhibited a negligible antimicrobial activity, evaluated by the *in vitro* paper-disk diffusion method, against eight selected Gram+ and Gram- bacteria *Bacillus cereus* (PCI 213), *Bacillus subtilus* (ATCC 6633), *Staphylococcus aureus* (ATCC 25923), *Streptococcus epidermidis* (ATCC 12228), *Escherichia coli* (ATCC 25922), *Proteus mirabilis* (ATCC 12453), *Pseudomonas aeruginosa* (ATCC 27853), *Salmonella paratyphi* A (ATCC 12176), while that of *M. globosum* ssp *libanoticum* showed a low activity, mostly against Gram+ bacteria [36]. The authors attribute this to the content in this oil of a good amount of caryophyllene and the presence of some other components like linalool, α-terpineol, eugenol that, even if present in low amounts, may synergisticallyincrease the action of carvacrol.

On the contrary, the study conducted by Petrovic, S. *et al*. revealed that EO of *M. incanum* exhibited antimicrobial activity against all microorganisms tested but with some differences [39]. These microorganisms consist of four G+ bacteria *Staphylococcus aureus* (ATCC 25923), *S. epidermidis* (ATCC 12228), *Micrococcus flavus* (ATCC 10240), *Enterococcus faecalis* (ATCC 29212); three G- bacteria *Escherichia coli* (ATCC 25922), *Klebsiella pneumonia* (NCIMB 9111) (National Collection of Industrial, Food and Marine Bacteria), *Pseudomonas aeruginosa* (ATCC 27853) and a yeast *Candida albicans* (ATCC 10259 and ATCC 24433). The antimicrobial activity was assayed using the agar diffusion and broth microdillution methods. Results were carried out by measuring diameters of zone of inhibitions and by determining minimum inhibitory (MIC) and minimum microbiocidal (MMC) concentrations. According to this study, the best inhibitory and bactericidal effect was detected against *M. flavus* (MIC 6.25 µg/mL; MMC 12.5 µg/mL), followed by *E. coli* and *K. pneumonia* (MIC 12.5 µg/mL; MMC 25 µg/mL, both) while *S. epidermidis* appeared to be the most resistant (MIC 100 µg/mL; MMC 200 µg/mL). The lowest MIC and MMC (6.25 µg/mL and 12.5 µg/mL, respectively) was also found against *C. albicans* (ATCC 24433), whereas *C. albicans* (ATCC 10259) was less sensitive than for the previous one (MIC 12.5µg/mL; MMC 25 µg/mL). The authors attribute d the antimicrobial activity of the oil, to an appreciable degree, to the presence of (E)-caryophyllene.

Allergic conjunctivitis

One third of the world population is affected by some form of allergic disease and ocular involvement is estimated to be present in 40-60% of this population [48]. Pathophysiology of ocular allergies and allergic responses are well discussed [48,49]; it involves sensitization, activation, mast cell degranulation and performed mediators. Histamine is a chemical mediator stored in mast cells; it is released in the early phase reaction with granulocytes degranulation [48]. It plays an important role in inflammatory and allergic reactions and for the treatment of allergic conjunctivitis, antihistamines are used among others [49]. The study conducted by Skaltsa, H. *et al*., showed that the EO of *M. cylleneum* enhances the amount of histamine present in the rat conjunctiva by acting through a mechanism yet to be identified; this increase in histamine may result from an increase in the rate of synthesis or storage of the amine, which remains to be determined [32].

Anticholinesterase activity

The EO of *M. deserti* was tested for its anticholinesterase activities by measuring the inhibition activity of acethylcholinesterase (AchE) and butyrylcholinesterase (BchE) enzymes using the spectrophotometric method [29]. According to the authors, the EO was inactive against both AchE and BchE, however the methanol extract of this species exhibits weak inhibition against both enzymes when compared to galantamine, used as a standard drug. The importance of

acethylcholinesterase and butyrylcholinesterase enzymes for human body is highlighted in the review of Patočka, J. *et al*. [50].

Antibiofilm formation

The effect of *M. deserti* EOs on Bacterial biofilm formation of microorganisms (*Staphylococcus aureus* ATCC 25923, *Staphylococcus aureus* ATCC6538P, *Staphylococcus epidermidis* MU 30, *Bacillus subtilus* ATCC 6633, *Bacillus cereus* RSKK 863, *Micrococcus luteus* NRRL B-4375, *Streptococcus mutans* CNCTC 8/77 and *Candida albicans* ATCC 10239) was tested with a microplate biofilm assay by Chemsa, A.E. *et al*. [29]. The results showed that EO at the MIC's inhibited biofilm formations of all microorganisms tested in various percentage (1, 1/2, 1/4, 1/8 and 1/16 MIC). The highest antibiofilm was obtained against *C. albicans* at 25 µg/mL (MIC) concentration with 36.31%. On the other hand, the authors found that the antibiofilm activity of EO on tested strains was lower than that of the methanol extract.

Conclusions

The essential oils of seventeen *Marrubium* species have been studied. Characterization and chemical composition analysis identified germacrene D, *β*-caryophyllene, caryophyllene oxide, bicyclo-germacrene and spathulenol as either main or minor constituents of the *Marrubium* species essential oils. Other identified components included hydrocarbon compounds and sesquiterpenes.

The EOs extracted from only three *Marrubium* species, *M. globosum*, *M. deserti* and *M. peregrinum*, have been investigated for their antioxidant activity. All these oils exhibit a greater activity when compared to standard antioxidants like BHT.

Studies have shown that some *Marrubium* EOs have moderate antimicrobial activity or negligible, while others were ineffective. This difference in antimicrobial activity might be attributed to the change of chemical composition of EOs and concentrations used in tests. The antimicrobial activity of the essential oils has been attributed to the presence of carvacrol and caryophyllene, and some other components like linalool, *α*-terpineol, eugenol that, even if present in low amounts, may synergistically increase the action of carvacrol.

Species of this genus may be regarded as a potential source of natural chemical compounds and could be used in the fields of food and pharmaceutical industries.

Acknowledgments

This study was supported by the Algerian Ministry of Higher Education and Scientific Research (Project CNEPRU code D04N01UN170120150002).

References

1. Chemat, F.; Cravotto, G. Eds. Microwave-assisted extraction for bioactive compounds: theory and practice. Springer: New York, 2013, pp. 53-66. DOI: https://doi.org/10.1007/978-1-4614-4830-3
2. Li, Y.; Fabiano-Tixier, A.S.; Chemat, F. Essential Oils as Reagents in Green Chemistry. Springer International Publishing: Switzerland, 2014, 78 p. DOI: https://doi.org/10.1007/978-3-319-08449-7
3. Sangwan, N.S.; Farooqi, A.H.A.; Shabih, F.; Sangwan, R.S. Regulation of essential oil production in plants. Plant Growth Regulation, 2001, 34(1), pp. 3-21. DOI: https://doi.org/10.1023/A:1013386921596
4. Bruneton J. Pharmacognosy. Phytochemistry. Medicinal Plants. Ph.D. Thesis, Lavoisier, Paris, 1999, 1120 p. (in French).
5. Senatore, F. Influence of harvesting time on yield and composition of the essential oil of a Thyme (*Thymus pulegioides* L.) growing wild in Campania (Southern Italy). Journal of Agricultural and Food Chemistry, 1996, 44(5), pp. 1327-1332. DOI: 10.1021/jf950508z
6. Baser, K.H.C.; Buchbauer, G. Eds. Handbook of Essential Oils: Science, Technology, and Applications. CRC Press Taylor & Francis Group: Florida, 2010, pp. 39-81. https://www.crcpress.com/
7. Scheffer, J.J.C. Various methods for the isolation of essential oils. Phytotherapy Research, 1996, 10, pp. s6-s7. https://onlinelibrary.wiley.com/loi/10991573/year/1996
8. Lahlou, M. Methods to study the phytochemistry and bioactivity of essential oils. Phytotherapy Research, 2004, 18(6), pp. 435-448. DOI: https://doi.org/10.1002/ptr.1465
9. Nakatsu, T.; Lupo, Jr.A.T.; Chinn, Jr.J.W.; Kang, R.K.L. Biological activity of essential oils and their constituents. Studies in Natural Products Chemistry, 2000, 21(B), pp. 571-631. DOI: https://doi.org/10.1016/S1572-5995(00)80014-9
10. El-Gazzar, A.; Watson, L. Some economic implications of the taxonomy of *Labiatae* essential oils and rusts. New Phytologyst, 1970, 69(2), pp. 487-492. DOI: https://doi.org/10.1111/j.1469-8137.1970.tb02444.x
11. Richard, A. Medical botany or natural and medical history. Béchet Jeune Librairy: Paris, 1823, 448 p. (in French). DOI: https://doi.org/10.5962/bhl.title.147978
12. Kadereit, J.W. Ed. Flowering Plants. Dicotyledons: Lamiales (except *Acanthaceae* including *Avicenniaceae*). Springer: Germany, 2004, 478 p. DOI: 10.1007/978-3-642-18617-2
13. Abu-Asab, M.S.; Cantino, P.D. Systematic implications of pollen morphology in subfamilies

Lamioideae and *Pogostemonoideae* (*Labiatae*). Annals of the Missouri Botanical Garden, 1994, 81(4), pp. 653-686. DOI: https://doi.org/10.2307/2399915
14. Akgul, G.; Ketenoglu, O.; Pinar, N.M.; Kurt, L. Pollen and seed morphology of the genus *Marrubium* (*Lamiaceae*) in Turkey. Annales Botanici Fennici, 2008, 45, pp. 1-10. http://www.sekj.org/AnnBot.html
15. Lawrence, B.M. *Labiatae* oils – Mother Nature's chemical factory. 11th International Congress of Essential Oils, Fragrance and flavours; Oxford& IBH Publishing Company Eds., 1989, 71 p.
16. Demirci, B.; Baser, K.H.C.; Kirimer, N. Composition of the essential oil of *Marrubium bourgaei* ssp. *caricum* P.H. Davis. Journal of Essential oil Research, 2004, 16(2), pp. 133-134. DOI: https://doi.org/10.1080/10412905.2004.9698674
17. Kürkçüoglu, M.; Başer, K.H.C.; Tosun, A.; Dogan, E.; Duman, H. Essential oil composition of an endemic species of Turkey: *Marrubium bourgaei* Boiss. ssp. *bourgaei* (*Labiatae*). Journal of Essential Oil Research, 2007, 19(1), pp. 34-36. DOI: https://doi.org/10.1080/10412905.2007.9699224
18. Kırımer, N.; Kürkçüoğlu, M.; Akgül, G.; Başer, K.H.C.; Mahmoud, A.A. Composition of the essential oil of *Marrubium anisodon* C. Koch of Turkish origin. Records of Natural Products, 2015, 9(2), pp. 234-236. http://www.acgpubs.org/RNP/2015/Volume9/Issue%201/25-RNP-EO-1404-023.pdf
19. Baher Nik, Z.; Mirza, M.; Shahmir, F. Essential oil of *Marrubium cuneatum* Russell and its secretory elements. Flavour and Fragrance Journal, 2004, 19(3), pp. 233-235. DOI: https://doi.org/10.1002/ffj.1293
20. Morteza-Semnani, K.; Saeedi, M. The essential oil composition of *Marrubium astracanicum* Jacq. from Iran. Journal of Essential Oil Bearing Plants, 2004, 7(3), pp. 239-242. DOI: https://doi.org/10.1080/0972-060X.2004.10643399
21. Khanavi, M.; Ghasemian, L.; Motlagh, E.H.; Hadjiakhoondi, A.; Shafiee, A. Chemical composition of the essential oils of *Marrubium parviflorum* Fisch. & C. A. Mey. and *Marrubium vulgare* L. from Iran. Flavour and Fragrance Journal, 2005, 20(3), pp. 324-326. DOI: https://doi.org/10.1002/ffj.1425
22. Javidnia, K.; Miri, R.; Soltani, M.; Khosravi, A.R. Constituents of the essential oil of *Marrubium astracanicum* Jacq. from Iran. Journal of Essential Oil Research, 2007, 19(6), pp. 559-561. DOI: https://doi.org/10.1080/10412905.2007.9699331
23. Tajbakhsh, M.; Khalilzadeh, M.A.; Rineh, A.; Balou, J. Essential oils of *Marrubium anisodon* C. Koch and *Marrubium propinquum* Fisch. et C.A. Mey., growing wild in Iran. Journal of Essential Oil Research, 2008, 20(2), pp. 161-162. DOI: https://doi.org/10.1080/10412905.2008.9699980
24. Teimori, M.; Khavari-Nejad, R.A.; Yassa, N.; Nejadsatari, T. Analysis of the essential oil of *Marrubium crassidens* Boiss. and *M. astracanicum* Jacq. Journal of Applied Science, 2008, 8(9), pp. 1793-1795. DOI: 10.3923/jas.2008.1793.1795
25. Masoudi, S.; Aghajani, Z.; Rustaiyan, A.; Feizbakhsh, A.; Kakhky, A.M. Volatile constituents of *Teucrium persicum* Boiss., *Thymus caucasicus* Willd. ex *Ronniger* subsp. *grossheimii* (Ronniger) Jalas. And *Marrubium crassidens* Boiss. Three Labiatae Herbs growing wild in Iran. Journal of Essential Oil Research, 2009, 21(1), pp. 5-7. DOI: https://doi.org/10.1080/10412905.2009.9700093
26. Mohammadhosseini, M. First report on screening of the profiles of the essential oils and volatiles from the aerial parts of *Marrubium persicum* using classical and advanced methods prior to gas chromatographic mass spectrometric determination. Journal of Medicinal Plants and By-products, 2016, 5(2), pp. 169-180. http://jmpb.areeo.ac.ir/article_109393.html
27. Hamdaoui, B.; Wannes, W.A.; Marrakchi, M.; Brahim, N.B.; Marzouk, B. Essential oil composition of two Tunisian horehound species: *Marrubium vulgare* L. and *Marrubium aschersonii* Magnus. Journal of Essential Oil Bearing Plants, 2013, 16(5), pp. 608-612. DOI: https://doi.org/10.1080/0972060X.2013.854492
28. Laouer, H.; Yabrir, B.; Djeridane, A.; Yousfi, M.; Beldovini, N.; Lamamra, M. Composition, antioxidant and antimicrobial activities of the essential oil of *Marrubium deserti*. Natural Product Communication, 2009, 4(8), pp. 1133-1138. https://www.ncbi.nlm.nih.gov/pubmed/19768999
29. Chemsa, A.E.; Zellagui, A.; Öztürk, M.; Erol, E.; Ceylan, O.; Duru, M.E.; Gherraf, N. Antibiofilm formation, antioxidant and anticholinesterase activities of essential oil and methanol extract of *Marrubium deserti* de Noé. Journal of Materials and Environmental Science, 2016, 7(3), pp. 993-1000. https://www.jmaterenvironsci.com/Journal/vol7-3.html
30. Argyropoulou, C.; Skaltsa, H. Identification of essential oil components of *Marrubium thessalum* Boiss. & Heldr., growing wild in Greece. Natural Product Research, 2012, 26(7), pp. 593-599. DOI: https://doi.org/10.1080/14786419.2010.535153
31. Golmakani, H.; Rabbani Nasab, H.; Sharifan, M.; Kamali, H.; Yadollahi, A. The essential oil composition and antibacterial activity of *Marrubium duabense* Murata from North Khorassan province, Iran. Journal of Essential Oil Bearing Plants, 2016, 19(4), pp. 963-971. DOI: https://doi.org/10.1080/0972060X.2014.998722
32. Skaltsa, H.; Lazari, D.; Loukis, A.; Aslanis, D.; Tiligada, E. Chemical and biological studies on the essential oil of *Marrubium cylleneum* Boiss. & Heldr. Phamaceutical and Pharmacological Letters, 1997, 7(4), pp.184-186. https://www.ncbi.nlm.nih.gov/nlmcatalog/9214513

33. Lazari, D.M.; Skaltsa, H.D.; Constantinidis, T. Essential oils of *Marrubium velutinum* Sm. and *Marrubium peregrinum* L., growing wild in Greece. Flavour and Fragrance Journal, 1999, 14(5), pp. 290-292. DOI: https://doi.org/10.1002/(SICI)1099-1026(199909/10)14:5<290::AID-FFJ828>3.0.CO;2-4
34. Chebrouk, F.; Hammoudi, R.; Hadj, M.M.; Ferfad, T.B. Composition of essential oils of *Marrubium deserti* from Ghardaia (Septentrional East Algerian Sahara). Algerian Journal of Arid Environment, 2011, 1(2), pp. 82-87. (in French). https://www.asjp.cerist.dz/en/article/596
35. Hamedeyazdan, S.; Fathiazad, F.; Asnaashari, S. Chemical composition of the essential oil from *Marrubium persicum* C.A. Mey. (*Lamiaceae*). Pharmaceutical sciences, 2013, 19(2), pp. 35-38. http://journals.tbzmed.ac.ir/PHARM/Abstract/PHARM_200_20131216101051
36. Grassia, A.; Senatore, F.; Arnold, N.A.; Bruno, M.; Piozzi, F.; Rigano, D.; Formisano, C. Chemical composition and antimicrobial activity of essential oils from aerial parts of two *Marruibium* sp. (*Lamiaceae*) growing wild in Lebanon. Polish Journal of Chemistry, 2006, 80(4), pp. 623-628. http://www.ichf.edu.pl/pjch/pj-2006/pj-2006-04c.htm
37. Sarikurkcu, C.; Tepe, B.; Daferera, D.; Polissiou, M.; Harmandar, M. Studies on the antioxidant activity of the essential oil and methanol extract of *Marrubium globosum* subsp. *globosum* (*Lamiaceae*) by three different chemical assays. Bioresource Technology, 2008, 99(10), pp. 4239-4246. DOI: https://doi.org/10.1016/j.biortech.2007.08.058
38. Kaurinovic, B.; Vlaisavljevic, S.; Popovic, M.; Vastag, D.; Djurendic-Brenesel, M. Antioxidant properties of *Marrubium peregrinum* L. (*Lamiaceae*) essential oil. Molecules, 2010, 15(9), pp. 5943-5955. DOI: https://doi.org/10.3390/molecules15095943
39. Petrović, S.; Pavlović, M.; Maksimović, Z.; Milenković, M.; Couladis, M.; Tzakouc, O.; Niketić, M. Composition and antimicrobial activity of *Marrubium incanum* Desr. (*Lamiaceae*) essential oil. Natural Product Communication, 2009, 4(3), pp. 431-434.
40. Nagy, M.; Svajdlenka, E. Comparison of essential oils from *Marrubium vulgare* L. and *M. peregrinum* L. Journal of Essential Oil Research, 1998, 10(5), pp. 585-587. DOI: https://doi.org/10.1080/10412905.1998.9700978
41. Bal, Y.; Kaban, S.; Kirimer, N.; Baser, K.H.C. Composition of the essential oil of *Marrubium parviflorum* Fisch. *et* Mey. subsp. Oligodon (Boiss.) Seybold. Journal of Essential Oil Research, 1999, 11(3), pp. 300-302. DOI: https://doi.org/10.1080/10412905.1999.9701138
42. Baher Nik, Z.; Mirza, M. Composition of the essential oil of *Marrubium astracanicum* Jacq. Journal of Essential Oil Research, 2003, 15(5), pp. 342-343. DOI: https://doi.org/10.1080/10412905.2003.9698607
43. Zawiślak, G. Comparison of chemical composition of the essential oil from *Marrubium vulgare* L. and *M. incanum* Desr. during the second year of cultivation. Acta Agrobotanica, 2015, 68(1), pp. 59-62. DOI: http://doi.org/10.5586/aa.2015.002
44. ISO, International Standard 9235: Aromatic natural raw materials-vocabulary. International Organization for Standardization, Geneva: Switzerland, 1997. https://www.iso.org/obp/ui/#iso:std:iso:9235:ed-2:v1:en
45. Kaufmann, B.; Christen, P. Recent extraction techniques for natural products: microwave-assisted extraction and pressurised solvent extraction. Phytochemical Analysis, 2002, 13(2), pp. 105-113. DOI: https://doi.org/10.1002/pca.631
46. Leitner, J. A contribution to the knowledge of the pollen grains of the *Labiatae*. Österreichische Botanische Zeitschrift, 1942, 91(1), pp. 29-40 (in German). https://www.jstor.org/stable/43804961
47. Ruzicka, L. The isoprene rule and the biogenesis of terpenic compounds. Experientia, 1953, 9(10), pp. 357-367. DOI https://doi.org/10.1007/BF02167631
48. Leonardi, A. Allergy and allergic mediators in tears. Experimental Eye Research, 2013, 117, pp. 106-117. DOI: https://doi.org/10.1016/j.exer.2013.07.019
49. Abelson, M.B.; Smith, L.; Chapin, M. Ocular allergic disease: mechanisms, disease sub-types, treatment. The Ocular Surface, 2003, 1(3), pp. 127-149. DOI: https://doi.org/10.1016/S1542-0124(12)70140-4
50. Patočka, J.; Kuca, K.; Jun, D. Acetylcholinesterase and butyrylcholinesterase – important enzymes of human body. Acta Medica (Hradec Kralove), 2004, 47(4), pp. 215-228. ftp://orbis.lfhk.cuni.cz/Acta_Medica/2004/AM-4_04.pdf

CHEMISTRY JOURNAL OF MOLDOVA. General, Industrial and Ecological Chemistry. 2018, 13(2), 24-31
ISSN (p) 1857-1727 ISSN (e) 2345-1688
http://cjm.asm.md
http://dx.doi.org/10.19261/cjm.2018.502

THE EFFECT OF RICE HUSK ON THE PHASE FORMATION AND CEMENT CLINKER PROPERTIES

Lev Chernyak [*], Liubov Melnyk, Natalia Dorogan

National Technical University of Ukraine "Igor Sikorsky Kyiv Polytechnic Institute",
37, Peremohy ave., Kyiv 03056, Ukraine
[*]e-mail: lpchernyak@ukr.net; phone: (+38) 067 298 57 75

Abstract. The features of the cement clinker containing rice husk are investigated. The dependence of the raw mixture composition on the set product burning characteristics has been analysed using the software "CLINKER". The mixture compositions have been identified on the basis of the chalk–clay–rice husk system, with the introduction of man-made stock of 6.0–18.0 mass%. The features of the phase composition and the binder properties, by varying the rice husk content, mixture ratio and burning temperature were studied.

Keywords: cement, clinker, rice husk, crystalline phase, property.

Received: 10 July 2018/ Revised final: 26 September 2018/ Accepted: 28 September 2018

Introduction

Increased volumes of manageable large-tonnage wastes from metallurgy, chemical industry and agrarian production call for complex solving of tasks related to the silicate production development for environment and resource preservation [1-3]. Solving of these tasks requires a corresponding development of scientific and technical principles of silicate chemical technologies, with the identification of regularities regarding the impact of different raw materials concentrations on the structure and properties of silicate materials [4,5].

Stock base expanding in the silicate materials production is studied by numerous researchers. Moreover, the use of wastes from other industries as the technological raw material into the processes is emphasized [6-8]. The largest practical achievement in this field of research was the use of nonferrous-metals industry wastes, namely blast furnace granulated slag and of thermal power sector wastes, namely fly ash from thermal power stations as the components of slag Portland cement and composite cements [9,10]. From among other large-tonnage wastes, the rice husk attracts attention [11,12]. It is stated that manufacturing of 1 kg of white rice gives 0.28 kg of rice husk as the by-product in the milling process. As a result, over 150 million tons of wastes are generated, considering an annual global rice production capacity of 750 million tons.

Large volumes of generated and accumulated rice production wastes may be regarded as hazardous to the environment; this emphasizes the urgency of development of new methods for waste disposal considering their physical and chemical properties and impact on characteristics of probable product types. In this connection, the application of rice husk in silicate productions is of particular interest. In addition, the rice husk can be a source of amorphous silica, as an activator of physical and chemical processes of silicate system structure formation [13-15]. This is proved experimentally by published scientific reports regarding the impact of rice husk additives on brick [16,17], porcelain [18] and concrete [19,20] properties. The results of most of these studies lead to the conclusion that the use of rice husk in manufacturing of silicate materials is directed towards its addition to raw compositions in the frames of the existing technology. However, most of the studies on the use of waste from rice production in the technology of astringent materials are associated with the preliminary thermal treatment of rice husk, the study of the properties of rice husk ash and the influence of its addition on the properties of cement and concrete [21-24]. These works do not address the issue of increasing the volume of utilization of rice husk as a significant component of raw mixtures for the manufacturing of cement clinker, and this underlines the actuality of our researches in this field.

The aim of the research presented in this work was to investigate the effect of rice husk on phase formation of the raw material mixture during burning and on the properties of cement clinker. The features of the phase composition and the binder properties were studied by varying the rice husk content, mixture ratio and burning temperature.

Experimental

Materials

Chalk (chalk, MD-2 type, Zdolbuniv deposit, Rivne area, Ukraine), clay (clay, polymineral type, Kryvyn deposit, Rivne area, Ukraine) and rice husk (wastes from the production of rice, LTD. "Rice of Ukraine", Kherson area, Ukraine) were used as raw materials.

The raw mixtures have been prepared by dispensing the components by mass, mixing and homogenizing in a ball mill, firing and milling of the final product in accordance with the modern technology of mineral binders.

Samples of raw mixtures have been bubbled in an oven for 15 hours in the range of maximum temperatures of 1200°C and 1400°C keeping a hold at a maximum of 1.5 hours. All samples of the mixtures that have been compared were blasted together to exclude the possibility of a difference in the degree of heat treatment. The properties of the binding material (setting time, compressive strength) were determined according to standardized procedures [25,26].

Methods

Methods of physical - chemical analysis of silicate raw materials and testing of properties of astringent substances which were used in this work included:

- *chemical composition analysis* using standardized procedures [27,28];
- *X-ray diffraction analysis* (powder - like preparations) using a diffractometer DRON-3M (radiation CuK_α 1-2, voltage 40 kV, current 20 mA, speed 2 degrees/min).

The raw mixtures based on the chalk–clay–rice husk systems were used in the present study to make Portland cement clinker. The chemical compositions of the output stock samples (Table 1) differ in terms of quantitative content of oxides and form the following rows, mass % for:

- SiO_2: chalk < rice husk < clay;
- Al_2O_3: clay > chalk and rice husk;
- CaO: chalk > clay > rice husk;
- Fe_2O_3: clay > chalk and rice husk.

The main rock-forming mineral of the rice husk is the amorphous silica (Figure 1) that is confirmed by the X-ray phase analysis [30].

Table 1

Chemical composition of raw materials (mass %).

Samples	*SiO_2*	*Al_2O_3*	*Fe_2O_3*	*TiO_2*	*CaO*	*MgO*	*SO_3*	*Na_2O*	*K_2O*	*LOI***
Chalk	0.77	0.25	0.13	-	55.0	0.25	0.08	-	-	43.49
Clay	60.96	15.66	5.57	0.79	3.33	2.04	0.16	0.30	2.70	8.48
Rice husk*	15.64	0.24	0.12	-	0.61	0.45	0.18	0.48	0.28	82

* *Correlated with known data [29];*

** *LOI is the loss on ignition.*

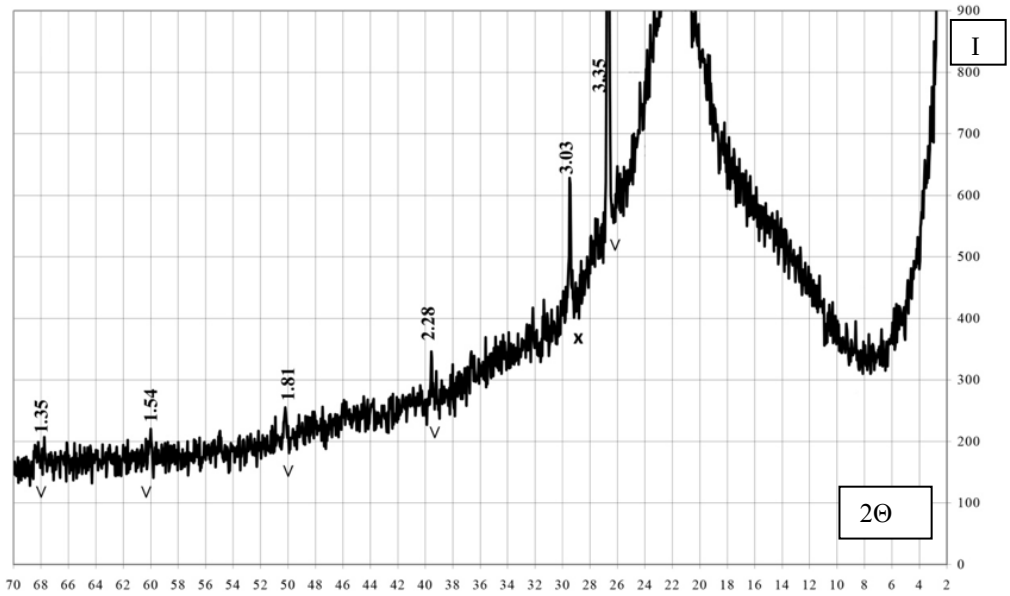

Figure 1. X-ray diffraction of rice husk: v - quartz, x – calcite [30].

It is evident that in the studied silicate system, the use of clay and rice husk for manufacturing of cement clinker will serve as the source of SiO_2, which is required to create the main clinker minerals in the process of burning. However, because of different crystallisation levels, the crystal *β*-quartz was introduced into the system with the clay, and amorphous silica was introduced with the rice husk.

The *calculations and the analysis of raw mixtures* to obtain Portland cement clinker have been performed with the software application "CLINKER" according to the recommendations for numerical values of the saturation factor (*SF*), and silica *n* and alumina *p* modules [31]. The basic steps of using the software are as follows:

1. A table listing chemical compositions of possible raw components is entered;
2. Values of *SF* and *n*, *p* modules are set;
3. Using the accepted calculation formulas, all combinations of two, three or four components that guarantee the required performance of the clinker are identified. To this end, if a rather large raw material base is available, rational proportions of components in the output raw mixture can be promptly identified.

Results and discussion

Analysis of raw mixtures containing rice husk for clinker production

The analysis of the obtained results showed that the concentration of the rice processing wastes as part of raw mixtures within the recommended intervals *SF* depends considerably on types and quantitative ratio of other components; moreover, an inverse proportional dependence exists between the content of wastes and saturation factor value (*SF*). The possible content of rice husk may vary within 5.6 to 18.4 mass % and it increases with the reduced *SF* value and clay quantity in the three-component mixture on the chalk–clay–rice husk (Figure 2).

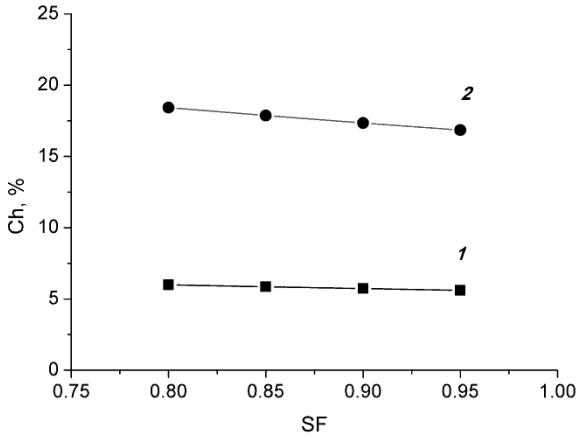

Figure 2. Correlation between the rice husk content (*Ch*) in the mixture chalk–clay–rice husk and the saturation factor (*SF*) of clinker in the silica module: *(1) n*= 3.0; *(2) n*= 3.5.

Based on computer calculations, 3-component raw mixtures were taken for further study and for manufacturing the Portland cement clinker on the basis of the chalk–clay–rice husk system (Table 2).

The studied mixtures differ in the rice husk content and different quantitative ratio of other components. Thus, sample 2S differs from sample 1S with the less (1.9 against 2.8) quantitative ratio of carbonate-containing component (chalk) to the sum of alumino- and silica-containing (clay and rice husk) components, and less quantitative ratio of clay to rice husk (0.9 to 3.4). The analysis of the chemical composition of the studied mixtures proves that when the rice husk content increases, sample 2S differs from sample 1S with the less content of CaO (47.0 versus 41.2 mass %) at a considerable reduction in the quantitative ratio $CaO:SiO_2$ (2.75 *versus* 2.80) and definite increase of $CaO:Al_2O_3$ (13.1 *versus* 11.6), and reduction in the content of Fe_2O_3 and MgO (Table 3).

Table 2

Composition of raw materials mixtures (mass %).

Code of mixture	*Chalk*	*Clay*	*Rice husk*
1S	73.5	20.5	6.0
2S	66.0	16.0	18.0

Table 3

Chemical composition of raw mixtures (mass %).

Code of mixture	*SiO_2*	*Al_2O_3*	*Fe_2O_3*	*CaO*	*MgO*	*SO_3*	*LOI*
1S	14.62	3.56	1.31	41.15	0.65	0.11	38.60
2S	13.47	2.82	1.04	37.04	0.59	0.11	44.93

Phase composition and clinker properties in the case of using rice husk

Three-component mixtures with different quantitative ratio of the components, different values of the clinker performance and phase composition were studied. In case of the mixtures on the basis of the chalk–clay–rice husk, sample 2S with the rice husk content of 18 mass% and its quantitative ratio to the clay of 1.1:1 must differ from sample 1S with 6 mass% and its quantitative ratio to the clay of 1:3.4 in an inconsiderable increase in C_3S and C_2S and some decrease in the quantity of C_3A and C_4AF (Table 4).

According to the X-ray phase analysis, some features of phase transformation have been defined during burning of the studied mixtures at the maximal temperatures of 1200°C and 1400°C (Figure 3-6).

Table 4

Description of the clinker.

Code of mixture	*Parameters of clinker*			*Crystalline phases, %*			
	SF	*n*	*p*	*C_3S*	*C_2S*	*C_3A*	*C_4AF*
1S	0.85	3.0	2.72	49.76	30.71	11.77	6.45
2S	0.85	3.5	2.71	51.12	31.55	10.36	5.74

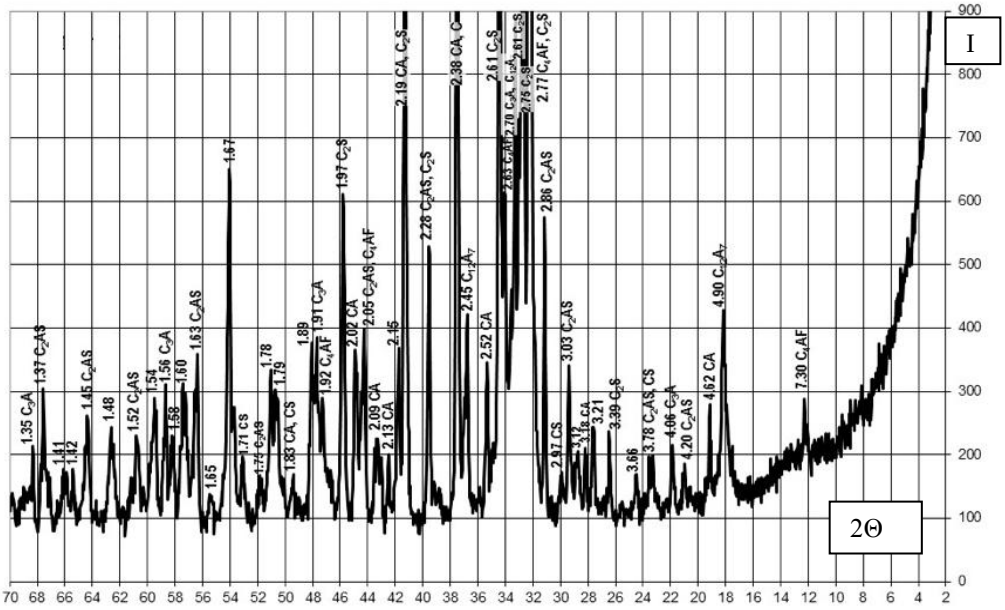

Figure 3. X-ray diffraction of clinker sample 1S (1200ºC).

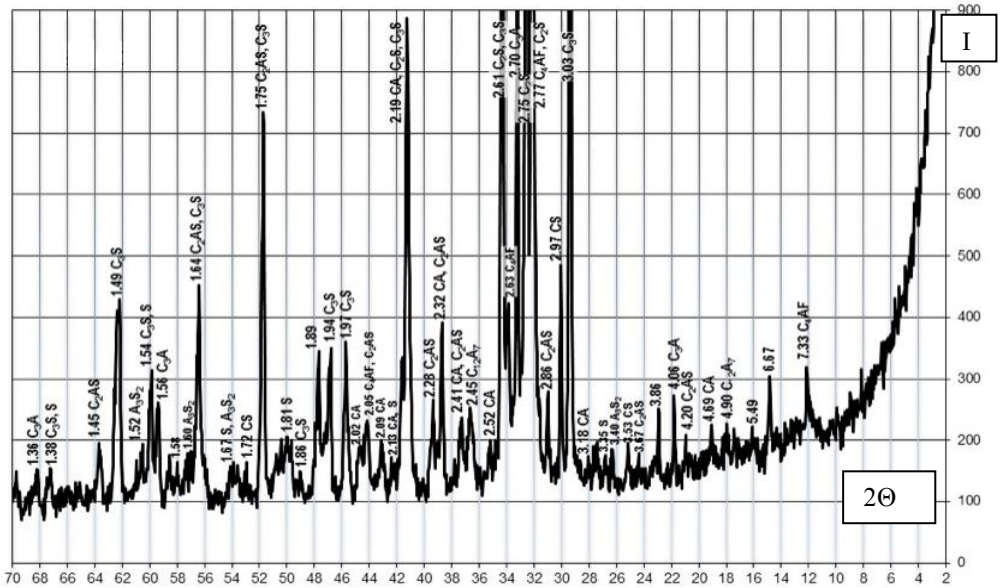

Figure 4. X-ray diffraction of clinker sample 1S (1400ºC).

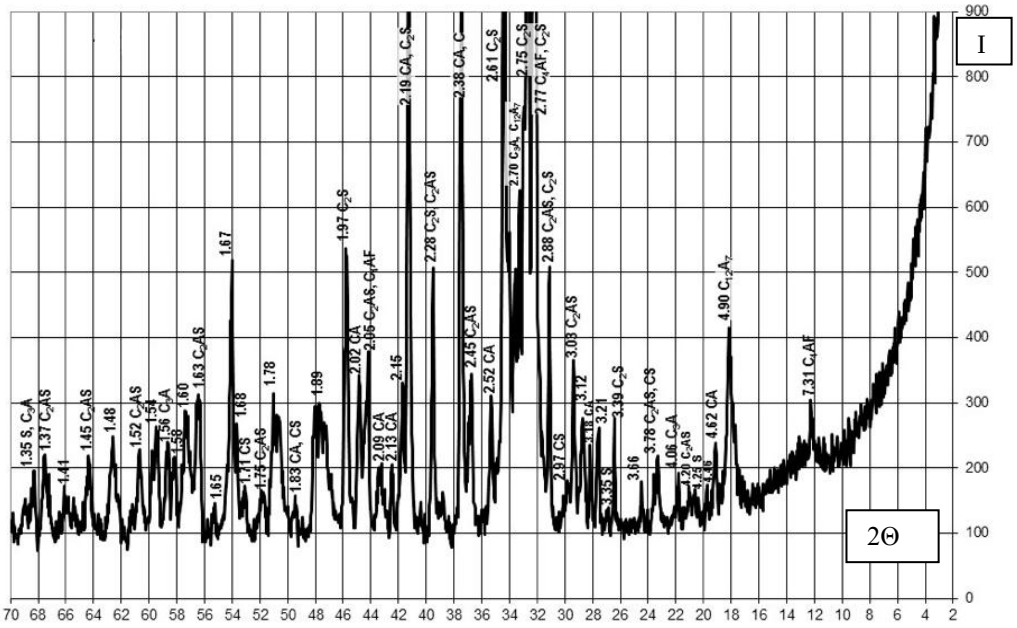

Figure 5. X-ray diffraction of clinker sample 2S (1200ºC).

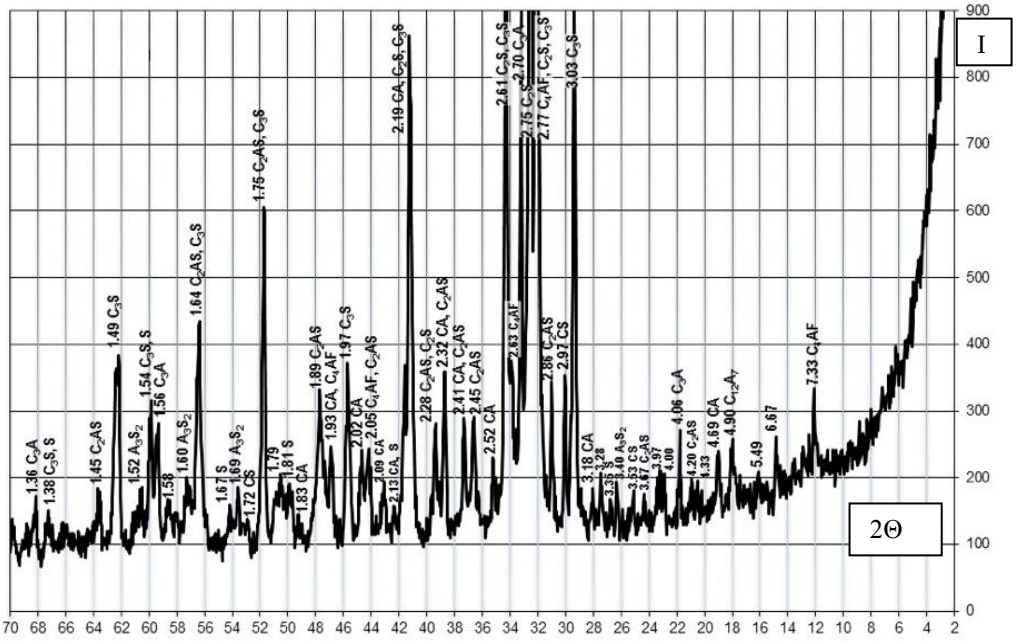

Figure 6. X-ray diffraction of clinker sample 2S (1400ºC).

It is evident that when the burning temperature increases from 1200°C to 1400°C, the samples with the composition of mixtures 1S and 2S show the same trends of the phase composition changing:

- as to the crystalline phases of calcium silicates – generation of C_3S (1.86, 3.03 Å), intensive production of wollastonite CS (2.97 Å), with minor differences in C_2S;
- as to the crystalline phases of calcium aluminosilicates - decreased content of gehlenite C_2AS (2.86 Å);
- as to the crystalline phases of calcium aluminates - intensive production of C_3A (2.70 Å); with decreased content of CA (2.52 Å) and mayenite $C_{12}A_7$ (4.90 Å);
- decreased content of CaO (2.38 Å) and C_4AF (2.63 Å).

However, in case of the same qualitative phase composition, sample 2S produced from the mixture with the 18 mass % of rice husk differs from sample 1S with the 6 mass % of rice husk by a smaller content in $CaO{\cdot}SiO_2$, $3CaO{\cdot}SiO_2$, $CaO{\cdot}Al_2O_3{\cdot}Fe_2O_3$ and a larger content of $CaO{\cdot}Al_2O_3$, $12CaO{\cdot}7Al_2O_3$ and $2CaO{\cdot}Al_2O_3{\cdot}SiO_2$. The obtained results of sample testing show the difference in composition of the output raw

mixtures and maximal value of the burning temperature (Table 5).

In accordance with the classification of DSTU B B.27-91-99, after burning at the maximal temperature of 1200°C and 1400°C, at a setting rate, the studied cement samples on the basis of the chalk – clay – rice husk were referred to different groups.

With a relatively less content of the rice husk after burning at a temperature of 1200ºC, sample 1S was referred to the group of quick setting ones (the term of beginning is 15 to 45 min). This is considered to be typical for anhydrite and aluminous cements. After increasing the burning temperature to 1400ºC, it was referred to normally setting ones (the term of beginning is 45 min to 2 h). This is considered to be typical for Portland cement and slag Portland cement.

When increasing the rice husk content to its quantitative ratio 1:1 to clay, sample 2S was referred to the group quickest setting ones (the term of beginning is up to 15 min) after burning at a temperature of 1200ºC. This is considered to be typical for expanding and self-stressing cement. After increasing the burning temperature to 1400ºC, it was referred to the group of quick setting ones.

In the course of the research undertaken, the rational composition of raw mixtures was determined on the basis of the system chalk – clay – rice husk for the manufacturing of cement clinker with baking on a maximum temperature of 1400ºC. In this case, the possibility of adjusting the binding properties of the material from the fast to normal setting is shown due to appropriate changes in the phase composition.

Among the positive aspects of this study should be denoted the directed use of rice husk as a component of the initial mixture, which becomes a source of amorphous silica with increased reactivity in the process of burning, and influences the phase formation and properties of cement clinker.

The main weakness of this study is the use of chalk as raw composition material. Obviously, the expansion of the number of basic carbonate components, first of all limestones and marls, will open up additional opportunities to achieve the goal and to increase efficiency of the study.

Table 5

Properties of clinker samples.

Quality index	*Code of sample and burning temperature*			
	1200ºC		*1400ºC*	
	1S	*2S*	*1S*	*2S*
Finesse of grinding, sieve residue no. 008, mass. %	7	8	7	8
Initial setting time, min	20	10	65	20
Final setting time, min	25	20	110	35
Compressive strength, MPa	33.4	31.7	40.2	38.6

Conclusions

The increase in the volumes of practically used large-tonnage of industrial wastes, including the rice husk resulted from the rice production in the agro-industrial sector, facilitates the solution of the complex issues related to ecology, resources preservation and technology of the manufacturing of silicate building materials.

The expediency of rice husk utilization in the binder technology is defined by the presence of amorphous silica in the chemical composition with an increased reactivity in the process of formation of silicate system structure during burning.

To produce the cement clinker, it is possible to introduce 6–18 mass % of rice husk into raw mixtures obtained based on the chalk–clay–rice husk system, when the quantitative ratio of rice husk to clay ranges between 1:3.4 and 1.1:1.

Due to the X-ray analysis and technological tests, the possibilities of adjustment of the quantitative ratio between clinker minerals and binders when varying the rice husk content in the output mixture by the maximum burning temperature were determined.

References

1. Udachkin, I.B.; Pashchenко, A.A.; Chernyak, L.P.; Zakharchenko. P.V.; Semididko, A.S.; Myasnikova, E.A. Complex development of source of raw materials for building materials industry. Kiev: Budivelnyk, 1988, 104 p. (in Russian).
2. Dvorkin, L.Y.; Dvorkin, O.L. Building materials from wastes of industry. Rostov on Don: Feniks, 2007, 368 p. (in Russian).
3. Ramesh, M.; Karthic, K.S.; Karthikeyan, T.; Kumaravel, A. Construction materials from

industrial wastes-a review of current practices. International Journal of Environmental Research and Development, 2014, 4(4), pp. 317-324. https://www.ripublication.com/ijerd_spl/ijerdv4n4spl_08.pdf
4. Shabanova, G.N.; Korogodskaya, A.N.; Kostyrkin, O.V.; Vorozhiyan, R.M. Establishment of possibility of utilization for wastes of industry in the production of alumina cement. Collection of scientific works of UkrDaz. Ukrainian State Academy of Railway Transport (UkrSART): Kharki, 2011, 122, pp. 288-292. (in Russian).
5. Chernyak, L.P. Particularities of structure formation of dispersed systems in the portland cement technology. Technology audit and production reserves, 2013, 5(14), pp. 8-10. (in Ukrainian). DOI: https://doi.org/10.15587/2312-8372.2013.19654
6. Allen, D.T.; Benmanesh, N. Wastes as Raw Materials. The Greening of Industrial Ecosystems. Washington: National Academy Press, 1994, pp. 69-89. https://www.nap.edu/read/2129/chapter/7
7. Shabanova, G.N.; Kiselyova, S.O.; Shapка, O.V. Utilization of industrial wastes at making of malmbrick is a way to the improvement of ecological situation. Scientific and technical collection is the Communal economy of cities. Kharkov: Osnova, 2010, 91, pp. 250-255. (in Ukrainian).
8. Wiemes, L.; Pawlowsky, U.; Mymrin, V. Incorporation of industrial wastes as raw materials in brick`s formulation. Journal of Cleaner Production, 2017, 142 (Part 1), pp. 69-77. DOI: https://doi.org/10.1016/j.jclepro.2016.06.174
9. Pashchenko, A.A.; Myasnikova, E.A.; Evsyutin, Yu.R. Energy-saving and zero-emission technologies of receipt of astringent substances. High school (Vyshcha shkola): Kiev, 1990, 223 p. (in Russian).
10. Klassen, V.K.; Borisov, I.N.; Manuylov, V.E. Technogenic materials in the production of cement: monograph. Belgorod: Izd-vo BGTU, 2008, 125 p. (in Russian). https://search.rsl.ru/ru/record/01004343586
11. Rice husk ash market. Electronic resource: https://www.transparencymarketresearch.com/rice-husk-ash-market.html
12. Vozhegova, R.; Vozhegov, S.; Yakub, V. Rice is in Ukraine: present and prospects tense. Electronic resource: http://propozitsiya.com/ua/ris-v-ukrayini-sogodennya-ta-perspektivi (in Ukrainian).
13. Sun, L.; Gong, K. Silicon-based materials from rice husks and their applications. Industrial & Engineering Chemistry Research, 2001, 40(25), pp. 5861-5877. DOI: 10.1021/ie010284b
14. Sergienko, V.I.; Zemnukhova, L.A.; Egorov, A.G.; Shkorina, E.D.; Vasiluk, N.S. Proceeded in the sources of chemical raw material: complex processing of wastes of production of rice and buckwheat. Russian chemical Journal, 2004, 48(3), pp. 116-124. (in Russian).
15. Mansha, M.; Javed, S.H.; Kazmi, M.; Feroze, N. Study of rice husk ash as potential source of acid resistance calcium silicate. Advances in Chemical Engineering and Science, 2011, 1(3), pp. 147-153, DOI: 10.4236/aces.2011.13022
16. Carter, G.W.; Cannor, A.M.; Mansell, D.S. Properties of bricks incorporating unground rice husks. Building and Environment, 1982, 17(4), pp. 285-291. DOI: https://doi.org/10.1016/0360-1323(82)90021-X
17. Sutas, J.; Mana, A.; Pitak, L. Effect of rice husk and rice husk ash to properties of bricks. Procedia Engineering, 2012, 32, pp. 1061-1067. DOI: https://doi.org/10.1016/j.proeng.2012.02.055
18. Prasad, C.S.; Maiti, K.N.; Venugopal, R. Effect of rice husk ash in whiteware compositions. Ceramics International, 2001, 27(6), pp. 629-635. DOI: https://doi.org/10.1016/S0272-8842(01)00010-4
19. Hwang, C.L.; Anh-Tuan, B.L.; Chen, C.T. Effect of rice husk ash on the strength and durability characteristics of concrete. Construction and Building Materials, 2011, 25(9), pp. 3768-3772. DOI: https://doi.org/10.1016/j.conbuildmat.2011.04.009
20. Kumar, P.Ch.; Venugopal, N.V.S.; Rao, P.M. Studies on the determination of compressive strengths of different grades of rice husk ash-an ecofriendly concrete. Journal of Environmental Protection, 2013, 4(4), pp. 329-332. DOI: 10.4236/jep.2013.44039
21. Ajiwe, V.I.E.; Okeke, C.A.; Akigwe, F.C. A preliminary study of manufacture of cement from rice husk ash. Bioresource Technology, 2000, 73(1), pp. 37-39. DOI: https://doi.org/10.1016/S0960-8524(99)00135-2
22. Habeeb, G.A.; Mahmud, H.B. Study on properties of rice husk ash and its use as cement replacement material. Materials Research, 2010, 13(2), pp. 185-190. DOI: http://dx.doi.org/10.1590/S1516-14392010000200011
23. Zareei, S.A.; Ameri,F.; Dorostkar, F.; Ahmadi, M. Rice husk ash as a partial replacement of cement in high strength concrete containing micro silica: Evaluating durability and mechanical properties. Case Studies in Construction Materials, 2017, 7, pp. 73-81. DOI: https://doi.org/10.1016/j.cscm.2017.05.001
24. Chindaprasirt, P.; Rukzon. S. Strength, porosity and corrosion resistance of ternary blend Portland cement, rice husk ash and fly ash mortar. Construction and Building Materials, 2008, 22(8), pp. 1601-1606. DOI: https://doi.org/10.1016/j.conbuildmat.2007.06.010
25. DSTU B.2.7-46. Cements of general construction purpose. Specifications - Introduction. 09/01/2011 - K.: Minregionstroy of Ukraine, 2011, 14 p. (in Ukrainian).
26. DSTU B EN 197-1. Part 1. Composition, specifications and conformity criteria for

conventional cements. Introduction. Minregionstroy of Ukraine, 2009, 24 p. (in Ukrainian).
27. DSTU B V.2.7-112-2002. Cements general specifications. Introduction. State Building of Ukraine, 2002, 39 p. (in Ukrainian).
28. GOST 5382-91. Cements and materials for cement production. Chemical analysis methods. (in Russian).
29. Orazimbetova, G.J. Analysis of hydration of cement made of marl and rice shuck. Published in the proceedings of the 5th international conference, Cooperation for waste issues, 2008, pp. 165-166. (in Russian).
30. Holoiukh, I.A.; Dorogan N.A.; Cherniak L.P. Aspects of waste utilization from rice production for Portland cement manufacturing. The first independent scientific Bulletin, 2016, 6, pp. 63-66. (in Russian).
31. Svidersky, V.A.; Chernyak, L.P.; Dorogan, N.O.; Soroka, A.S. Software of portland cement technology. Building materials and wares, 2014, 1(84), pp. 16-17. (in Ukrainian).

CHEMISTRY JOURNAL OF MOLDOVA. General, Industrial and Ecological Chemistry. 2018, 13(2), 32-37
ISSN (p) 1857-1727 ISSN (e) 2345-1688
http://cjm.asm.md
http://dx.doi.org/10.19261/cjm.2018.516

METALLURGICAL COKEMAKING WITH THE IMPROVED PHYSICOCHEMICAL PARAMETERS AT AVDEEVKA COKE PLANT

Oleg Zelenskii [a*], Yuriy Vasil'ev [a], Alexey Sytnik [a], Natalia Desna [a], Elena Spirina [a], Andrey Grigorov [b]

[a]*State Enterprise "Ukrainian State Research Institute for Carbochemistry", 7, Vesnina str., Kharkov 61023, Ukraine*
[b]*National Technical University "Kharkov Polytechnic Institute", 2, Kirpichova str., Kharkov 61002, Ukraine*
[*]*e-mail: zelenskii.ukhin@gmail.com; phone: (+380 66) 727 12 75; fax: (+380 57) 700 69 06*

Abstract. The article presents the results of studies regarding the improvement of the qualitative characteristics of blast furnace coke obtained from modified coal blend in industrial conditions of Avdeevka Coke Plant. Inorganic corundum powders are applied to modify the coal blend, namely electrocorundum (α-Al_2O_3) and carborundum (α-SiC). It has been found that the introduction of non-caking corundum materials in small concentrations (0.25 wt %) affects the structure of the organic mass of coal as it is assumed that the corundum materials act as centers of crystallization. The influence of a certain type of modifying additive on the quality of coke is significantly dependent on the brand composition of the blend. The use of electrocorundum and carborundum is especially important for blends with reduced caking ability.

Keywords: coal, electrocorundum, carborundum, blend, coke.

Received: 27 September 2018/ Revised final: 15 November 2018/ Accepted: 16 November 2018

Introduction

Coke performs three main functions in a blast furnace: it is a heat source for chemical reactions and phase transformations of a blast furnace charge, a reducing agent in chemical reactions, and a physical support - of a column of charge materials [1]. The normal course of the blast-furnace process depends on the performance of these coke functions, which are determined by the physical-chemical properties of this product [2].

The operation of blast furnaces with high productivity, long service life and low coke consumption is achievable only with the use of high-quality charge materials - iron ore with high iron content and high quality coke produced from coking coals with the necessary mineral composition and low sulphur content. It should be noted that most of coking coals produced in Ukraine have high sulphur content, allowing to obtain, on average, coke with the coke reactivity index (CRI) and coke strength after reaction (CSR) values within 40% [3,4]. In the U.S.A., Germany, Poland, China, Japan metallurgical plants impose very high requirements regarding the quality of blast furnace coke for these parameters (CRI $\leq$ 30%; CSR $\geq$ 60%) [2].

Coke consumption for iron blast furnaces in the Ukraine is on average up to 450 kg/t [1] while leading ironmakers in other countries have reduced coke usage to 300 kg/t. The specific coke consumption in Ukraine is much higher, which reduces the economy of smelting cast iron, because coke is the most expensive component of the blast furnace charge. Therefore, leading manufactures substitute coke (up to 40%) with additional fuels, primarily pulverized coal. To get the blast-furnace coke with necessary quality indicators at the existing coal base, coke-makers develop and use techniques that improve quality parameters of coal. One of such methods is the targeted influence of the coke quality by adding non-coking additives into the coal blend: coke dust and fines, anthracite, semi-coke, as well as inorganic additives (finely dispersed oxides of titanium, iron and aluminum) [5].

The use of nanomaterials as additives is known to be effective in improving the wear resistance, strength, crack resistance and other characteristics of hard alloys [6]. For example, Al_2O_3, SiC, B_4C, TiN, TiCN and WC nanopowders have been used successfully as modifying additives [7-9]. In this paper, the task was set to use micropowders of electrocorundum (α-Al_2O_3) and carborundum (α-SiC) as additives in coal blends for the production of metallurgical coke with improved quality parameters.

Experimental

Cokemaking procedure

One of the coke plants in Ukraine, Avdeevka Coke Plant has been selected for research. Cokemaking trials were carried out using metal coke boxes. The box dimensions were as follows: length 200 mm; width 200 mm; height 280 mm. The total mass of the coal batch in the box was 8 kg.

The packing density of the coal blend in the box was 800 kg/m^3 and the moisture content was 8–10%. To attain this density, the appropriate mass of coal was charged in the box corresponding to the density achieved industrially.

Four coking ovens in a coke oven battery No. 1 were selected to study. Four boxes with experimental blend were placed in each coking chamber. The boxes were loaded through the middle charging hole in the coking chamber. The coking time was set to 21 hours.

After the oven was pushed and the coke was quenched, the metal boxes were removed from the coke wharf and were water quenched, if necessary.

The additives that were selected for the use in this study, crystalline (α-modification) powders of aluminum oxide (electrocorundum) and silicon carbide (carborundum) with different particle size, were purchased from Private Joint Stock Company ZAPOROZHABRASIVE (Zaporozhe, Ukraine).

Characterization techniques of coal and coke

The technical analysis of coal and coke (volatility, sulphur and ash content) was performed using standard test methods [10-12]. The technical analysis was carried out on dried samples of coal and coke. Samples of coal and coke were dried in an oven for 1 hour at 105°C and 150°C respectively.

The mean vitrinite reflection coefficient (R_0) and *vitrinite content* (V_t) were performed using a Petrographic complex "OLYMPUS BX51M". For the analyses, the samples were prepared by standard methods [13,14].

The chemical composition of the ash was determined by the standard method [15]. *The basicity index* (B_b) and *the base/acid ratio* (I_b) were calculated by the Eqs.(1), (2) [16].

$$B_b = \frac{100A^d(Fe_2O_3+CaO+MgO+Na_2O+K_2O)}{(100-V^{daf})(SiO_2+Al_2O_3)} \quad (1)$$

where, A^d – ash content of coal in the dry state, %;
V^{daf} – volatile matter in the dry ash-free state, %.

$$I_b = \frac{Fe_2O_3+CaO+MgO+Na_2O+K_2O}{SiO_2+Al_2O_3} \quad (2)$$

The coke reactivity index (CRI) and *coke strength after reaction (CSR)* were determined by the standard methods [17].

The physicochemical properties of coke (*structural strength according to Gryaznov, abrasive hardness according to Ginzburg, reactivity, electrical resistivity* and *porosity)* were obtained by appropriate methods [18-20].

Results and discussion

The production blend of the plant from two coal preparation departments was used in this study. To determine the effect of additives on the coke quality, box coking was conducted on two different blends, Blend 1 - obtained from coal blend of ordinary quality and Blend 2 - obtained from coal blend with improved quality.

Table 1 presents the composition and characteristics of the coal used in the experiments and Table 2 presents the chemical composition of the ash, basicity index Eq.(1) and base/acid ratio Eq.(2).

Table 1

Characteristics of coal concentrate and coal blend.

Sample	*Supplier*	*Content, %*	*Ash A^d, %*	*Sulphur S^d_t, %*	*Volatility V^{daf}, %*	*Mean vitrinite reflection coefficient R_0, %*	*Vitrinite V_t, %*
Coal blend 1	Toldinskaya Yuzhnaya (Russia)	25.1	7.0	0.15	40.5	0.67	85
	Samsonovskaya Zapadnaya (Ukraine)	38.6	8.4	1.13	36.4	0.97	85
	Yunyaginskiy razrez (Russia)	22.7	8.1	0.68	25.4	0.98	82
	Suhodolskaya Vostochnaya (Ukraine)	3.6	8.1	0.99	24.9	1.30	96
	Kolosnikovskaya (Ukraine)	4.0	8.6	1.56	32.2	0.70	93
	Samsonovskaya (Ukraine)	3.0	8.7	2.67	27.0	1.12	92
	Uzlovskaya (Ukraine)	3.0	8.2	2.21	23.0	1.15	89
	Total	**100**	**8.2**	**1.34**	**29.9**	**0.98**	**89**

Continuation of Table 1

Sample	*Supplier*	*Content, %*	*Ash A^d, %*	*Sulphur S^d_t, %*	*Volatility V^{daf}, %*	*Mean vitrinite reflection coefficient R_0, %*	*Vitrinite V_t, %*
	Komsomolskaya (Ukraine)	4	6.1	1.09	37.0	0.88	70
	Prokopevskaya (Russia)	7	7.6	0.49	42.2	0.67	86
	Toldyinskiy razrez (Russia)	15	8.7	0.33	38.9	0.64	83
	Promugol (Russia)	4	9.8	0.72	33.2	1.01	90
	Duvanskaya (Ukraine)	7	8.5	2.04	33.2	0.99	92
Coal	Kievskaya (Ukraine)	6	8.7	2.06	31.3	1.04	93
blend	Samsonovskaya (Ukraine)	4	8.9	2.68	31.5	0.99	94
2	Pokrovskaya (Ukraine)	15	7.8	0.62	28.3	1.09	86
	Kalininskaya (Ukraine)	4	8.5	1.09	25.0	1.23	90
	Uzlovskaya (Ukraine)	4	8.2	2.21	23.0	1.45	91
	Wellmore (U.S.A.)	6	8.5	0.91	34.1	0.93	70
	Carter Roag (U.S.A.)	14	8.5	0.69	31.8	1.02	92
	Pocahontas (U.S.A.)	10	8.9	0.94	18.0	1.54	73
	Total	**100**	**8.4**	**1.01**	**31.3**	**1.03**	**85**

A^d – ash content of coal in the dry state;
S^d_t – sulphur content of coal in the dry state;
V^{daf} – volatile matter in the dry ash-free state;
R_0 – mean vitrinite reflection coefficient of coal;
V_t – vitrinite content of coal.

Table 2

Chemical composition and basicity of coal blend.

Coal blend	*Chemical composition of ash, %*								*Basicity*	
	SiO_2	*Al_2O_3*	*Fe_2O_3*	*MgO*	*CaO*	*Na_2O*	*K_2O*	*SO_3*	*B_b*	*I_b*
1	51.79	24.47	11.97	1.76	2.80	1.42	1.99	2.28	3.06	0.261
2	50.16	28.33	9.98	1.76	2.63	1.26	2.37	2.04	2.80	0.229

The additives added in the blend were crystalline (α-modification) powders of aluminum oxide (electrocorundum) and silicon carbide (carborundum) with different particle size. These powders were chosen as additives based on the fact that they are mass produced by abrasive companies and have a low cost. Additives were added to the coal blend in the amount of 0.25 wt % by mechanical stirring of the additive with a coal charge for box coking (8 kg). The choice of this range of additives was based on previous studies that showed an optimum level of additives in the blend of 0.25 wt % [21]. Table 3 presents sample compositions.

The technical analysis and CRI/CSR indicators of coke obtained by box coking is given in Table 4. The obtained results show that addition of additives into the coal blend in quantities up to 0.25 wt % has no effect on the ash content of the coke (Table 4).

The dynamics of the effect of additives on the qualitative indices of CRI and CSR of coke is shown in Figures 1 and 2, respectively. The CRI/CSR indexes for the reference coke samples No. 1 and No. 5 were considered as zero. Data showing improvement (decrease) in CRI index values is in the negative area with the sign "–" (Figure 1). The improvement (increase) in CSR index / parameter values (Figure 2) is shown in the positive area with the sign "+".

Table 3

Characteristics of bulk modifying additives.

Sample No.	*Additive*	*Amount of additive in the sample, wt %*	*Particle size, μm*
1	Standard coal blend – Variant 1	without additives	–
2	α-Al_2O_3	0.25	40-80
3	α-SiC v/g*	0.25	8-12
4	α-SiC	0.25	125-150
5	Standard coal blend – Variant 2	without additives	–
6	α-Al_2O_3	0.25	40-80
7	α-SiC v/g	0.25	8-12
8	α-SiC	0.25	125-150

** v/g – vibro-ground treatment.*

Figures 1 and 2 shows that the optimal results for improving coke quality from the Blend 1 were obtained while using the following additives:

- α-Al_2O_3 (0.25 wt %) with a registered 4.1% decrease in CRI and a 5.5% increase in CSR;

- α-SiC v/g (0.25 wt %) with a recorded 3.7% decrease in CRI and a 6.1% increase in CSR;

- α-SiC (0.25 wt %) with a registered 5.2% decrease in CRI and a 6.2% increase in CSR.

Other additives either slightly worsen the CRI and CSR values or maintain the level of the standard coke within the accuracy of measurement. The improvement in CRI/CSR indices of coke characteristics with additives No. 2, 3 and 4 was also confirmed by some other analyses of the physicochemical properties of coke (structural strength according to Gryaznov, reactivity), as follows from the data presented in Table 5.

Table 4

Technical analysis and values of CRI/CSR for coke produced.

Sample No.	*Ash A^d, %*	*Volatility V^{daf}, %*	*Sulphur S^d_t, %*	*Coke reactivity index CRI, %*	*Coke strength after reaction CSR, %*
1	11.2	0.3	0.81	37.3	39.5
2	11.6	0.2	0.84	33.2	45.0
3	11.5	0.6	0.82	33.6	45.6
4	11.4	0.4	0.81	32.1	45.7
5	10.6	0.2	0.72	34.2	46.7
6	10.6	0.2	0.71	33.4	47.1
7	11.1	0.3	0.74	34.8	47.4
8	10.6	0.2	0.72	32.2	49.3

A^d – ash content of coke in the dry state;
V^{daf} – volatile matter in the dry ash-free state;
S^d_t – sulphur content of coke in the dry state;
CRI – coke reactivity index;
CSR – coke strength after reaction with CO_2.

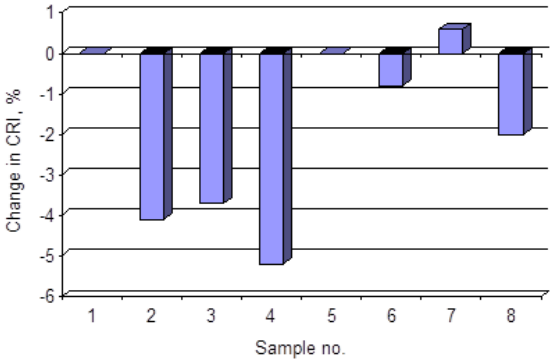

Figure 1. The dependence of various additives influence on CRI coke characteristics.

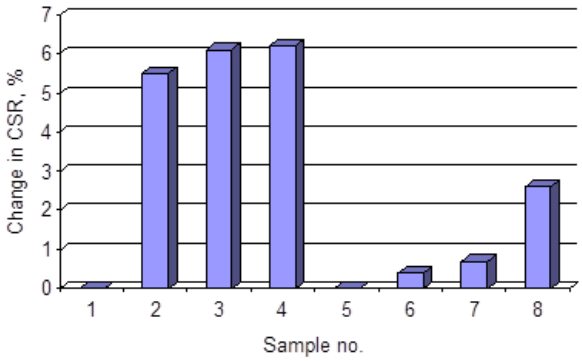

Figure 2. The dependence of various additives influence on CSR coke characteristics.

Table 5

Physicochemical parameters of experimental cokes.

Sample No.	*Structural strength according to Gryaznov, %*	*Abrasive hardness according to Ginzburg, mg*	*Electrical resistivity, Ω·cm*	*Reactivity, $cm^3/g{\cdot}sec$*	*Porosity, %*
1	83.0	95.7	0.163	0.37	50.2
2	89.1	103.1	0.207	0.26	47.1
3	87.1	101.1	0.230	0.23	49.9
4	87.0	100.6	0.248	0.21	49.3
5	83.3	96.7	0.210	0.65	50.1
6	88.0	105.1	0.193	0.53	47.3
7	86.0	105.5	0.163	0.50	50.3
8	81.3	100.6	0.223	0.46	49.2

By action on the indicators of CSR and CRI, inorganic additives may be divided into two: those that improve these indicators and those that significantly reduce CSR [22]. The first group comprises aluminum oxide, compounds of silicon and minerals: apatite, muscovite and orthoclase. Additives that improve the properties of coke, *i.e.* increase CRI and decrease CSR include magnesium oxide, iron compounds (Fe_2O_3, $FeCO_3$, $FeO{\cdot}Fe_2O_3$, FeS_2) and calcium oxides.

According to literature data, the addition of aluminum oxide and silicon compounds reduces the content of isotropic textures in the coke and increases the content of fine mosaic textures [22]. Thus, the introduction of inorganic additives in small concentrations affects the structure of the organic mass of coal, since it is assumed that the additives act as crystallization centers at the stage of plastic state of the coal blend.

Conclusions

The introduction of a specific quantity (0.25 wt %) of non-clinkering additives allows the modification of the processes that occur when the coal blend is plastic, with consequent improvement in coke strength.

The obtained results show that coke reactivity index (CRI) and coke strength after reaction (CSR) values of the coke are improved by introducing modifying additives in the coal blend in quantities of 0.25 wt %.

It was shown that positive results are obtained along with the additives 2 (α-Al_2O_3 0.25 wt %), 3 (α-SiC v/g 0.25 wt %) and 4 (α-SiC 0.25 wt %).

The influence of each specific additive on the coke properties depends significantly on the rank composition of the blend. Thus, the improvement in the coke quality with the addition of additives was obtained with Blend 1, and, accordingly, there was no improvement in the quality of the coke obtained from Blend 2 with the addition of additives. Therefore, it can be concluded that the use of these additives is relevant for batch materials with reduced caking index.

References

1. Filatov, Y.V.; Kovalev, E.T.; Shulga, I.V.; Kaufman, S.I.; Kolomiychenko, A.I. Theory and Practice of Production and Application of Blast-Furnace Coke of Improved Quality. Naukova dumka: Kiev, 2011, 128 p. (in Russian). http://www.ndumka.kiev.ua/
2. Zolotukhin, Yu.A.; Andreichikov, N.S.; Kukolev, Ya.B. Quality requirements on coke for blast furnaces operating with coal-dust fuel. Coke and Chemistry, 2009, 52(3), pp. 110-115. DOI: https://doi.org/10.3103/S1068364X09030053
3. Ryshchenko, A.I.; Kovalev, E.T.; Shulga, I.V.; Miroshnichenko, D.V.; Shmalko, V.M. The influence of the properties of coals on the reactivity and the post-reactive strength of coke. Coal Chemistry Journal, 2009, 5-6, pp. 11-17. (in Russian). http://www.ukhin.org.ua
4. Gusak, V.G.; Rubchevskiy, V.N.; Tkalich, G.M.; Chernyshov, Yu.A.; Ovchinnikova, S.A.; Podlubnyy, A.V.; Kovalev, E.T.; Drozdnik, I.D.; Kaftan, Yu.S. Producing high-quality coke from blends of domestic and imported coal at PAO Zaporozhkoks. Coke and Chemistry, 2014, 57(4), pp. 141-146. DOI: https://doi.org/10.3103/S1068364X14040024
5. Zelenskii, O.I. Modern trends in the use of nonmetallurgical additives in the coke production. Coal Chemistry Journal, 2013, 3-4, pp. 21-28. (in Russian). http://www.ukhin.org.ua/
6. Ryzhonkov, D.I.; Levina, V.V.; Dzidziguri, E.L. Nanomaterials: Manual, BINOM: Moscow, 2008, 365 p. (in Russian). http://www.lbz.ru/
7. Tsikarev, D.A. Effect of mineral additives in coal blends on the properties of blast furnace coke. Coke and Chemistry, 1993, 4, pp. 30-32. (in Russian). http://vlib.ustuarchive.urfu.ru/cox_chem/index.html
8. Semchenko, G.D.; Panasenko, M.A.; Zelenskii, O.I.; Baklan, V.Yu. Carbon precursors for synthesizing oxygen-free refractory new formations in carbon-graphite materials. Refractories and Industrial Ceramic, 2010, 51(3), pp. 193-196. DOI: https://doi.org/10.1007/s11148-010-9287-4.
9. Fuping, T.; Xiaoyang, L.; Xu, W.; Xibo, M. Coal blending coking technology. China Patent, 2010, No. 102559230A.
10. ISO 1171:2010. Solid mineral fuels. Determination of ash. https://www.iso.org/standard/55944.html
11. ISO 334:2013. Solid mineral fuels. Determination of total sulphur. Eschka method. https://www.iso.org/standard/63441.html
12. ISO 562:2010. Hard coal and coke. Determination of volatile matter. https://www.iso.org/standard/55943.html
13. ISO 7404-5:2009. Methods for the petrographic analysis of coals. Part 5: Method of determining microscopically the reflectance of vitrinite. https://www.iso.org/standard/42832.html
14. ISO 7404-3:2009. Methods for the petrographic analysis of coals. Part 3: Method of determining maceral group composition. https://www.iso.org/standard/42831.html
15. GOST 10538-87. Solid fuel. Methods for determination of chemical composition of ash. (in Russian).
16. Lyalyuk, V.P.; Sokolova, V.P.; Shmeltser, E.O.; Timofeeva, D.Yu.; Beryeza V.V. Predicting the reactivity and hot strength of coke on the basis of ash basicity. Coke and Chemistry, 2014, 57(6), pp. 238-244. DOI: https://doi.org/10.3103/S1068364X14060052

17. ISO 18894:2018. Coke. Determination of coke reactivity index (CRI) and coke strength after reaction (CSR). https://www.iso.org/standard/72266.html
18. Sklyar, M.G.; Tutunnikov, Yu.B. Chemistry of Solid Fossil Fuels. Laboratory Practical Work. Vischa shkola: Kiev, 1985, 247 p. (in Russian).
19. SSU 7664:2014. Coke. Method for determination of reactivity. (in Ukrainian).
20. ISO 1014:1985. Coke. Determination of true relative density, apparent relative density and porosity. https://www.iso.org/standard/5483.html
21. Zelenskii, O.I.; Gaidaenko, A.S.; Tkalich, G.M. Coking of batch with modifying additives at ChAO Zaporozhkoks. Coke and Chemistry, 2017, 60(5), pp. 189-192. DOI: https://doi.org/10.3103/S1068364X17050088
22. Price, J.T.; Gransden, J.F.; Khan, M.A.; Ryan, B.D. Effect of Selected Minerals on High Temperature Properties of Coke. 2-nd International Cokemaking Congress; The Institute of Materials: London, 1992, vol. 2, pp. 286-292.

CHEMISTRY JOURNAL OF MOLDOVA. General, Industrial and Ecological Chemistry. 2018, 13(2), 38-47
ISSN (p) 1857-1727 ISSN (e) 2345-1688
http://cjm.asm.md
http://dx.doi.org/10.19261/cjm.2018.368

NMR STUDIES OF SOME Zn AND Cd COORDINATION COMPOUNDS BEARING 1,2-CICLOHEXANEDIONEDIOXIME

Elena Gorincioi [a,b*], Eduard Coropceanu [a,b]

[a]*Institute of Chemistry, 3, Academiei str., Chisinau MD-2028, Republic of Moldova*
[b]*Tiraspol State University, 5, Iablocikin str., Chisinau MD-2069, Republic of Moldova*
[*]*e-mail: elena.gorincioi@gmail.com; phone: (+373 22) 73 96 11; fax: (+373 22) 72 54 91*

Abstract. A series of homobi- and polynuclear zinc and cadmium coordination compounds supported by 1,2-cyclohexanedionedioxime (nioxime, $NioxH_2$) and bridging bidentate ligands: 4,4'-bipyridyl (bpy), 1,2-bis(4-pyridyl) ethane (bpe), 1,3-bis(4-pyridyl) propane (bpp) and dipyridyl sulphide (dps) have been characterized by the experimental techniques of ^{1}H and ^{13}C NMR spectroscopy. Individual NMR data of the compounds are consistent with their assignment as complexes.

Keywords: NMR, zinc, cadmium, oxime, homodinuclear complex, coordination polymer.

Received: 30 May 2018/ Revised final: 20 June 2018/ Accepted: 20 June 2018

Introduction

Nowadays the state of the art in analytical technologies is frequently found in the bioanalytical area, NMR spectroscopy being amongst the fast, effective and information rich methods for solving a wide range of essential purposes for human health [1-5]. Nevertheless, it still remains one of the most important analytical tools available to the classical chemist. A unique and powerful methodology of NMR for the characterization of the self-assembled complexes and the investigation of their dynamic behaviour in solution has been reviewed in a comprehensive manner [6].

Metal-organic frameworks are one of the important domains of materials science due to their useful properties that are continuously explored in gas storage, chemical separation, catalysis and luminescence. Recently the fabrications of metal-organic frameworks have been reported, whose chemical composition and shape of building units can be multiply varied within a particular structure and may lead to materials that offer a synergistic combination of properties [7]. In the light of this, designing strategies for assembling from mono- to polynuclear compounds for capitalization of their application potential is one of the priority directions in coordination chemistry.

Zinc and cadmium coordination compounds with a varied molecular composition and architecture, possessing different convenient properties, have found diverse applications, primarily related to photochemistry and luminescence [8-11].

It should be mentioned that the literature data on zinc compounds containing oxime ligands are scarce and almost missing regarding the cadmium compounds [12-14]. Mononuclear zinc and cadmium complexes are known with neutral mono- and dioximes that have been synthesized and studied in the presence of organic and inorganic anions [15,16]. A homologous series of Zn bimetallic complexes bridged by neutral, radical anionic and dianionic 4,4'-bipyridine has been reported [17]. Bimetallic zinc complexes supported by salicilaldiminato and anilido-aldimine ligands were targeted [18], which can potentially mimic phosphomonoesterase activity in protic media [19].

In search for the methods of obtaining novel materials endowed with valuable properties, new synthetic approaches were recently developed that include tuning the dimensionality from the low nuclearity complexes decorated by oxime ligands to polynuclear compounds [20-24]. Our contribution to the Zn- and Cd/oxime chemistry has demonstrated the efficacy of the oxime/anion/bipyridyne "blend" approach that resulted in the mixed-ligand discrete complexes of different nuclearity. In these articles the synthesis, some mechanistic considerations were discussed, as well as various properties, such as: supramolecular isomerism, chirality, luminescence and adsorption capacity for

homobi- and polynuclear zinc and cadmium coordination compounds supported by $NioxH_2$ and bridging bidentate ligands: bpy, bpe, bpp and dps **1-14** (Table 1), their structures being confirmed by elemental analyses, IR-spectroscopy and X-ray analyses.

Table 1

Bibliographic data on complexes 1-14.

Complex		*Reference*
Dinuclear polymers		
$[Zn_2(CH_3COO)_4(NioxH_2)_2(H_2O)_2bpy]$	**1**	[20]
$[Cd_2(CH_3COO)_4(NioxH_2)_2(H_2O)_2bpy]$	**2**	[20]
$[Cd_2(HCOO)_4(NioxH_2)_2(H_2O)_2bpy]$	**3**	[20]
$[Cd_2(CH_3COO)_4(NioxH_2)_2(H_2O)_2bpe]$	**4**	[22]
Polymers containing SO_4^{2-} anion		
$\{[Zn(NioxH_2)(SO_4)bpy]\cdot 0.5H_2O\cdot DMF\}_n$	**5**	[21]
$\{[Cd(NioxH_2)(SO_4)bpy]_3(NioxH_2)(H_2O)_3\}_n$	**6**	[20]
$[Zn(NioxH_2)(SO_4)bpe]_n$	**7**	[21]
$[Cd(NioxH_2)(SO_4)bpe]_n$	**8**	[22]
Polymers without SO_4^{2-} anion		
$[Zn(CH_3COO)_2(NioxH_2)(H_2O)bpe]_n$	**9**	[22]
$\{[Cd(HCOO)_2(NioxH_2)bpe]\cdot DMF\}_n$	**10**	[24]
$[Cd(HCOO)_2(NioxH_2)bpp]_n$	**11**	[23]
$[Zn(CH_3COO)_2(NioxH_2)dps]_n$	**12**	[24]
$[Cd(CH_3COO)_2(NioxH_2)dps]_n$	**13**	[24]
$[Cd(HCOO)_2(NioxH_2)dps]_n$	**14**	[24]

The current report furnishes complementary data on the coordination compounds **1-14**. For the first time, the spectral ^1H and ^{13}C NMR individual characteristics for complexes **1-14** are presented. The diamagnetic nature of these coordination compounds allowed the assignment of all ^1H and ^{13}C signals in the respective spectra. The signals confirming ligand-metal coordination are put into discussion, in connection with the corresponding signals in free ligands.

Experimental

Complexes **1-14** were prepared according to the reported synthetic protocols (Table 1).

NMR spectroscopy

NMR spectra were recorded on a Bruker AVANCE 400 spectrometer equipped with a 5-mm broadband reverse probe with field *z* gradient, operating at 400.13 and 100.61 MHz for ^1H and ^{13}C nuclei, respectively. DMSO-d_6 (isotopic enrichment 99.95%) was used as solvent, containing tetramethylsilane (TMS) as an internal standard. Chemical shifts (δ) are reported in parts per million (ppm) and are referenced to the residual non-deuterated solvent peak (2.50 ppm for ^1H and 39.50 ppm for ^{13}C). The 1D and 2D NMR experiments were performed through standard pulse sequences.

DOSY NMR experiments. The spectra were recorded on a Bruker Avance 400 spectrometer, at 9.395 tesla, at the resonating frequency of 400.13 MHz for ^1H nuclei, using a BBI Bruker 5 mm gradient probe. The temperature was regulated at 298 K and no spinning was applied to the NMR tube. The diffusion NMR experiments were performed with a 2D sequence for diffusion measurement using double stimulated echo for convection compensation (dstebpgp3s), using bipolar gradients. The bipolar gradient duration and the diffusion time were in the range of 1 to 1.5 ms and 200 ms, respectively. The evolution of the pulsed-field gradient during the NMR diffusion experiments was established in 32 steps, applied linearly between 1 and 50 Gcm^{-1}. Data analysis was performed using Bruker TOPSPIN software.

Results and discussion

Figure 1 depicts the used atom numbering for description of the chemical shifts of the ^1H and ^{13}C nuclei, as follows: in dinuclear complexes **1-4** - as shown in structure **A**, in polymers **5-10** - as shown in structure **B**, in polymer **11** - as shown in structure **C**, and in polymers **12-14** - as shown in structure **D.**

NMR characteristics for complexes **1-14** have been obtained on the basis of their 1D (^1H, ^{13}C, DEPT-135,) and 2D homo- ($^1H/^1H$ COSY-45,) and heteronuclear ($^1H/^{13}C$ HSQC and $^1H/^{13}C$ HMBC) correlation spectra. For comparison, the chemical shifts of ^1H and ^{13}C NMR nuclei in ligands are presented (Table 2). All the ^1H and ^{13}C NMR signals are given for binuclear complexes **1-4** and the data for monomers of polymeric compounds **5-14** are presented, as well (Tables 3-5). The relative areas of signals are proportional to the number of hydrogen atoms in one structural unit of the compounds.

Nioxime moiety

The ^1H NMR spectra of the compounds under discussion **1-14** contain the characteristic signals of the coordinated $NioxH_2$, except for the polymer **11** (Table 5). The resonances of nioxime protons showed some variation with respect to the free ligand that was more noticeable for oxime protons. Thus, in the ^1H spectra of complexes **1-14** the methylene groups were identified by the multiplets centred in 1.53–1.72 and 2.47–2.70 ppm regions (Tables 2-5). The resonances of these methylene carbon atoms vary insignificantly for compounds **1-14**, being found in their ^{13}C NMR spectra at 21.3–22.1 and 24.6–25.1 ppm, respectively. These values practically remain in the range of the data characterizing the free $NioxH_2$ (Table 1).

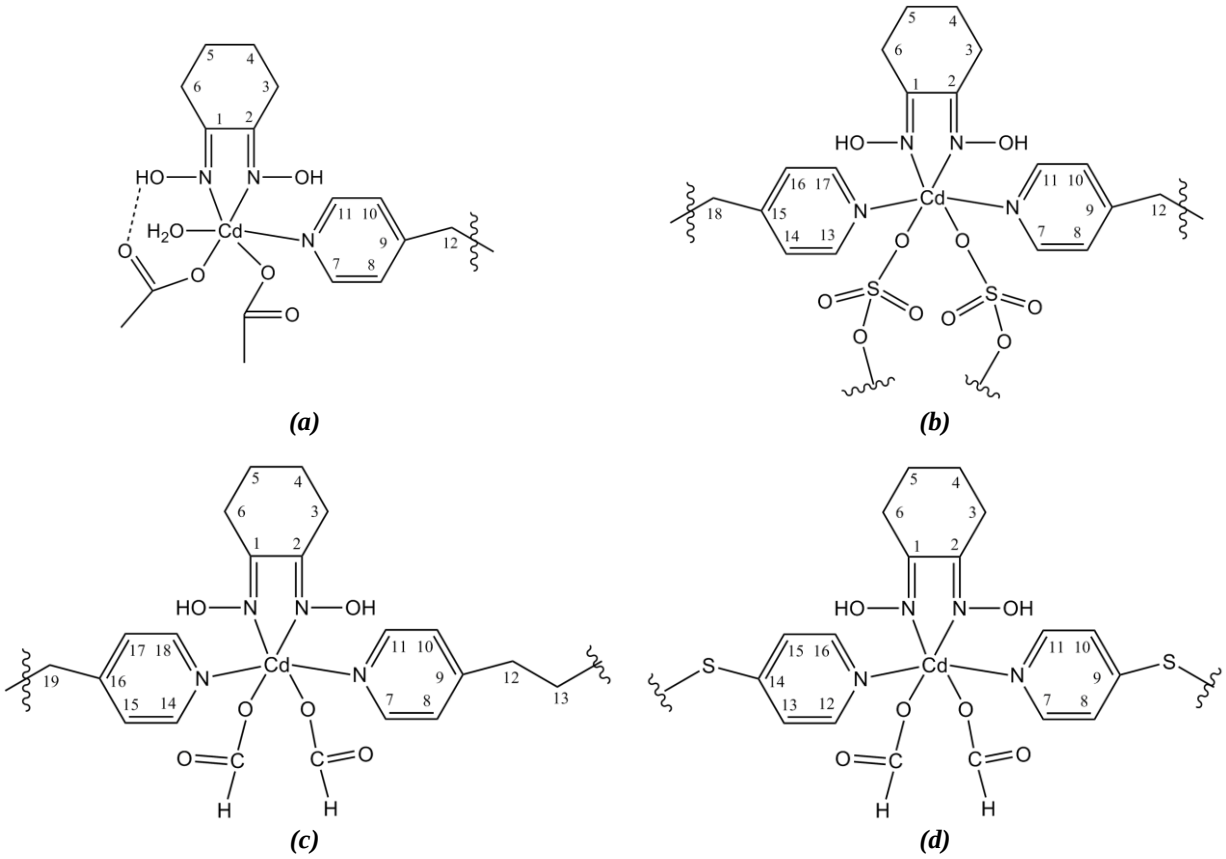

(a) ***(b)*** ***(c)*** ***(d)***

Figure 1. One unit in the structure of dimer 4 *(a)*, polymer 8 *(b)*, polymer 11 *(c)* and polymer 14 *(d)*.

Table 2

^{1}H and ^{13}C NMR spectral data for ligands (δ ppm; *J*, Hz) in DMSO-d_6 solutions.

NMR data[1] / *Ligand*[2]	*^{1}H NMR*	*^{13}C NMR*
$NioxH_2$	1.54 (m, 4H, $2CH_2$), 2.49 (m, 4H, $2CH_2$), 11.17 (br. s, 2H, $N\text{-}OH_{exchangeable}$)	22.0 C(4,5), 24.9 C(3,6), 152.2 C(1,2)
bpy[3]	7.82 (app.dd, 4H, *J*= 4.5, 1.6, C(3,5 and 3',5')H), 8.72 (app.dd, 4H, *J*= 4.5, 1.6, C(2,6 and 2',6')H)	121.8 C(3,5 and 3',5'), 144.8 C(4 and 4'), 151.0 C(2,6 and 2',6')
bpe	2.93 (s, 4H, ethylene bridge), 7.25 (app.dd, 4H, *J*= 4.4, 1.6, C(3,5 and 3',5')H), 8.43 (app.dd, 4H, *J*= 4.4, 1.6, C(2,6 and 2',6')H)	34.8 (ethylene), 124.5 C(3,5 and 3',5'), 149.8 C(2,6 and 2',6'), 150.3 C(4 and 4')
bpp	1.89 (q, 2H, *J*= 7.7, CH_2), 2.60 (t, 4H, *J*= 7.7, CH_2), 7.23 (app.dd, 4H, *J*= 4.6, 1.6, C(3,5 and 3',5')H), 8.44 (app.dd, 4H, *J*= 4.6, 1.6, C(2,6 and 2',6')H)	30.6, 34.2 (propane), 124.4 C(3,5 and 3',5'), 149.9 C(2,6 and 2',6'), 151.2 C(4 and 4')
dps	7.53 (app.dd, 4H, *J*= 4.6, 1.5, C(3,5 and 3',5')H), 8.50 (app.dd, 4H, *J*= 4.6, 1.5, C(2,6 and 2',6')H)	120.6 C(3,5 and 3',5'), 146.2 C(4 and 4'), 150.4 C(2,6 and 2',6')

[1] *s: singlet; br. s: broad singlet; app. dd: apparent doublet of doublets; m: multiplet; t: triplet; q: quartet.*
[2] *for $NioxH_2$ the atom numbering was used, as depicted in Figure 1.*
[3] *for bpy, bpe, bpp and dps the pyridine atom numbering was used.*

Signals of oxime protons in complexes **1-14** were a clear proof of the ligand/metal coordination. Thus, in $NioxH_2$ oxime protons resonate at 11.17 ppm as a broad singlet, whilst in complexes **1-14** the corresponding singlets are often shifted downfield, being found in the ^{1}H NMR spectra in the range of 11.20-13.37 ppm (Tables 2-5 and Figure 2). This confirms that coordination of the ligand to the metal occurs with the participation of oximic nitrogen atoms: coordination enhances the electron depletion of oxime proton, *i.e*. deshields its nucleus, moving the corresponding resonance to higher frequencies. At the same time, the characteristic shape of signal - broad singlet - attests the presence of intra- and intermolecular hydrogen atom bonds, as it was also documented by IR and X-ray analyses [20-24]. According to the

^{13}C NMR spectra, the peaks for the nuclei of azomethine carbon atoms in complexes **1-14** do not markedly differentiate from the corresponding chemical shifts in the free ligand, being found in the range of 150.4-152.5 ppm *versus* 152.2 ppm for $NioxH_2$ (Table 1 and Tables 2-5 for comparison).

Table 3

^{1}H and ^{13}C NMR spectral data for dinuclear polymers 1-4 (δ ppm; *J*, Hz)[1,2] in DMSO-d_6 solutions.

NMR data / *Complex*	*^{1}H NMR*	*^{13}C NMR*
1	1.55 (m, 8H, C(4,5 and 4',5')H_2), 1.84 (s, 12H, COCH_3), 2.52 (m, 8H, C(3,6 and 3',6')H_2), 7.86 (app.dd, 4H, *J*= 4.5, 1.7, C(8,10 and 8',10')H), 8.73 (app.dd, 4H, *J*= 4.5, 1.7, C(7,11 and 7',11')H), 11.62 (br. s, 4H, N-$OH_{exchangeable}$)	21.9 C(4,5 and 4',5'), 22.6 (COCH_3), 24.9 C(3,6 and 3',6'), 121.6 C(8,10 and 8',10'), 144.7 C(9 and 9'), 150.8 C(7,11 and 7',11'), 151.9 C(1,2 and 1',2'), 176.4 (COCH_3)
2	1.59 (m, 8H, C(4,5 and 4',5')H_2), 1.88 (s, 12H, COCH_3), 2.54 (m, 8H, C(3,6 and 3',6')H_2), 7.85 (app.dd, 4H, *J*= 4.5, 1.7, C(8,10 and 8',10')H), 8.72 (app.dd, 4H, *J*= 4.5, 1.7, C(7,11 and 7',11')H), 13.60 (br. s, 4H, N-$OH_{exchangeable}$)	21.4 C(4,5 and 4',5'), 23.5 (COCH_3), 24.8 C(3,6 and 3',6'),121.7 C(8,10 and 8',10'), 144.8 C(9 and 9'), 150.5 C(1,2 and 1',2'), 150.8 C(7,11 and 7',11'), 177.6 (COCH_3)
3	1.59 (m, 8H, C(4,5 and 4',5')H_2), 2.55 (m, 8H, C(3,6 and 3',6')H_2), 7.84 (app.dd, 4H, *J*= 4.4, 1.6, C(8,10 and 8',10')H), 8.30 (s, 4H, OCOH), 8.72 (app.dd, 4H, *J*= 4.4, 1.6, C(7,11 and 7',11')H), 13.11 (br. s, 4H, N-$OH_{exchangeable}$)	21.3 C(4,5 and 4',5'), 24.6 C(3,6 and 3',6'),121.5 C(8,10 and 8',10'), 144.6 C(9 and 9'), 150.7 C(7,11 and 7',11'), 150.8 C(1,2 and 1',2'), 167.9 (OCOH)
4	1.59 (m, 8H, C(4,5 and 4',5')H_2), 1.85 (s, 12H, COCH_3), 2.53 (m, 8H, C(3,6 and 3',6')H_2), 2.95 (s, 4H, C(12 and 12')H_2), 7.27 (app.dd, 4H, *J*= 4.4, 1.6, C(8,10 and 8',10')H), 8.44 (app.dd, 4H, *J*= 4.4, 1.6, C(7,11 and 7',11')H), 12.92 (br. s, 4H, N-$OH_{exchangeable}$)	21.6 C(4,5 and 4',5'), 22.8 (COCH_3), 24.8 C(3,6 and 3',6'), 34.8 (C(12 and 12'), 124.4 C(8,10 and 8',10'), 149.8 C(7,11 and 7',11'), 150.2 C(9 and 9'), 150.9 C(1,2 and 1',2'), 177.5 (COCH_3)

[1] s: singlet, br. s: broad singlet; app. dd: apparent doublet of doublets, m: multiplet.

*[2] here the number of protons is presented for both units of binuclear complexes **1-4**. Integration of the signals in ^{1}H NMR spectra offers information regarding one structure unit, the binuclearity of complexes being proved by X-ray data, as stated before [20,22]. For numbering the atoms of the second structural unit, the prime symbol was used.*

Table 4

^{1}H and ^{13}C NMR spectral data for polymers containing SO_4^{2-} anion 5-8 (δ ppm; *J*, Hz)[1] in DMSO-d_6 solutions.

NMR data / *Complex*	*^{1}H NMR*	*^{13}C NMR*
5	1.56 (m, 4H, C(4,5)H_2), 2.51 (m, 4H, C(3,6)H_2), 2.73 (s, 3H, DMF), 2.89 (s, 3H, DMF), 7.86 (app.dd, 4H, *J*= 4.5, 1.5, C(8,10 and 14,16)H), 7.95 (s, 1H, DMF), 8.74 (app.dd, 4H, *J*= 4.5, 1.5, C(7,11 and 13,17)H), 11.50 (br. s, 2H, N-$OH_{exchangeable}$)	21.9 C(4,5), 24.9 C(3,6), 30.7 and 35.7 (DMF), 121.5 C(8,10 and 14,16), 144.6 C(9 and 15), 150.7 C(7,11 and 13,17), 152.1 C(1,2), 162.7 (DMF)
6[2]	1.54 (m, 4H, C(4,5)H_2), 2.51 (m, 4H, C(3,6)H_2), 7.83 (app.dd, 4H, *J*= 4.4, 1.6, C(8,10 and 14,16)H), 8.73 (app.dd, 4H, *J*= 4.4, 1.6, C(7,11 and 13,17)H), 11.16 (br. s, 2H, N-$OH_{exchangeable}$)	22.1 C(4,5), 24.9 C(3,6), 121.5 C(8,10 and 14,16), 144.6 C(9 and 15), 150.7 C(7,11 and 13,17), 152.3 C(1,2)
7	1.56 (m, 4H, C(4,5)H_2), 2.48 (m, 4H, C(3,6)H_2), 2.95 (s, 4H, C(12 and 18)H_2), 7.26 (app.dd, 4H, *J*= 4.4, 1.4, C(8,10 and 14,16)H), 8.44 (app.dd, 4H, *J*= 4.4, 1.4, C(7,11 and 13,17)H), 11.25 (br. s, 2H, N-$OH_{exchangeable}$)	22.0 C(4,5), 24.9 C(3,6), 34.7 (C(12 and 18), 124.3 C(8,10 and 14,16), 149.6 C(7,11 and 13,17),150.2 C(9 and 15), 152.2 C(1,2)
8	1.56 (m, 4H, C(4,5)H_2), 2.49 (m, 4H, C(3,6)H_2), 2.95 (s, 4H, C(12 and 18)H_2), 7.26 (app.dd, 4H, *J*= 4.5, 1.5, C(8,10 and 14,16)H), 8.44 (app.dd, 4H, *J*= 4.5, 1.5, C(7,11 and 13,17)H), 11.27 (br. s, 2H, N-$OH_{exchangeable}$)	21.7 C(4,5), 24.6 C(3,6), 34.5 (C(12 and 18), 123.9 C(8,10 and 14,16), 149.2 C(7,11 and 13,17),149.5 C(9 and 15), 152.5 C(1,2)

[1] s: singlet, br. s: broad singlet; app. dd: apparent doublet of doublets, m: multiplet.

[2] only protons of the coordination sphere are described.

Table 5

^{1}H and ^{13}C NMR spectral data for polymers 9-14 (δ ppm; *J*, Hz)[1] in DMSO-d_6 solutions.

NMR data / *Complex*	*^{1}H NMR*	*^{13}C NMR*
9	1.56 (m, 4H, C(4,5)H_2), 1.84 (s, 6H, CO*C*H_3), 2.52 (m, 4H, C(3,6)H_2), 2.97 (s, 4H, C(12 and 18)H_2), 7.31 (app.dd, 4H, *J*= 4.4, 1.5, C(8,10 and 14,16)H), 8.45 (app.dd, 4H, *J*= 4.4, 1.5, C(7,11 and 13,17)H), 11.74 (br. s, 2H, N-OH$_{exchangeable}$)	21.8 C(4,5), 22.6 (CO*C*H_3), 24.8 C(3,6), 34.7 (C(12 and 18), 124.4 C(8,10 and 14,16), 149.6 C(7,11 and 13,17),150.6 C(9 and 15), 151.8 C(1,2), 176.7 (*C*OCH_3)
10	1.60 (m, 4H, C(4,5)H_2), 2.55 (m, 4H, C(3,6)H_2), 2.73 (s, 3H, DMF), 2.89 (s, 3H, DMF), 2.95 (s, 4H, C(12 and 18)H_2), 7.29 (app.dd, 4H, *J*= 4.5, 1.6, C(8,10 and 14,16)H), 8.32 (s, 2H, OCO*H*), 7.95 (s, 1H, DMF), 8.43 (app.dd, 4H, *J*= 4.5, 1.6, C(7,11 and 13,17)H), 13.20 (br. s, 2H, N-OH$_{exchangeable}$)	21.4 C(4,5), 24.9 C(3,6), 30.7 (DMF), 34.9 (C(12 and 18), 35.7 (DMF), 124.6 C(8,10 and 14,16), 149.8 C(7,11 and 13,17),150.7 C(9 and 15), 150.9 C(1,2), 162.7 (DMF), 168.2 (O*C*OH)
11[2]	1.72 (m, 4H, C(4,5)H_2), 2.03 (m, 2H, C(13)H_2), 2.70 (m, 4H, C(3,6)H_2), 2.74 (t, 4H, *J*=7.5, C(12,19)H_2), 7.34 (app.dd, 4H, *J*= 4.1, 1.5, C(8,10 and 15,17)H), 8.42 (app.dd, 4H, *J*= 4.1, 1.5, C(7,11 and 14,18)H), 8.48 (s, 2H, OCO*H*)	21.0 C(4,5), 24.3 C(3,6), 30.3 (C(13), 34.1 (C(12 and 19), 124.4 C(8,10 and 15,17), 148.5 C(7,11 and 14,18), 151.9 C(1,2), 152.9 C(9 and 16), 168.8 (O*C*OH)
12[3]	1.56 (m, 4H, C(4,5)H_2), 1.84 (s, 6H, CO*C*H_3), 2.51 (m, 4H, C(3,6)H_2), 7.41 (app.dd, 4H, *J*= 4.5, 1.5, C(8,10 and 13,15)H), 8.56 (app.dd, 4H, *J*= 4.5, 1.5, C(7,11 and 12,16)H), 11.61 (br. s, 2H, N-OH$_{exchangeable}$)	21.9 C(4,5), 22.7 (CO*C*H_3), 24.9 C(3,6), 125.0 C(8,10 and 13,15), 143.5 C(9 and 14), 150.7 C(7,11 and 12,16), 151.9 C(1,2), 177.5 (*C*OCH_3)
13	1.58 (m, 4H, C(4,5)H_2), 1.85 (s, 6H, CO*C*H_3), 2.52 (m, 4H, C(3,6)H_2), 7.40 (app.dd, 4H, *J*= 4.4, 1.6, C(8,10 and 13,15)H), 8.54 (app.dd, 4H, *J*= 4.4, 1.6, C(7,11 and 12,16)H), 13.37 (br. s, 2H, N-OH$_{exchangeable}$)	21.2 C(4,5), 23.2 (CO*C*H_3), 24.5 C(3,6), 124.8 C(8,10 and 13,15), 143.3 C(9 and 14), 150.4 C(1,2), 150.5 C(7,11 and 12,16), 177.3 (*C*OCH_3)
14	1.60 (m, 4H, C(4,5)H_2), 2.55 (m, 4H, C(3,6)H_2), 7.40 (app.dd, 4H, *J*= 4.5, 1.7, C(8,10 and 13,15)H), 8.30 (s, 2H, OCO*H*), 8.56 (app.dd, 4H, *J*= 4.5, 1.7, C(7,11 and 12,16)H), 13.02 (br. s, 2H, N-OH$_{exchangeable}$)	21.4 C(4,5), 24.8 C(3,6), 125.0 C(8,10 and 13,15), 143.4 C(9 and 14), 150.7 C(7,11 and 12,16), 151.1 C(1,2), 168.0 (O*C*OH)

[1] *s: singlet, br. s: broad singlet; app. dd: apparent doublet of doublets, m: multiplet.*
[2] *for polymer **11** NOH proton has not been detected.*
[3] *C(1,2) signals found by ^{1}H/^{13}C HMBC correlation.*

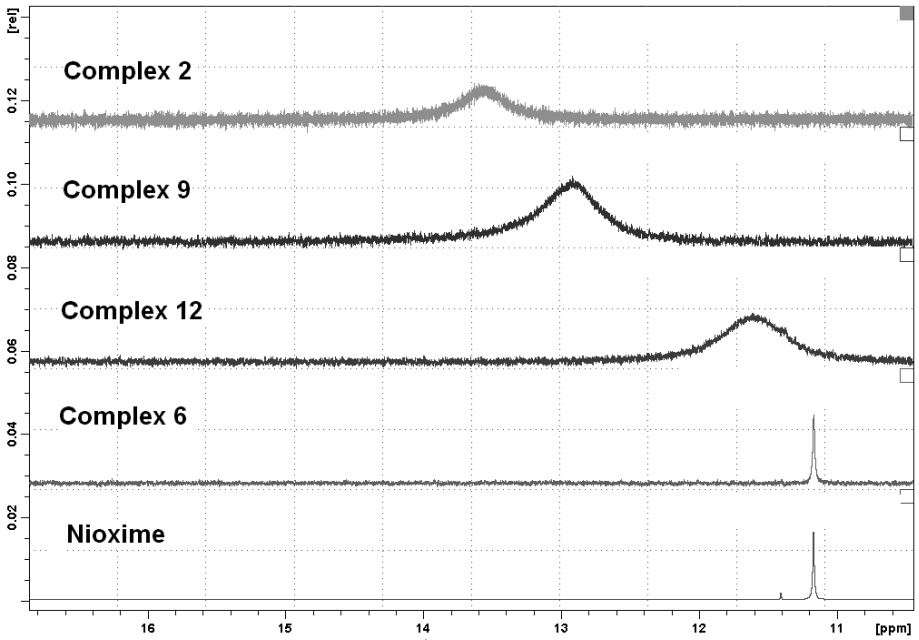

Figure 2. Selected signals for oxime protons in the ^{1}H NMR spectra of NioxH_2 and complexes 2, 6, 9 and 12.

Pyridyl fragment

In the ^{1}H NMR spectra of compounds **1-14** the AA'XX' pattern identifying the pyridyl ring is present. Thus, the bpy moiety in the molecules of compounds **1-3, 5** and **6** is attested by the AA'XX' system in the corresponding ^{1}H spectra that appeared as two apparent doublets of doublets in aromatic region with *J*= 4.5 and 1.7 Hz, due to the presence of *ortho*- (δ_H ~ 8.70 ppm (two AA'- parts of AA'XX' system, 4H)) and *meta*-bpy protons (δ_H ~ 7.80 ppm (two XX'- parts of AA'XX' system, 4H)). Comparison of the AA'XX' patterns in the ^{1}H spectra of complexes **1-3, 5** and **6** with the one of bpy, revealed their similarity, both as the value of chemical shift and shape of the signal (Figure 3, Tables 2-4).

Likewise, analysis of AA'XX' systems in the aromatic region of the ^{1}H NMR spectra of complexes **4, 7-9** and **10,** containing bpe as bridging ligand, showed almost a complete similarity to the corresponding region in the ^{1}H NMR spectrum of free bpe, both by the shape of the signal and its position in the ^{1}H spectrum (Tables 2-5, Figure 3). In complexes **4, 7-9** and **10,** the singlets characteristic for ethylene protons remain almost unshifted with respect to free bpe, as well (Tables 2-5).

Some comments can be made here, regarding the NMR particularities of the involved in this study bpe ligand, which is closely related to bpy. One can suppose that insertion of the ethylene moiety between pyridyl rings diminishes the diamagnetic ring current; that is why the chemical shifts of the aromatic protons in bpe are slightly upfield in comparison with bpy. *Meta*-pyridyl protons are more affected by the proximity of the ethylene fragment, their chemical shift being moved by 0.57 ppm to the region of low resonances, when compared to bpy ligand (for *ortho*- protons the upfield shift constitutes 0.29 ppm) (Table 2 and Figure 3).

^{13}C NMR spectra of compounds **1-10** showed the distinct resonances consistent with the proposed structures. According to the ^{13}C NMR spectra of complexes **1-10**, metal/bpy complexation has no distinguishable impact upon the resonance frequency of the pyridyl carbon atoms (Tables 2-4, Figures 4 and 6).

In the case of polymer **11** bpp serves as bridging ligand; the AA'XX' pattern in its ^{1}H spectrum is again rather close to that of free ligand (Tables 2, 5 and Figure 5). As observed for the bpe-containing polymeric complexes **4, 7-9** and **10**, complexation to the metal has no major impact upon the resonance frequency of the protons from neighbouring pyridyl rings. It should be mentioned, that protons of pyridyl rings in free bpp resonate at lower frequencies too, in comparison with bpy ligand (δ_H 8.44 and 7.23 ppm in bpp *versus* δ_H 8.72 and 7.82 ppm in bpy), thus demonstrating that the propane moiety also decreases the diamagnetic ring current, as it was afore-discussed for the homologous bpe ligand (Table 2). Signals of propane protons are slightly downfield in the ^{1}H spectrum of polymer **11** (δ_H 2.03 and 2.74 ppm), with respect to the signals identifying the free bpp (δ_H 1.89 and 2.60 ppm) (Tables 2 and 5).

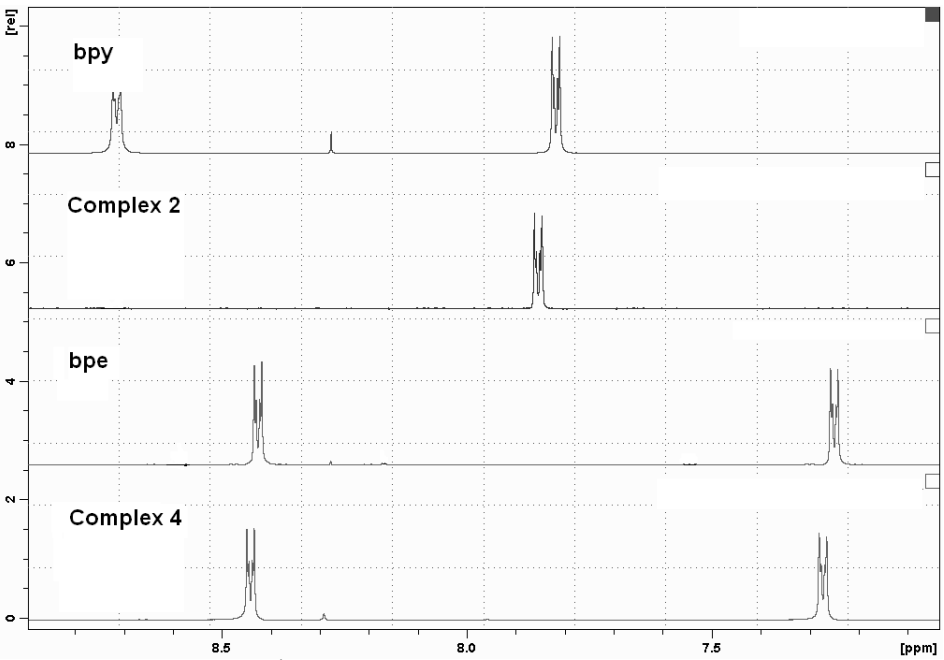

Figure 3. Aromatic region in the ^{1}H NMR spectra of complexes 2 and 4 *versus* ligands: bpy and bpe.

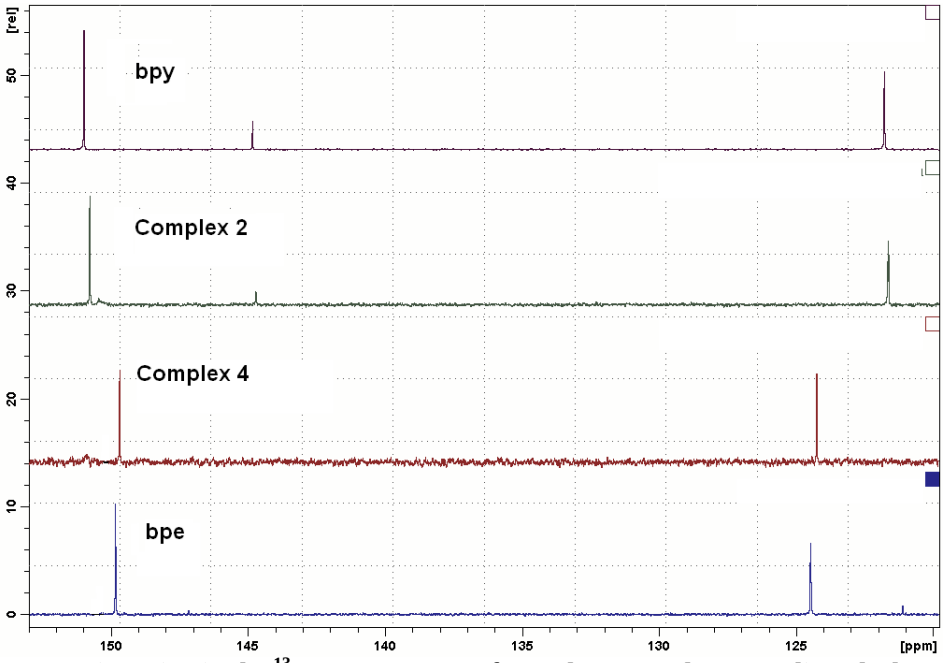

Figure 4. Aromatic region in the ^{13}C NMR spectra of complexes 2 and 4 *versus* ligands: bpy and bpe.

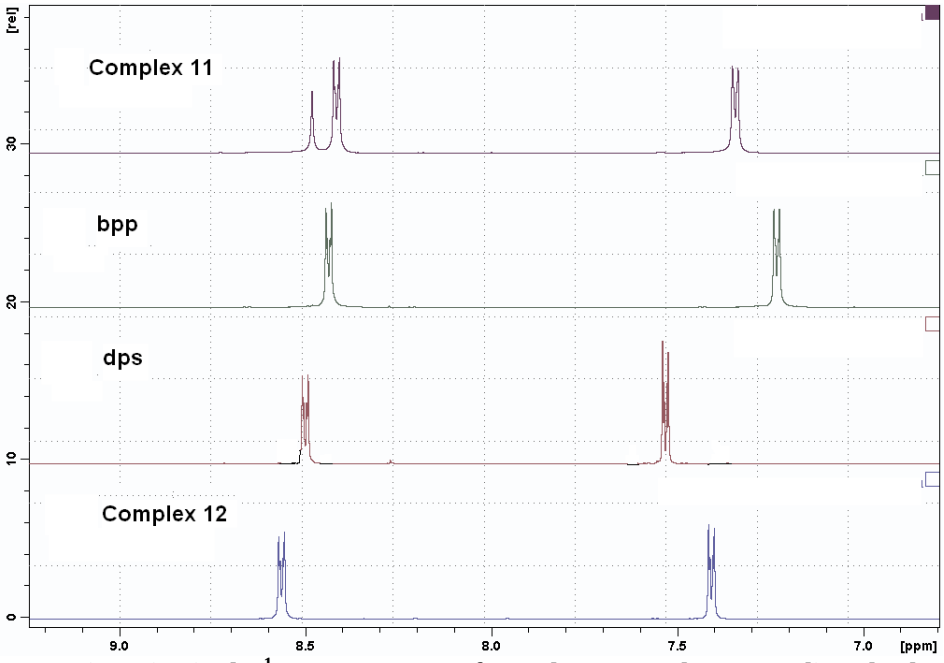

Figure 5. Aromatic region in the ^{1}H NMR spectra of complexes 12 and 11 *versus* ligands: dps and bpp.

In the ^{1}H spectrum of polymer **11** the shape of signal for magnetically equivalent protons at C(12) and C(19) remains unmodified (t, *J*= 7.5 Hz), in comparison with the corresponding signal in free bpp (t, *J*= 7.7 Hz), while the characteristic quartet for two propane protons at δ_H 1.89 ppm with the coupling constant of 7.7. Hz in bpp becomes a multiplet centred at δ_H 2.03 ppm in complex **11**. Signals of *ortho*-carbon atoms in pyridyl fragment of complex **11** are shifted upfield by 1.4 ppm, while the carbon atoms adjacent to the propane moiety resonate at a higher frequency (the downfield shift of 1.7 ppm), with respect to the corresponding signals in ^{13}C spectrum of bpp (Tables 2 and 5 and Figure 6).

Finally, we present the peculiarities observed by us of dps and dps-containing polymers **12-14.** In the AA'XX' systems from the ^{1}H NMR spectra of complexes **12-14**, a small upfield shift has been noted for the close to sulphur heteroatom *meta*-protons of pyridyl rings (by ~ 0.13 ppm), in comparison with the ^{1}H NMR data of free dps (Tables 2 and 5, Figure 5).

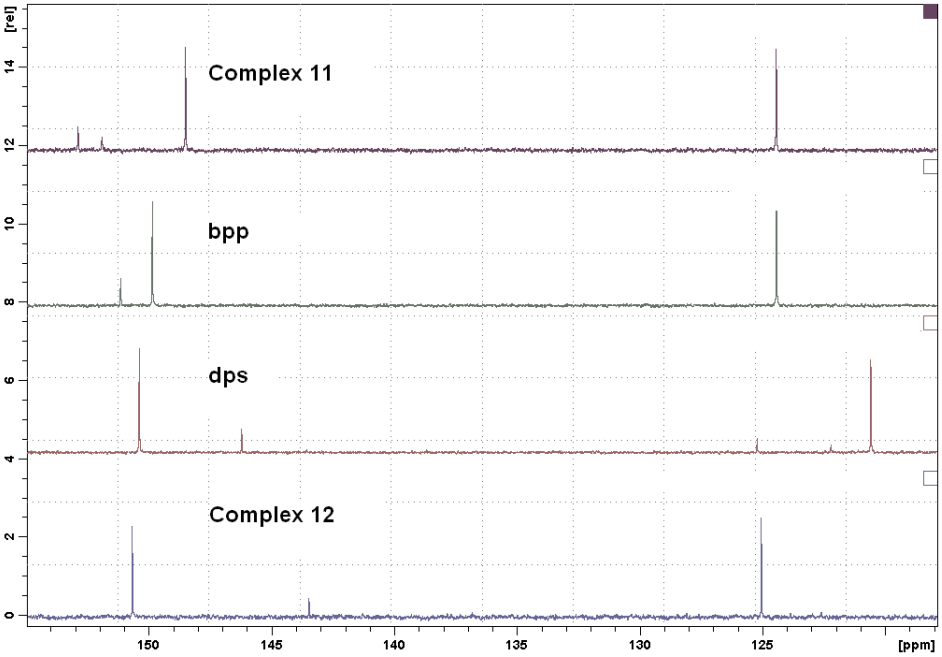

Figure 6. Aromatic region in the ^{13}C NMR spectra of complexes 12 and 11 *versus* ligands: dps and bpp.

Interestingly and differently from the bpy-, bpe- and bpp- containing complexes, the resonances of these *meta*- carbons in pyridyl moieties of polymers **12-14** were found downfield by ~4.4 ppm in the ^{13}C NMR spectra, in comparison with free dps (*e.g.*, δ_C 125.0 ppm for complex **12** *versus* δ_C 120.6 ppm for dps). Vicinal to sulphur atom pyridyl quaternary carbons, on the contrary, have shown an upfield shift (*e.g.*, δ_C 143.5 ppm for complex **12** *versus* 146.2 ppm for free dps), whilst the resonance frequency for *ortho*- pyridyl carbons does not significantly change (150.7 ppm *versus* 150.4 ppm (Tables 2 and 5, Figure 6). In our opinion, the noted specific features in the ^{13}C NMR data of complexes **12-14** can be explained by the concerted expression of the effects from the conjugation of p lone electron pairs of sulphur with neighbouring π-electron systems, and chelation. According to the classics in electrophilic aromatic substitution, in dps the electronegative sulphur atom with its two lone pairs of electrons represent a resonance donating agent that augment the electron density in the ring through resonance at C(3,5 and 3',5'; δ_C 120.6 ppm). However, in the molecules of complexes **12-14**, most probably due to the metal-dps coordination, the electron density in the aromatic rings is redistributed, the nuclei of carbons under discussion becoming deshielded (in complexes **12-14** these are nuclei of atoms C(8,10 and 13,15)), that causes the downfield shift of these nuclei (δ_C 125.0 ppm), as afore-described. Likewise, the induced by chelation electron density fluctuation can determine the shielding of C(9 and 14) nuclei in polymers **12-14**, when compared to the respective C(4 and 4') atoms in dps.

Additional room-temperature (298 K) diffusion experiments on compound $[Zn(CH_3COO)_2(NioxH_2)dps]_n$ **12**, as well as $NioxH_2$ and dps, were also conducted to establish the structure of **12** in solution (Figure 7). The translational diffusion coefficient value (D), which is a function of the molecular size and shape [25], was determined for complex **12** showing a magnitude of 2.238×10^{-10} m^2/s. To calculate D, the Stokes-Einstein equation has been used [25]. The observed D value is significantly different to those obtained for the solutions of dps and $NioxH_2$ of the same molarities (3.09×10^{-10} m^2/s and 1.778×10^{-10} m^2/s, respectively). Thus, no dissociation of complex **12** was found in DMSO-d_6 solution. For solvent species present in solution, the following D values were calculated: 6.025×10^{-10} m^2/s (DMSO) and 7.762×10^{-10} m^2/s (H_2O).

The presence of acetate/formate ligands in the molecules of complexes **1-4** and **9-14** was duly attested by the corresponding signals in the ^{1}H and ^{13}C NMR spectra of compounds (Tables 3 and 5). Inclusion of the DMF molecules in the polymer matrixes of compounds **5** and **10** was ascertained by the characteristic chemical shifts for ^{1}H and ^{13}C nuclei of DMF that were present in the spectra of these compounds. The presence of crystallisation water in the studied complexes could not be ascertained by ^{1}H NMR due to signal overlapping with the dissolved in DMSO-d_6 water.

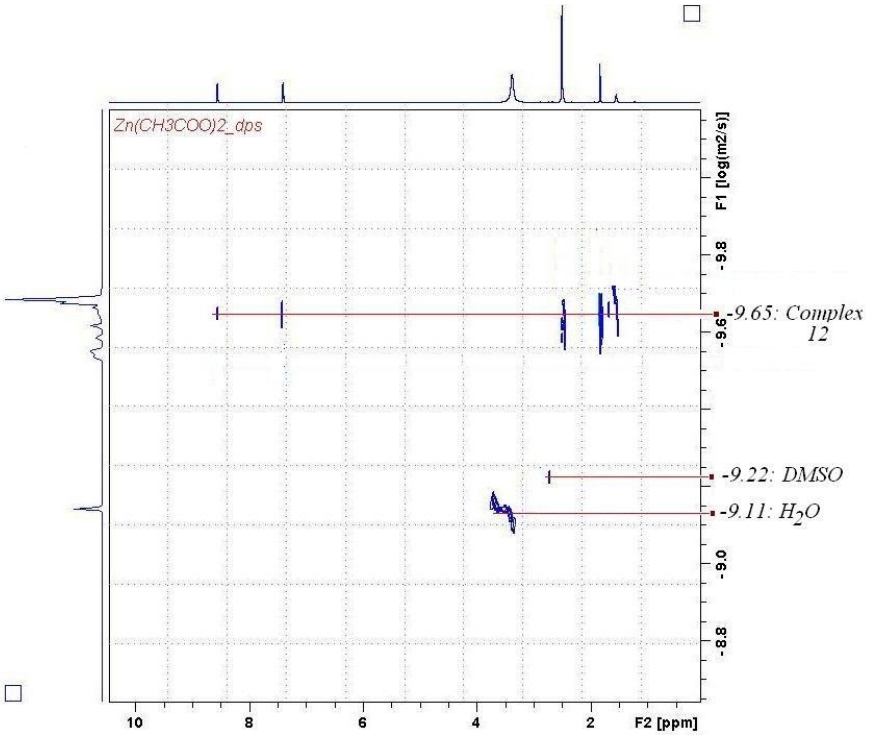

Figure 7. DOSY spectrum of complex 12.

Conclusions

Homodinuclear Zn and Cd complexes **1-4,** as well as coordination polymers **5-14** supported by 1,2-cyclohexanedionedioxime and bridging bidentate ligands: 4,4'-bipyridyl, 1,2-bis(4-pyridyl) ethane, 1,3-bis(4-pyridyl) propane and dipyridyl sulphide have been characterized by using the 1D (^{1}H, ^{13}C, DEPT-135') and 2D homo- (^{1}H/^{1}H COSY-45') and heteronuclear (^{1}H/^{13}C HSQC and ^{1}H/^{13}C HMBC) NMR experiments in DMSO-d_6 solutions. For the first time the spectral ^{1}H and ^{13}C NMR individual characteristics for complexes **1-14** are presented. The broad singlets identifying oxime protons were found to be particularly relevant for confirmation of the nioxime-metal coordination, also confirming the presence of intra- and intermolecular hydrogen atom bonds in the molecules under investigation. The resonance frequencies of the protons from the pyridyl fragments do not undergo significant changes after chelation. In the ^{13}C spectra of complexes **12-14** containing dipyridyl sulphide, noticeable change in the chemical shift for the *para*- (vicinal to sulphur) and *meta*- pyridyl carbon atoms, with respect to the free ligand, can serve as a proof of dps-metal coordination.

References

1. Berkowitz, S.A.; Engen, J.R.; Mazzeo, J.R.; Jones, G.B. Analytical tools for characterizing biopharmaceuticals and the implications for biosimilars. Nature Reviews Drug Discovery, 2012, 11(7), pp. 527-540. DOI: https://doi.org/10.1038/nrd3746
2. García-Álvarez, L.; Busto, J.H.; Avenoza, A.; Sáenz, Y.; Peregrina, J.M.; Oteo, J.A. Proton nuclear magnetic resonance spectroscopy as a technique for gentamicin drug susceptibility studies with *Escherichia coli* ATCC 25922. Journal of Clinical Microbiology, 2015, 53(8), pp. 2433-2438. DOI: 10.1128/JCM.00604-15
3. Prade, E.; Bittner, H.J.; Sarkar R.; Lopez Del Amo, J.M.; Althoff-Ospelt, G.; Multhaup, G.; Hildebrand, P.W.; Reif, B. Structural mechanism of the interaction of Alzheimer's disease Aβ fibrils with the NSAID sulindac sulfide. Journal of Biological Chemistry, 2015, 290(48), pp. 28737-28745. DOI: 10.1074/jbc.M115.675215
4. Popescu, R.; Costinel, D.; Dinca, O.R.; Marinescu, A.; Stefanescu, L.; Ionete, R.E. Discrimination of vegetable oils using NMR spectroscopy and chemometrics. Food Control, 2015, 48, pp. 84-90. DOI: https://doi.org/10.1016/j.foodcont.2014.04.046
5. Geana, E.I.; Popescu, R.; Costinel, D.; Dinca, O.R.; Ionete, R.E, Stefanescu, I.; Artem, V.; Bala, C. Classification of red wines using suitable markers coupled with multivariate statistic analysis. Food Chemistry, 2016, 192, pp. 1015-1024. DOI: http://doi.org/10.1016/j.foodchem.2015.07.112
6. Pastor, A.; Martınez-Viviente, E. NMR spectroscopy in coordination supramolecular chemistry: A unique and powerful methodology. Coordination Chemistry Reviews, 2008, 252(21-22), pp. 2314-2345. DOI: https://doi.org/10.1016/j.ccr.2008.01.025
7. Furukawa, H.; Cordova, K.E.; O'Keeffe, M.; Yaghi, O.M. The chemistry and applications of

metal–organic frameworks. Science, 2013, 341(6149), 1230444, pp. 974-986. DOI: https://doi.org/10.1126/science.1230444
8. Zheng, S.L.; Chen, X.M. Recent advances in luminescent monomeric, multinuclear, and polymeric Zn(II) and Cd(II) coordination complexes. Australian Journal of Chemistry, 2004, 57(8), pp. 703-712. DOI: https://doi.org/10.1071/CH04008
9. Wang, D.; Zhang, L.; Li, G.; Huo, Q.; Liu, Y. Luminescent MOF material based on cadmium(II) and mixed ligands: Application for sensing volatile organic solvent molecules. RSC Advances, 2015, 5(23), pp. 18087-18091. DOI: 10.1039/C4RA16599C
10. Barsukova, M.; Goncharova, T.; Samsonenko, D.; Dybtsev, D.; Potapov, A. Synthesis, crystal structure, and luminescent properties of new zinc(II) and cadmium(II) metal-organic frameworks based on flexible bis(imidazol-1-yl)alkane ligands. Crystals, 2016, 6(10), pp. 132. DOI: https://doi.org/10.3390/cryst6100132
11. Farnum, G.A.; Lucas, J.S.; Wang, C.Y.; LaDuca, R.L. Luminescent cadmium and zinc diphenate coordination polymers containing pyridyl-piperazine type ligands: Grids, diamondoid lattices, and a rare 4-connected net. Inorganica Chimica Acta, 2011, 368(1), pp. 84-95. DOI: https://doi.org/10.1016/j.ica.2010.12.053
12. Milios, C.; Stamatatos, T.; Perlepes, S. The coordination chemistry of pyridyl oximes. Polyhedron, 2006, 25(1), pp. 134-194. DOI: https://doi.org/10.1016/j.poly.2005.07.022
13. Chaudhuri, P. Homo- and hetero-polymetallic exchange coupled metal-oximates. Coordination Chemistry Reviews, 2003, 243(1-2), pp. 143-190. DOI: https://doi.org/10.1016/S0010-8545(03)00081-X
14. Canpolat, E.; Kaya, M. The synthesis, characterization, and spectral studies of Co(II), Ni(II), Cu(II), Zn(II) and Cd(II) complexes with N,N-bis(2-{[(2-methyl-2-phenyl-1,3-dioxolan-4-yl)methyl]amino}butyl N′,N′-dihydroxyethanediimidamide. Journal of Coordination Chemistry, 2005, 58(10), pp. 875-882. DOI: https://doi.org/10.1080/00958970500048802
15. Papatriantafyllopoulou, C.; Kostakis, G.E.; Raptopoulou, C.P.; Terzis, A.; Perlepes, S.P.; Plakatouras, J.C. Investigation of the $MSO_4 \cdot xH_2O$ (M= Zn, x= 7; M= Cd, x= 8/3)/methyl 2-pyridyl ketone oxime reaction system: A novel Cd(II) coordination polymer versus mononuclear and dinuclear Zn(II) complexes. Inorganica Chimica Acta, 2009, 362(7), pp. 2361-2370. DOI: https://doi.org/10.1016/j.ica.2008.10.033
16. Konidaris, K.F.; Polyzou, C.D.; Kostakis, G.E.; Tasiopoulos, A.J.; Roubeau, O.; Teat, S.J.; Manessi-Zoupa, E.; Powell, A.K.; Perlepes, S.P. Metal ion-assisted transformations of 2-pyridinealdoxime and hexafluorophosphate. Dalton Transactions, 2012, 41(10), pp. 2862-2865. DOI: 10.1039/C1DT11881A
17. Irwin, M.; Kramer, T.; McGrady, J.E.; Goicoechea, J.M. On the structural and electronic properties of $[Zn_2(4,4'\text{-bipyridine})(mes)_4]n^-$ (n= 0-2), a homologous series of bimetallic complexes bridged by neutral, anionic, and dianionic 4,4'-bipyridine. Inorganic Chemistry, 2011, 50(11), pp. 5006-5014. DOI: 10.1021/ic200241d
18. Doyle, D.J.; Gibson, V.C.; White, A.J.P. Synthesis and structures of bimetallic and polymeric zinc coordination compounds supported by salicylaldiminato and anilido–aldimine ligands. Dalton Transactions, 2007, 0(3) pp. 358-363. DOI: 10.1039/B615080B
19. Parkin, G. Synthetic Analogues Relevant to the Structure and Function of Zinc Enzymes. Chemical Reviews, 2004, 104(2), pp. 699-768. DOI: 10.1021/cr0206263
20. Croitor, L.; Coropceanu, E.; Jeanneau, E.; Dementiev, I.; Goglidze, T.; Chumakov, Iu.; Fonari, M. Anion-induced generation of binuclear and polymeric Cd(II) and Zn(II) coordination compounds with 4,4′-bipyridine and dioxime ligands. Crystal Growth & Design, 2009, 9(12), pp. 5233-5243. DOI: 10.1021/cg900746w
21. Croitor, L.; Coropceanu, E.; Siminel, A.; Kravtsov, V.; Fonari, M. Polymeric Zn(II) and Cd(II) sulfates with bipyridine and dioxime ligands: supramolecular isomerism, chirality, and luminescence. Crystal Growth & Design, 2011, 11(8), pp. 3536-3544. DOI: 10.1021/cg200465f
22. Croitor, L.; Coropceanu, E.; Siminel, A.; Botoshansky, M.; Fonari, M. Synthesis, structures, and luminescence properties of mixed ligand Cd(II) and Zn(II) coordination compounds mediated by 1,2-bis(4-pyridyl)ethane. Inorganica Chimica Acta, 2011, 370(1), pp. 411-419. DOI: https://doi.org/10.1016/j.ica.2011.02.014
23. Coropceanu, E.; Croitor, L.; Siminel, A.; Chumakov, Iu.; Fonari, M. The luminescence attenuation in the solid state by fluoride anion entrapped in the one-dimensional Zn(II) dioximate and mononuclear Cd(II) dioxime compounds. Polyhedron, 2016, 109, pp. 107-114. DOI: http://doi.org/10.1016/j.poly.2016.01.043
24. Croitor, L.; Coropceanu, E.; Siminel, A.; Kulikova, O.; Zelentsov, V.; Datsko, T.; Fonari, M. 1,2-Cyclohexanedionedioxime as a useful co-ligand for fabrication of one-dimensional Zn(II) and Cd(II) coordination polymers with wheel-and-axle topology and luminescent properties. CrystEngComm, 2012, 14(10), pp. 3750-3758. DOI: 10.1039/C2CE00020B
25. Waldeck, A.R.; Kuchel, P.W.; Lennon, A.J.; Chapman, B.E. NMR diffusion measurements to characterise membrane transport and solute binding. Progress in Nuclear Magnetic Resonance Spectroscopy, 1997, 30(1-2), pp. 39-68. DOI: https://doi.org/10.1016/S0079-6565(96)01034-5

CHEMISTRY JOURNAL OF MOLDOVA. General, Industrial and Ecological Chemistry. 2018, 13(2), 48-55
ISSN (p) 1857-1727 ISSN (e) 2345-1688
http://cjm.asm.md
http://dx.doi.org/10.19261/cjm.2018.504

SYNTHESIS AND X-RAY CHARACTERISATION OF A NEW MIXED-VALENCE TRINUCLEAR IRON CLUSTER

Olesea Cuzan-Munteanu [a*], Silvia Melnic [a,b], Sergiu Shova [a]

[a] *Institute of Chemistry, 3, Academiei str., Chisinau MD 2028, Republic of Moldova*
[b] *"Nicolae Testemitanu" State University of Medicine and Pharmacy, 165, Stefan cel Mare si Sfant Blvd., Chisinau MD 2004, Republic of Moldova*
[*] *e-mail: olesea_cuzan@yahoo.com*

Abstract. This paper reports on the synthesis of a new trinuclear homometalic mixed-valence iron carboxylate cluster with furan-2-carboxylic acid. The complex with the formula $[Fe_2^{III}Fe^{II}O(C_4H_3OCOO)_6(H_2O)_3]\cdot 0.5CH_3CN\cdot 2.25H_2O$ was characterized by X-ray analysis that revealed that the compound crystalizes in the triclinic centrosymmetric group *P*-1, with the following unit cell parameters: a= 10.2758(6) Å, b= 11.5991(9) Å, c= 19.7349(15) Å, α= 105.060(7)°, β= 94.216(6)°, γ= 101.662(6)°.

Keywords: iron cluster, mixed valence, X-ray analysis, μ_3-oxo, crystal structure, hydrogen bond.

Received: 28 June 2018/ Revised final: 14 August 2018/ Accepted: 15 August 2018

Introduction

Transition metal carboxylate compounds have a significant importance in coordination chemistry [1]. The big variety of carboxylic acids and the extraordinary ability of carboxylic groups towards coordination favoured the existence of a great number of metal carboxylate complexes. Carboxylate groups can coordinate to the metal in different ways [2], thus leading to the formation of different types of structures: mononuclear, polynuclear, polymeric or supramolecular compounds.

The class of oxo-centered trinuclear complexes with the general formula $[M_3O(OOCR)_6L_3]^{n+}$ have been widely studied during the last centuries [3,4] not only due to the structural particularities but also due to the large spectrum of properties which emerge from the metal-metal interaction in the cluster.

Although trinuclear iron complexes were studied for a long time, mixed-valence iron clusters began to be a research subject much later. The first detailed review of iron mixed-valence carboxylates was published by Robin, M. and Day, P. in 1967 [5]. However the class of mixed-valence iron carboxylate compounds was studied in detail by Turta, C. *et al.* [6-15] and they also performed the study of carboxylates by Mössbauer spectroscopy. The electron transfer processes were also studied by Oh, S. [16-19] and Wohler, S. [20].

Recently, it has been reported the possibility of using trinuclear clusters as precursors for the nanoparticle synthesis [21,22]. Some studies were devoted to the study of magnetic interaction between heterometallic atoms [23,24], another to the study of thermal behaviour of the trinuclear clusters [25].

Polynuclear homo- and hetero- clusters with furan-2-carboxylic acid as a ligand were determined to manifest a large scale of properties as interesting magnetic behaviour [26], luminescent activity [27], biological activity with anti-tuberculosis properties [28], and ability of regulation of the biochemical composition of cyanobacterium *Spirulina platensis* biomass [29].

To continue the research on the use of the furan-2-carboxylic acid as a ligand in the synthesis of trinuclear clusters, we have synthesized and structurally characterized the $[Fe_2^{III}Fe^{II}O(C_4H_3OCOO)_6(H_2O)_3]\cdot 0.5CH_3CN\cdot 2.25H_2O$ compound by single crystal X-ray method. The presence of both iron(II) and iron(III) species was confirmed by using analytical methods of identification [30].

Experimental

Materials

All chemicals were purchased from commercial sources and used as received without further purification.

Starting materials were $Cu_2(C_4H_3OCOO)_4 \cdot 4H_2O$, $FeCl_2 \cdot 4H_2O$, CH_3OH (methanol), CH_3CN (acetonitrile). The $Cu_2(C_4H_3OCOO)_4 \cdot 4H_2O$ compound was synthesized by the reaction between $(CuOH)_2CO_3$ and furan-2-carboxylic acid. The $FeCl_2 \cdot 4H_2O$ salt was synthesized by the reaction between metallic iron with hydrochloric acid.

Synthesis of $[Fe_2^{III}Fe^{II}O(C_4H_3OCOO)_6(H_2O)_3] \cdot 0.5CH_3CN \cdot 2.25H_2O$

The mixture of copper(II) furan-2-carboxylate salt (0.58 g, 1.8 mmol) and iron(II) chloride (0.36 g, 1.8 mmol) in methanol was stirred under argon atmosphere upon heating. After cooling, a yellow crystalline product was separated upon filtration and was further washed with methanol. Yellow prismatic crystals, suitable for X-ray analysis, were isolated upon recrystallization from acetonitrile solution.

IR (cm^{-1}): 3137.8 vw, 2971.8 vw, 2902.0 vw, 1708.6 vw, 1597.8 w, 1578.8 m, 1565.8 m, 1469.9 s, 1417.7 s, 1372.9 s, 1232.8 w, 1203.7 m, 1140.5 w, 1076.3 w, 1015.7 m, 935.15 w, 884.31 w, 799.5 w, 777.4 m, 758,44 m, 702,46 vw.

Physical measurements

The IR spectrum of the complex was recorded using a Perkin Elmer Spectrum 100 FT-IR spectrometer in the range 4000–650 cm^{-1}.

X-ray crystallography. Suitable crystals for single crystal X-ray diffraction study of $[Fe_2^{III}Fe^{II}O(C_4H_3OCOO)_6(H_2O)_3] \cdot 0.5CH_3CN \cdot 2.25H_2O$ complex were grown by slow evaporation of CH_3CN solution.

X-ray diffraction measurements were carried out with an Oxford-Diffraction XCALIBUR E CCD diffractometer equipped with graphite-monochromated MoKα radiation. The unit cell determination and data integration were carried out using the CrysAlis package of Oxford Diffraction [31]. The structure was solved by direct methods using the Olex2 [32] software with the SHELXS structure solution program and refined by full-matrix least-squares on F^2 with SHELXL-97 [33] using an anisotropic model for non-hydrogen atoms. All H atoms were introduced in idealised positions (d_{CH}= 0.96 Å) using the riding model. The positional parameters for H-atoms attached to O were verified by the geometric parameters of the possible hydrogen bonds. The molecular plots were obtained using the Olex2 program. The crystallographic data and refinement details are quoted in Table 1. CCDC 1851865 contains the supplementary crystallographic data for this contribution. These data can be obtained free of charge *via* www.ccdc.cam.ac.uk/conts/retrieving.html (or from the Cambridge Crystallographic Data Centre, 12 Union Road, Cambridge CB2 1EZ, UK; fax: (+44) 1223-336-033; or deposit@ccdc.ca.ac.uk).

Table 1

Crystal data and details of data collection for $[Fe_2^{III}Fe^{II}O(C_4H_3OCOO)_6(H_2O)_3] \cdot 0.5CH_3CN \cdot 2.25H_2O$.

Parameter	*Value*
Empirical formula	$C_{31}H_{30}Fe_3N_{0.5}O_{24.25}$
Fw	965.10
T, K	293
Space group	P-1
a, Å	10.2758(6)
b, Å	11.5991(9)
c, Å	19.7349(15)
α, °	105.060(7)
β, °	94.216(6)
γ, °	101.662(6)
V, Å^3	2204.7(3)
Z	2
$\rho_{calcd.}$ g cm^{-3}	1.454
μ, mm^{-1}	1.056
Crystal size, mm	0.2 × 0.15 × 0.15
2Θ range	5.952 to 57.76
Reflections collected	16839
Independent reflections	9896 [R_{int}= 0.0730]
Data/restraints/parameters	9896/59/492
R_1[a]	0.0826
wR_2[b]	0.2087
GOF[c]	1.000
Largest diff. peak/hole / e Å^{-3}	0.93/-0.51

[a] $R_1 = \Sigma||F_o| - |F_c||/\Sigma|F_o|$.
[b] $wR_2 = \{\Sigma[w(F_o^2 - F_c^2)^2]/\Sigma[w(F_o^2)^2]\}^{1/2}$.
[c] $GOF = \{\Sigma[w(F_o^2 - F_c^2)^2]/(n-p)\}^{1/2}$, *where n is the number of reflections and p is the total number of parameters refined.*

Results and discussion

The reaction between copper furoate and iron(II) chloride under argon atmosphere in methanol solution upon heating leads to the formation of a new mixed-valence trinuclear complex with the composition $[Fe_2^{III}Fe^{II}O(C_4H_3OCOO)_6(H_2O)_3] \cdot 0.5CH_3CN \cdot 2.25H_2O$. It should be mentioned that in the case of furan-2-carboxylic acid, the typical reaction with an iron salt does not result in the formation of a trinuclear cluster, in this case a copper(II) furoate salt should be used instead [29].

According to X-ray crystallography, the investigated compound has a molecular crystal structure, which is built up from trinuclear mixed-valence $[Fe_2^{III}Fe^{II}O(C_4H_3OCOO)_6(H_2O)_3]$ neutral entities co-crystallized with acetonitrile and water molecules in 1:0.5:2.25 ratio. The trinuclear units exhibit a typical μ_3-oxo structure

where three iron atoms situated in the edges of a triangle are linked by μ_3-oxigen atom as well as the six furan-2-carboxylic groups acting as bridging ligands (Figure 1).

The geometric parameters of the coordination polyhedron of the metals, especially Fe-O1 bond distances could serve as a criterion for the analysis of the distribution of the Fe^{2+} and Fe^{3+} within the trinuclear cluster. Nevertheless, the difference in the Fe1-O1 1.909(5) Å, Fe2-O1 1.891(4) Å and Fe3-O1 1.923(5) Å is not so pronounced giving rise to the statistically distribution of the metal cations in 1:2 ratio for each metal center (Table 2).

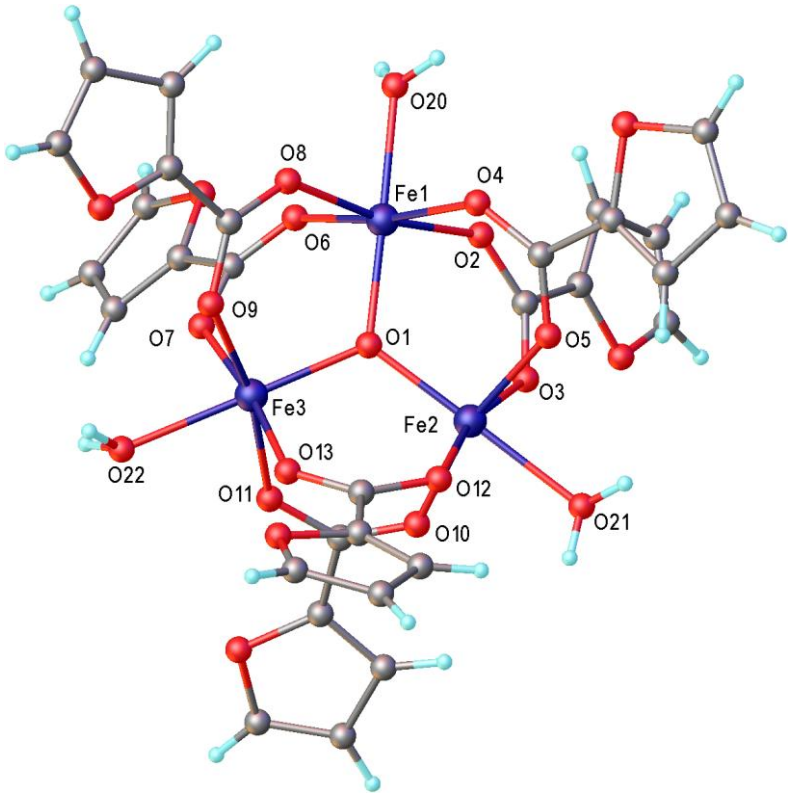

Figure 1. Molecular structure of the $[Fe_2^{III}Fe^{II}O(C_4H_3OCOO)_6(H_2O)_3]$ complex. Only one position of disordered moieties is shown for clarity.

Each pair of iron atoms in the trinuclear core are separated at 3.2981(16), 3.2909(18) and 3.3237(17) Å for Fe1···Fe2, Fe2···Fe3, Fe3···Fe1 atoms, respectively. The values of Fe1-O1-Fe2, Fe2-O1-Fe3, Fe3-O1-Fe1 angles vary in the range between 120.5(3) and 119.2(3)°. The sum of the angles around the μ_3-oxygen atom is of 360(8)° which confirms the planar configuration of the $\{Fe_3\mu_3\text{-}O\}$ fragment. The iron atoms are displaced from the mean plane defined by four equatorial oxygen atoms at 1.909(5), 1.891(4), 1.923(5) Å towards the central μ_3-O1 atom, respectively.

Each iron atom has six-oxygen coordination in a slightly distorted octahedral geometry formed by four carboxylate oxygen atoms in the equatorial plane, the μ_3-O atom and water molecules in the apical positions.

The analysis of crystal structure packing shows the presence of dimeric aggregates formed due to intermolecular hydrogen bonding between one of the coordinated water molecule as donor and two carboxylate oxygen atoms of adjacent trinuclear complex as acceptor of protons, as shown in Figure 2.

A similar aggregation of trinuclear complexes was observed previously for a hetero-trinuclear complex with the composition $[Fe_2MnO(CHCl_2COO)_6(THF)_2H_2O]$ [34] where the water molecule involved in H-bonding is coordinated to Mn^{II} atom.

The crystal structure packing (Figure 3) is described as a three-dimensional supramolecular network consolidated through the hydrogen bonds between coordinated and solvate water molecules. A specific feature of 3D packing consists in the formation of the parallel channels along crystallographic axis *a*, accommodating statistically distributed solvate water molecules.

Table 2

Selected bond lengths and angles for the $[Fe_2^{III}Fe^{II}O(C_4H_3OCOO)_6(H_2O)_3]\cdot 0.5CH_3CN\cdot 2.25H_2O$ complex.

Bond	*d, (Å)*	*Bond*	*d, (Å)*
Fe1–O1	1.909(5)	Fe2– O10	2.024(5)
Fe1– O2	2.015(5)	Fe2– O12	2.026(6)
Fe1– O4	1.992(5)	Fe2– O21	2.099(4)
Fe1– O6	1.993(5)	Fe3–O1	1.923(5)
Fe1– O8	2.013(5)	Fe3–O7	1.999(6)
Fe1– O20	2.043(6)	Fe3–O9	1.991(5)
Fe2– O1	1.891(4)	Fe3–O11	1.985(5)
Fe2– O3	1.987(6)	Fe3–O13	2.010(6)
Fe2– O5	2.012(5)	Fe3–O22	2.107(5)
Angle	*ω, (°)*	*Angle*	*ω, (°)*
O1–Fe1–O2	95.1(2)	O5–Fe2–O10	167.2(2)
O1–Fe1–O4	94.5(2)	O5–Fe2–O12	87.5(2)
O1–Fe1–O6	94.4(2)	O5–Fe2–O21	83.78(19)
O1–Fe1–O8	95.2(2)	O10–Fe2–O12	91.9(2)
O1–Fe1–O20	178.9(2)	O10–Fe2–O21	83.4(2)
O2–Fe1–O20	85.7(2)	O12–Fe2–O21	82.2(2)
O4–Fe1–O2	88.5(2)	O1–Fe3–O7	91.6(2)
O4–Fe1–O6	170.6(3)	O1–Fe3–O9	96.1(2)
O4–Fe1–O8	90.4(2)	O1–Fe3–O11	95.2(2)
O4–Fe1–O20	86.2(2)	O1–Fe3–O13	95.0(2)
O6–Fe1–O2	88.0(2)	O1–Fe3–O22	177.3(2)
O6–Fe1–O8	91.5(2)	O7–Fe3–O13	173.4(3)
O6–Fe1–O20	84.8(2)	O7–Fe3–O22	85.9(2)
O8–Fe1–O2	169.7(3)	O9–Fe3–O7	92.6(2)
O8–Fe1–O20	84.0(2)	O9–Fe3–O13	87.0(2)
O1–Fe2–O3	96.2(2)	O9–Fe3–O22	85.2(2)
O1–Fe2–O5	96.03(19)	O11–Fe3–O7	88.8(2)
O1–Fe2–O10	96.8(2)	O11–Fe3–O9	168.6(2)
O1–Fe2–O12	96.3(2)	O11–Fe3–O13	90.3(2)
O1–Fe2–O21	178.5(2)	O11–Fe3–O22	83.6(2)
O3–Fe2–O5	89.9(2)	O13–Fe3–O22	87.5(2)
O3–Fe2–O10	87.9(2)	Fe1–O1–Fe3	120.3(2)
O3–Fe2–O12	167.4(2)	Fe2–O1–Fe1	120.5(3)
O3–Fe2–O21	85.3(2)	Fe2–O1–Fe3	119.2(3)

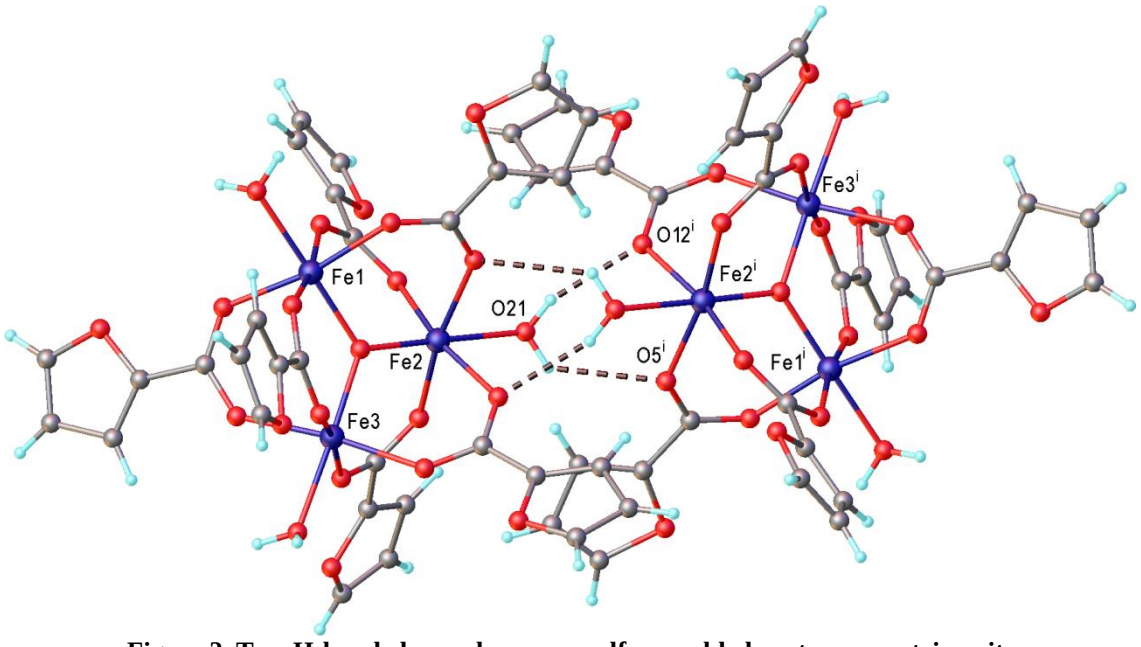

Figure 2. Two H-bonded complexes as a self-assembled centrosymmetric unit. Symmetry transformation used to generate equivalent atoms: *-x, 2-y, 1-z*.

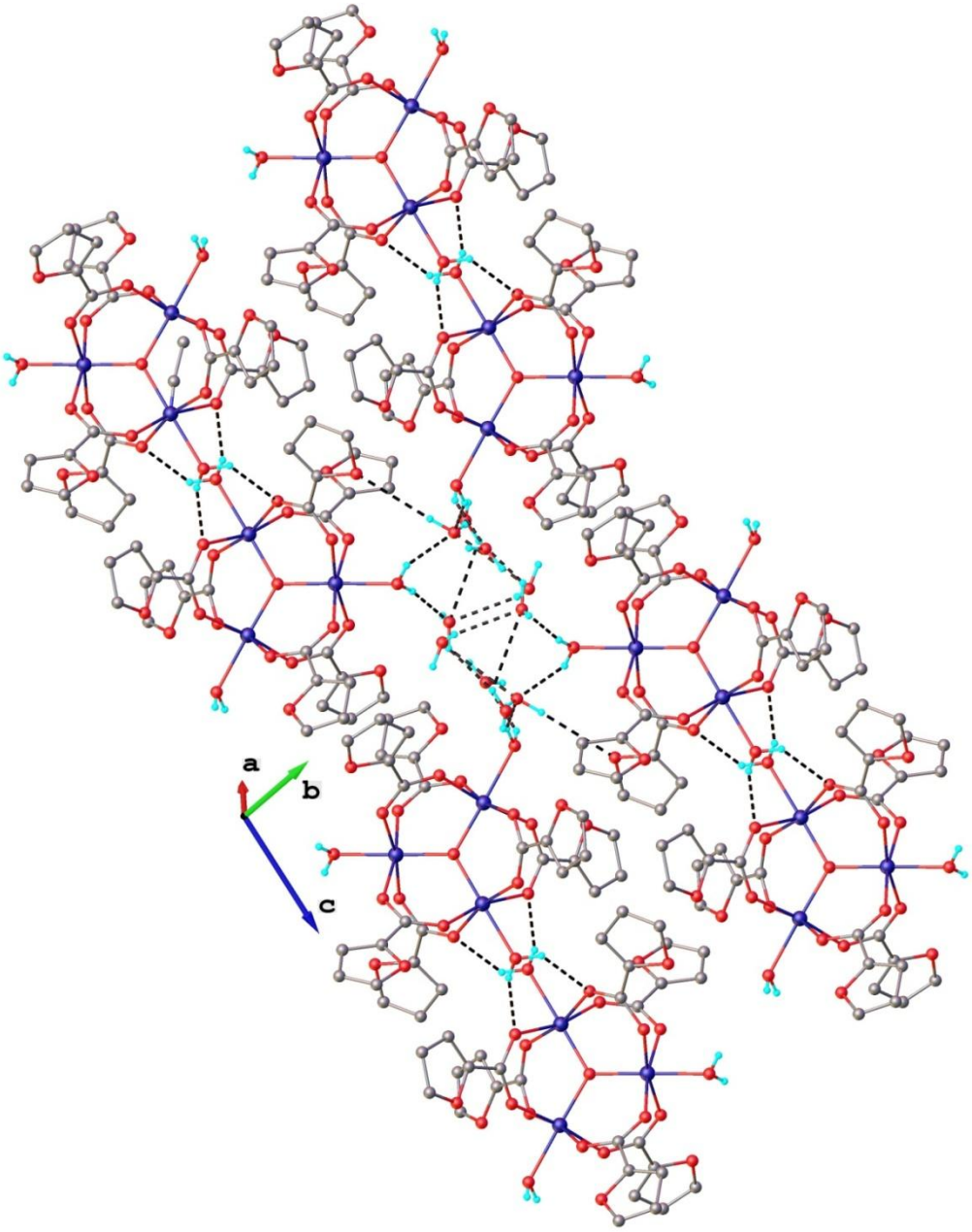

Figure 3. Partial view of the packing diagram.

The IR spectrum of the title compound shows multiple bands in the range of 4000–650 cm^{-1}, which were analysed according to the oscillation group concept [35]. According to this concept, the bands interpretation in a complex compound with many atoms is made on the basis of adsorption bands characteristic to certain functional groups.

The minimal number of characteristic bands of a polyatomic compound is calculated according to the formula 3n-6, where n is the total number of atoms in the molecule, thus for 85 atoms present in the studied complex, can be found 249 characteristic bands. Due to the fact that the range of the spectrum starts from 650 cm^{-1}, the number of bands decreases. Also, the same value of wave number $1/\lambda$ is characteristic for many functional groups, thus the peaks overlapping phenomenon is also present.

According to the oscillation group theory, the presence of hydrogen bonds in water molecules is characterized by a broad signal (the broader the signal, the stronger the hydrogen bonds) in the range of 3200–2800 cm^{-1}. In the given spectrum, this signal overlaps with the signals at: 3137.8; 2971.8; 2902.0 cm^{-1}, which are characteristic for ν(C-H) oscillations of the furanic ring.

The presence of protonated carboxylic groups, according to the same concept, can be identified by the presence of oscillations characteristic to the wave number of 1700 cm^{-1}.

It is worth mentioning that as the result of complexation (the proton substitution and the formation of oxygen – metal bonds) the band characteristic to the wave number is shifted with 150–200 cm^{-1}, and we can identify the presence of two types of vibrations: symmetric and asymmetric valence vibrations. Thus in the studied spectrum, the bands characteristic for ν_{as}, ν_s(COO) were identified at 1565.8 and 1417.7 cm^{-1}. The magnitude of the separation between the carboxylate stretches, $\Delta = \nu_{as}(COO) - \nu_s(COO)$ has the value of 148.1 cm^{-1} which confirms the bridging behaviour of the carboxylate group of the furan-2-carboxylic ligand [36].

The values of the wave number oscillations characteristic to the 2-furan-carboxylic ligand, present in the IR spectrum follows: 1597.8; 1578.8, 1469.9, 1372. 9 cm^{-1} for ν(ring), 1232.8; 1140.5; 1076.3 cm^{-1} for β(C-H), 1015.7 cm^{-1} for ν(C-O-C), 935.15 for ring pulsation, 884.31 for β(ring), 777.4; 758.44 cm^{-1} for γ(C-H) [37].

From the oscillations presented above should be mentioned that the band at 884.31 cm^{-1} is essential in the determination of the presence of furan-2-carboxylic acid while the band at 1015.7 cm^{-1} suggests that the oxygen atom from the furanic ring does not participate in the coordination of the ligand to the metal, thus the coordination occurs solely through the carboxylate groups.

Simultaneously, all the bands in the wave number range 1400–650 cm^{-1} can be assigned to the fingerprint region of this complex [36,38].

Conclusions

In this work, it is reported the synthesis of a new trinuclear mixed-valence iron carboxylate complex with the furan-2-carboxylic acid. The single-crystal X-ray characterization shows that the complex has a typical μ_3-oxo structure with the composition $[Fe_2^{III}Fe^{II}O(C_4H_3OCOO)_6(H_2O)_3]\cdot 0.5CH_3CN \cdot 2.25H_2O$. The presence of intermolecular hydrogen bonds favours the formation of a supramolecular structure by forming channels along crystallographic axis *a*.

Acknowledgements

This work was realised under the supervision of Prof. Constantin Turta (20.12.1940 – 23.03.2015).

References

1. Mehrotra, R.C.; Bohra, R. Metal carboxylates. Academic Press: New York, 1983, 396 p. https://www.elsevier.com/books-and-journals/academic-press
2. Gómez, V.; Corbella, M. Versatility in the coordination modes of *n*-chlorobenzoato ligands: synthesis, structure and magnetic properties of three types of polynuclear Mn^{II} compounds. European Journal of Inorganic Chemistry, 2009, (29-30), pp. 4471-4482. DOI: https://doi.org/10.1002/ejic.200900532
3. Weinland, R.; Holtmeier, H. About iron-nickel-etc. Acetates and a very basic crystallized iron acetate. Zeitschrift Für Anorganische Und Allgemeine Chemie, 1928, 173(1), pp. 49-62. (in German). DOI: https://doi.org/10.1002/zaac.19281730106
4. Schmoldt, A.; Benthe, H.F.; Haberland, G. Digitoxin metabolism by rat liver microsomes. Biochemical Pharmacology, 1975, 24(17), pp. 1639–1641. DOI: https://doi.org/10.1016/0006-2952(75)90094-5
5. Robin, M.B.; Day, P. Mixed valence chemistry – a survey and classification. Advances in Inorganic Chemistry and Radiochemistry, 1968, 10, pp. 247-422. DOI: https://doi.org/10.1016/S0065-2792(08)60179-X
6. Ponomareov, V.I.; Turta, C.I.; Shilov, G.V.; Bobcova, S.A.; Avtomean, L.O.; Stucan, R.A. X-ray diffraction and gamma spectroscopic study of a thinuclear mixed-valence iron complex $Fe_3(\mu_3\text{-}O)(CF_3COO)_6(C_6H_5PO)_3$. Russian Journal of Coordination Chemistry, 1986, 12(3), pp. 398-403. (in Russian). http://www.maik.ru/ru/journal/kordkhim/
7. Ponomareov, V.I.; Shilov, G.V.; Avtomean, L.O.; Turta, C.I.; Bobcova, S.A. The crystal and molecular structure of a trinuclear mixed-valence iron cluster $[Fe_3\text{-}\mu_3\text{-}O)(CCl_3COO)_6(CH_3OH)_3]\cdot 1.5H_2O$. Fast electron hopping. Russian Journal of Coordination Chemistry, 1987, 13, pp. 1097-1100. (in Russian). http://www.maik.ru/ru/journal/kordkhim/
8. Turta, C.I.; Bobcova, S.A.; Stucan, R.A.; Shova, S.G. Synthesis and study of trinuclear iron clusters of mixed valence (III, II, III) with chloroacetic acids. Russian Journal of Coordination Chemistry, 1981, 7, pp. 1682-1691. (in Russian). http://www.maik.ru/ru/journal/kordkhim/
9. Turta, C.I.; Bobcova, S. A.; Stucan, R.A. Synthesis and study of iron clusters of mixed valence (II, III, III) with fluorine-substituted carboxylic acids. Russian Journal of Inorganic Chemistry, 1982, 27, pp. 954-960. (in Russian). http://www.maik.ru/ru/journal/nergkhim/
10. Garbalau, N.V.; Timco, G.A.; Turta, C.I.; Popovici G.A.; Bobcova, S.A.; Indricean, C.M. Synthesis and study of μ_3-oxo-carboxylates of iron of mixed valence (II, III, III). Russian Journal of Inorganic Chemistry, 1986, 31, pp. 684-690. (in Russian). http://www.maik.ru/ru/journal/nergkhim/
11. Stucan, R.A.; Turta, C.I.; Ablov, A.V.; Bobcova, S.A. Gamma resonance spectra of the basic acetate complexes of mixed valence iron with pyridine, β- and γ-picolines. Russian Journal of

Coordination Chemistry, 1979, 5, pp. 95-102. (in Russian). http://www.maik.ru/ru/journal/kordkhim/
12. Turta, C.I.; Bobcova, S.A.; Stucan, R.A.; Dorogan, A.V.; Vekseliman, M.E. Synthesis and study of the basic acetates of iron (III) and mixed valence iron (III, II, III) with isoquinoline. Russian Journal of Coordination Chemistry, 1982, 8, pp. 794-800. (in Russian). http://www.maik.ru/ru/journal/kordkhim/
13. Stucan, R.A.; Turta, C. I.; Goldanski, V.I.; Kaplan, A.M.; Volikenau, N.A.; Sirotkina, E.I. Investigation of the temperature dependence of gamma-resonance spectra and phase transformations. Theoretical and Experimental Chemistry, 1971, 7, pp. 74-80. (in Russian). https://www.springer.com/chemistry/journal/11237
14. Turta, C.I.; Bobcova, S.A.; Stucan, R.A. Study by the Gamma Resonance Spectroscopy method of frozen solutions of trinuclear mixed valence iron clusters with trichloro- and trifluoroacetic acids. Russian Journal of Inorganic Chemistry, 1984, 29, pp. 731-734. (in Russian). http://www.maik.ru/ru/journal/nergkhim/
15. Ivleva, I.N.; Echmaev, S.B.; Stucan, R.A.; Turta, C.I.; Bobcova, S.A.; Vekseliman, M.E. Magnetochemical studies of mixed valence iron complexes with acetic acid and some of its derivatives. Russian Journal of Inorganic Chemistry, 1982, 27, pp. 1479-1485. (in Russian). http://www.maik.ru/ru/journal/nergkhim/
16. Oh, S.M.; Hendrickson, D.N.; Hassett, K.L.; Davis, R.E. Electron transfer in mixed-valence, oxo-centered, trinuclear iron acetate complexes: effect of statically disordered to dynamically disordered transformation in the solid state. Journal of the American Chemical Society, 1984, 106(25), pp. 7984-7985. DOI: 10.1021/ja00337a063
17. Oh, S.M.; Henderickson, D.N.; Hassett, K.L.; Davis, R.E. Valence-detrapping modes for electron transfer in the solid state of mixed-valence, oxo-centered, trinuclear iron acetate complexes: x-ray structure and physical data for $[Fe_3O(O_2CCH_3)_6(4\text{-Et-Py})_3](4\text{-Et-Py})$. Journal of the American Chemical Society, 1985, 107(26), pp. 8009-8018. DOI: 10.1021/ja00312a035
18. Oh, S.M.; Kambara, T.; Hendrickson, D.N.; Sorai, M.; Kaji, K.; Woehler, S.E.; Wittebort, R.J. Phase transitions affecting intramolecular electron transfer in mixed-valence trinuclear iron acetate complexes. Journal of the American Chemical Society, 1985, 107(19), pp. 5540-5541. DOI: 10.1021/ja00305a044
19. Sorai, M.; Kaji, K.; Hendrickson, D.N.; Oh, S.M. Heat capacity and phase transitions of the mixed-valence compound $[Fe_3O(O_2CCH_3)_6(Py)_3](Py)$. Journal of the American Chemical Society, 1986, 108(4), pp. 702-708. DOI: 10.1021/ja00264a021
20. Woehler, S.E.; Wittebort, R.J.; Oh, S.M.; Hendrickson, D.N.; Inniss, D.; Strouse, C.E. Solid-state deuterium NMR, Iron-57 Moessbauer, and X-ray structural characteristics of μ_3-oxo-bridged mixed-valence $[Fe_3O(O_2CCH_3)_6(4\text{-Me-Py})_3](C_6H_6)$: Dynamics of the benzene solvate molecules influencing intramolecular electron transfer. Journal of the American Chemical Society, 1986, 108(11), pp. 2938-2946. DOI: 10.1021/ja00271a024
21. Iacob, M.; Racles, C.; Tugui, C.; Stiubianu, G.; Bele, A.; Sacarescu, L.; Timpu, D.; Cazacu, M. From iron coordination compounds to metal oxide nanoparticles. Beilstein Journal of Nanotechnology, 2016, 7, pp. 2074-2087. DOI: 10.3762/bjnano.7.198
22. Turta, C.; Melnic, S.; Prodius, D.; Macaev, F.; Stoeckli-Evans, H.; Ruiz, P.; Muraviev, D.; Pogrebnoi, S.; Ribkovskaia, Z.; Mereacre, V.; Lan, Y.; Powell, A.K. Sunflower oil coating on the nanoparticles of iron(III) oxides. Inorganic Chemistry Communications, 2010, 13(12), pp. 1402-1405. DOI: https://doi.org/10.1016/j.inoche.2010.07.046
23. Gorinchoy, V.V.; Zubareva, V.E.; Shova, S.G.; Szafranski, V.N.; Lipkowski, J.; Stanica, N.; Simonov, Yu.A.; Turta, C.I. Homo- and heteronuclear iron complexes $\{Fe_2MO\}$ with salicylic acid: synthesis, structures, and physicochemical properties. Russian Journal of Coordination Chemistry, 2009, 35(10), pp. 731-739. DOI: https://doi.org/10.1134/S1070328409100042
24. Lupu D. Magnetic exchange in a heterogenous trinuclear system. Revue Roumaine de Chimie. 1970, 15, pp. 417-422. http://revroum.lew.ro
25. Gorinchoy, V.; Shova, S.; Melnic, E.; Kravtsov, V.; Turta, C. Homotrinuclear Fe_3^{III} μ– oxo salicylate cluster. Synthesis, structure and properties. Chemistry Journal of Moldova, 2013, 8(2), pp. 83-89. DOI: dx.doi.org/10.19261/cjm.2013.08(2).10
26. Melnic, S.; Prodius, D.; Shova, S.; Stoeckli-Evans, H.; Simonov, Yu.; Feher, A.; Gdaniec, M.; Turta, C. Synthesis, crystal structure and magnetic behaviour of novel 4f-2s heterometalic one-dimensional coordination polymers on the base of 2-furan-carboxylic acid. Chemistry Journal of Moldova, 2009, 4(2), pp. 60-67. DOI: dx.doi.org/10.19261/cjm.2009.04(2).10
27. Turta, C.; Melnic, S.; Bettinelli, M.; Shova, S.; Benelli, C.; Speghini, A.; Caneschi, A.; Gdaniec, M.; Simonov, Yu.; Prodius, D.; Mereacre, V. Synthesis, crystal structure, magnetic and luminescence investigations of new $2Ln^{3+}$–Sr^{2+} heteronuclear polymers with 2-furoic acid. Inorganica Chimica Acta, 2007, 360(9), pp. 3047-3054. DOI: https://doi.org/10.1016/j.ica.2007.02.045
28. Melnic, S.; Prodius, D.; Stoeckli-Evans, H.; Shova, S.; Turta, C. Synthesis and anti-tuberculosis activity of new hetero(Mn, Co, Ni)trinuclear iron(III) furoates. European Journal of Medicinal Chemistry, 2010, 45(4), pp. 1465-1469.

DOI: https://doi.org/10.1016/j.ejmech.2009.12.053
29. Melnic, S.; Prodius, D.; Simmons, C.; Zosim, L.; Chiriac, T.; Bulimaga, V.; Rudic, V.; Turta, C. Biotechnological application of homo- and heterotrinuclear iron(III) furoates for cultivation of iron-enriched *Spirulina*. Inorganica Chimica Acta, 2011, 373(1), pp. 167-172. DOI: https://doi.org/10.1016/j.ica.2011.04.011
30. Shapiro, S.A.; Shapiro, M.A. Analytical Chemistry. Vysshaya Shkola: Moscow, 1979, 384 p. (in Russian). http://www.vshkola.ru/en/
31. CrysAlis RED, Version 1.171.36.32, 2003; Oxford Diffraction Ltd.: Abingdon, UK, 2003. http://www.oxford-diffraction.com
32. Dolomanov, O.V.; Bourhis, L.J.; Gildea, R.J.; Howard, J.A.K.; Puschmann, H. OLEX2 : A complete structure solution, refinement and analysis program. Journal of Applied Crystallography, 2009, 42, pp. 339-341. DOI: https://doi.org/10.1107/S0021889808042726
33. Sheldrick, G.M. A Short History of SHELX. Acta Crystallographica, Section A, Foundations and Advances, 2008, A64, pp. 112-122. DOI: https://doi.org/10.1107/S0108767307043930
34. Shova, S.; Prodius, D.; Mereacre, V.; Simonov, Yu.A.; Lipkowski, J.; Turta, C. Discernible apical coordination in μ_3-oxo-bridged mixed metal trinuclear carboxylate $[Fe_2MnO(CHCl_2COO)_6(THF)_2H_2O]$. Inorganic Chemistry Communications, 2004, 7(2), pp. 292-295. DOI: https://doi.org/10.1016/j.inoche.2003.10.038
35. Drago, R.S. Physical methods for chemists, 2nd Ed. Saunders: Gainesville, Florida, 1992, 750 p. https://www.elsevier.com
36. Nakamoto, K. Infrared and Raman spectra of inorganic and coordination compounds. John Wiley & Sons: New York, 1986, 484 p. https://www.wiley.com/en-md
37. Avram, M.; Mateescu, Gh.D. Infrared spectroscopy: Applications in organic chemistry. Technical Publishing House: Bucharest, 1966, 552 p. (in Romanian) http://www.worldcat.org/
38. Tel'zhenskaya, P.N.; Shvarts, E.M. Complex compounds of salicylic acid and its derivatives. Russian Journal of Coordination Chemistry, 1977, 3, pp. 1279. (in Russian) http://www.maik.ru/ru/journal/kordkhim/

CHEMISTRY JOURNAL OF MOLDOVA. General, Industrial and Ecological Chemistry. 2018, 13(2), 56-62
ISSN (p) 1857-1727 ISSN (e) 2345-1688
http://cjm.asm.md
http://dx.doi.org/10.19261/cjm.2018.513

SYNTHESIS AND CRYSTAL STRUCTURE OF BIS(CITRATO)GERMANATE AND STANNATE WITH TRIS(PHENANTHROLINE)NICKEL(II) CATION

Elena Martsinko [a*], Inna Seifullina [a], Elena Chebanenko [a], Olha Pirozhok [a], Viktoriya Dyakonenko [b], Svitlana Shishkina [b,c]

[a]*I.I. Mechnikov Odessa National University, 2, Dvoryanskaya str., Odessa 65082, Ukraine*
[b]*SSI "Institute for Single Crystals", National Academy of Sciences of Ukraine, 60, Nauki ave., Kharkiv 61001, Ukraine*
[c]*V.N. Karazin Kharkiv National University, 4, Svobody sq., Kharkiv 61077, Ukraine*
[*]*e-mail: lborn@ukr.net*

Abstract. The new complexes $[Ni(phen)_3][Ge(HCit)_2]\cdot 2H_2O$ (**1**), $[Ni(phen)_3][Sn(HCit)_2]\cdot 3H_2O$ (**2**) (where phen is 1,10-phenanthroline, H_4Cit is citric acid) were synthesized. The identity, composition, and thermal stability of the complexes were established by elemental analysis, thermogravimetry, and IR spectroscopy. According to the data of X-ray diffraction, the bis(citrate)germanate/bis(citrate)stannate $[Ge/Sn(HCit)_2]^{2-}$ is the anion, while $[Ni(phen)_3]^{2+}$ is the cation in the studied complexes. The coordination polyhedrons of Ge, Sn and Ni atoms are octahedral and are formed by three pairs of oxygen atoms of different types of two $HCit^{-3}$ ligands or by three 1,10-phenanthroline molecules.

Keywords: citric acid, 1,10-phenanthroline, germanium(IV), tin(IV), nickel(II) complex.

Received: 01 September 2018/ Revised final: 28 September 2018/ Accepted: 03 October 2018

Introduction

Obtaining and determining of the structure of coordination compounds formed with biometals and hydroxycarbonic acids is of great interest nowadays because of the creation of new medicines on their basis. Citric acid is the direct participant of a cycle of three carbonic acids (the Krebs cycle) and is present in blood plasma [1]; germanium lactate-citrate possesses radioprotective properties [2].

In the past few years, authors have shown that germanium(IV) and tin(IV) in water solution are able to form cation–anion coordination compounds with bis(citrate)germanate $[Ge(HCit)_2]^{2-}$ or bis(citrate)stannate $[Sn(HCit)_2]^{2-}$ anions and octahedral $[M(H_2O)_6]^{2+}$ cations (M= Mg, Mn, Fe, Co, Ni, Cu, Zn) [3,4]. Such a type of coordination compounds show antihypoxic, cerebroprotective and antiviral properties [5]. Subsequently, new complexes with similar bis(citrate)germanate anions and cations $[M(phen)_3]^{2+}$ (phen - 1,10-phenantroline, M= Fe(II), Co(II)) and $[CuCl(phen)_2]^{+}$ have been synthesized and described by the authors [6,7]. A group of British and Portuguese scientists also have synthesized a number of complex compounds, which contain tris(oxalato-O,O')germanate anion $[Ge(C_2O_4)_3]^{2-}$ and transition-metal cationic complexes $[M(phen)_3][Ge(C_2O_4)_3]xH_2O$ (where M^{2+} = Cu^{2+}, Fe^{2+}, Ni^{2+}, Co^{2+}) [8]. Synthesis of new analogical bis(citrato)stannates is also of particular interest. These complexes can not be prepared from SnO_2 because of its poor solubility in water and acids.

This work is dedicated to the development of new synthesis methods and study of structure of new heterometal-different-ligand complexes of germanium(IV) or tin(IV) and nickel(II) with citric acid and 1,10-phenanthroline as promising biologically active compounds.

Experimental

Materials

Germanium(IV) oxide (GeO_2, 99.99%), tin(IV) chloride ($SnCl_4$, 98%), citric acid ($H_4Cit\cdot H_2O$, 99%), 1,10-phenanthroline (phen, 99%), nickel(II) salts $NiCl_2\cdot 6H_2O$ (99%) and $Ni(CH_3COO)_2\cdot 4H_2O$ (98%) were used as initial reagents for the synthesis of new complexes.

Methods

Elemental analysis for germanium, tin and nickel was performed using inductively coupled plasma atomic emission spectroscopy with an Optima 2000 DV instrument (PerkinElmer).

Analysis for C, H, and N was performed using a CE-440 Elemental Analyzer.

Thermogravimetric analysis (TGA) was carried out using a Q-1500D with a heating rate of 10°C/min on air in the temperature range 20-1000°C.

The IR spectra in the range of 4000-400 cm^{-1} were recorded as potassium bromide pellets on a Frontier spectrometer (PerkinElmer). The absorption bands were attributed according to the reference data for citric acid and our earlier obtained germanium(IV) coordination compounds with hydroxycarboxylic acids [3,4,6,7].

X-ray crystallography. Crystal data for structures **1** and **2** were measured on a Xcalibur-3 diffractometer (graphite monochromated MoKα radiation, CCD detector, ω-scanning). The structures were solved by the direct method using the SHELXTL package [9]. Full-matrix least-squares refinement against F^2 in anisotropic approximation was used for non-hydrogen atoms. Positions of hydrogen atoms were determined from electron density difference maps and refined by "riding" model with $U_{iso}= nU_{eq}$ of the carrier atom (n= 1.5 for hydroxyl groups and n= 1.2 for other hydrogen atoms). CCDC 1854034 and 1854035 contains the supplementary crystallographic data for **1** and **2**, respectively. These data can be obtained free of charge *via* http://www.ccdc.cam.ac.uk/conts/retrieving.html, or from the Cambridge Crystallographic Data Centre, 12 Union Road, Cambridge CB2 1EZ, UK; fax: (+44) 1223-336-033; or e-mail: deposit@ccdc.cam.ac.uk. Full use of the CCDC package was also made for searching in the CSD Database.

Synthesis

$[Ni(phen)_3][Ge(HCit)_2]\cdot 2H_2O$ (1)

A suspension of germanium(IV) oxide (0.0523 g, 0.5 mmol) and citric acid (0.21 g, 1 mmol) in 100 mL of hot distilled water was stirred to dissolve reagents completely and slowly evaporated at 50°C to a 20 mL volume. After cooling the solution to the room temperature, 20 mL of a 95% ethanol solution containing 1,10-phenanthroline (0.27 g, 1.5 mmol) and $NiCl_2\cdot 6H_2O$ (0.119 g, 0.5 mmol) were added. After 3 days, a pink-colored crystalline solid precipitated. Single crystals suitable for X-ray diffraction were collected from the reaction medium.

Elemental composition, based on single-crystal data for $C_{48}H_{38}GeN_6NiO_{16}$ (1086.14), analytically calculated in %: C 53.03, H 3.50, Ge 6.68, N 7.73, Ni 5.43; found for the as-synthesized bulk material (in %): C 52.78, H 3.29, Ge 6.57, N 7.63, Ni 5.38.

The thermal destruction of **1** (weight losses, Δm): 80-140°C, endothermic peak 100°C (-3.3%); 290-360°C, endothermic peak 350°C (-24.7%); 420-580°C, exothermic peak 530°C (-54.0%).

Selected IR data for **1** (in cm^{-1}): 3396 ν(OH), 1722 ν(C=O), 1626 $\nu_{as}(COO^-)$, 1588, 1518 $\nu(C–C_{Ar})$, 1393 $\nu_s(COO^-)$, 1349 ν(C–N), 1086 ν(C–O), 1151, 905, 855 δ(CH), 641 ν(Ge–O).

The $[Ni(phen)_3][Ge(HCit)_2]\cdot 2H_2O$ (**1**) crystal data (M= 1086.14 g/mol): monoclinic, space group $P2/c$, a= 23.012(2), b= 11.3384(6), c= 18.5747(8) Å, β= 94.660(5)°, V= 4830.4(5) $Å^3$, Z= 4, T= 294 K, $\mu(MoK_\alpha)$= 1.090 mm^{-1}, D_{calc}= 1.494 g/cm^3, 41649 reflections measured, 9454 unique (R_{int}= 0.221, R_{sigma}= 0.214), which were used in all calculations. The final R_1 was 0.086 for 3980 reflections with I> 2σ(I)) and wR_2 was 0.213 (all data), S= 0.936.

$[Ni(phen)_3][Sn(HCit)_2]\cdot 3H_2O$ (2)

It was prepared by dissolving citric acid (0.01 mol, 4.2 g) in water (20 mL), further, this solution was brought to boiling, $SnCl_4$ (0.005 mol, 0.625 mL) was added, heated for 10 min and cooled. After addition of tin tetrachloride to the acid solution, pH was brought to 1 by adding ammonium hydroxide. This was done because the complexation does not take place in a highly acidic medium, while further increase in the pH results in hydrolysis.

In the second step, the solution of $Ni(CH_3COO)_2\cdot 4H_2O$ in water (5 mL) was added, the mixture was stirred and the complex $[Ni(H_2O)_6][Sn(HCit)_2]\cdot 4H_2O$ [3] crystallized at room temperature. The blue precipitate was filtered off on a Schott glass filter, washed with cold water, and dried at room temperature (20°C).

In the third step, a suspension of $[Ni(H_2O)_6][Sn(HCit)_2]\cdot 4H_2O$ (0.0523 g, 0.5 mmol) and 1,10-phenanthroline (0.27 g, 1.5 mmol) was stirred in 20 mL of warm distilled water. On the next day, a red crystalline solid precipitated, from which single crystals were collected mechanically and analyzed by X-ray crystallography.

Elemental composition, based on single-crystal data for $C_{48}H_{40}N_6NiO_{17}Sn$ (1150.25), analytically calculated in %: C 50.12, H 3.39, N 7.31, Ni 5.13, Sn 10.35; found for the as-synthesized bulk material (in %): C 50.00, H 3.11, N 7.58, Ni 5.10, Sn 10.24.

The thermal destruction of **2** (weight losses, Δm): 80-160°C, endothermic peak 150°C (-4.7%); 270-320°C, endothermic peak 280°C (-15.7%);

320-360°C, endothermic peak 330°C (-7.7%); 360-680°C, exothermic peak 570°C (-50.2%).

Selected IR data for **2** (in cm^{-1}): 3417 ν(OH), 1723 ν(C=O), 1625 $\nu_{as}(COO^{-})$, 1589, 1518 $\nu(C–C_{Ar})$, 1427 $\nu_s(COO^{-})$, 1341 ν(C–N), 1077 ν(C–O), 1144, 940, 869 δ(CH), 537 ν(Sn–O).

The $[Ni(phen)_3][Sn(HCit)_2]\cdot 3H_2O$ (**2**) crystal data (M= 1150.26 g/mol): monoclinic, space group *P*2/*c*, *a*= 23.026(1), *b*= 11.2346(7), *c*= 18.5169(8) Å, β= 93.917(3)º, *V*= 4778.8(4) $Å^3$, *Z*= 4, *T*= 294 K, $\mu(MoK_\alpha)$= 0.998 mm^{-1}, D_{calc}= 1.599 g/cm^3, 41535 reflections measured, 9367 unique (R_{int}= 0.096, R_{sigma}= 0.082) which were used in all calculations. The final R_1 was 0.066 for 6794 reflections with I> 2σ(I)) and wR_2 was 0.164 (all data), *S*= 1.073.

Results and discussion

Complexes **1** and **2** are crystalline solids which are stable on air with the similar molar ratio Ge(Sn):citrate:Ni:phen= 1:2:1:3, molecular structures are presented in Figure 1. The crystal packing of $[Ni(phen)_3][Ge/Sn(HCit)_2]\cdot nH_2O$ is presented in Figure 2.

The thermal decomposition of **1** starts with an endotherm peak within the temperature range of 80-140°C, which is due to the elimination to the gas phase of two molecules of crystallized water. During further heating within the temperature range from 290 to 360°C, complex **1** eliminates one molecule of phenanthroline and two CO_2 molecules from the malate ligands.

The first endothermic peak on the thermogravimetric curve of **2** is due to the elimination of three water molecules to the gas phase. The second endothermic peak corresponds to the loss of two CO_2 molecules; complex **2** eliminates one molecule of phenanthroline (the third endothermic peak) within the temperature range 320-360°C.

Finally, complexes **1** and **2** undergo oxidative thermal degradation and combustion of the organic part of their molecules. According to the calculated weight loss on the thermogravimetric curve of complexes, the extensive thermal decomposition (1000°C) of **1** gives nickel(II) metagermanate while in the case of **2**, nickel(II) stannate is formed.

The IR spectra of compounds **1** and **2** were found to exhibit similar sets of absorption bands, which were compared with the data obtained for other different-metal and different-ligand bis(citrato)germanates and bis(citrate)stannates [3,4,6,7]. The presence of a free carboxyl group –COOH in the molecules of the obtained complexes is indicated by the ν(C=O) band at 1720 cm^{-1} in their IR spectra [11]. In comparison with the IR spectrum of citric acid, the spectra of complexes **1** and **2** show characteristic $\nu_{as}(COO^{-})$ and $\nu_s(COO^{-})$ bands, alkoxide type ν(C–O) bands at 1080 cm^{-1}, and Ge–O, Sn-O stretching bands.

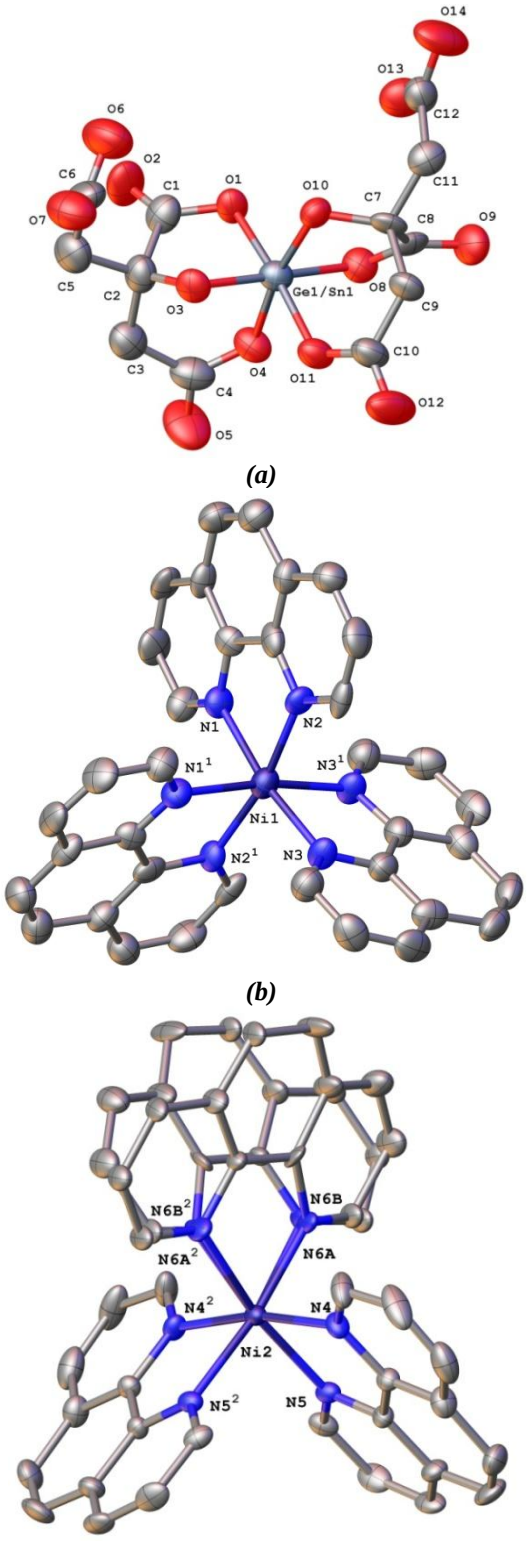

Figure 1. Molecular structure of the $[Ge/Sn(HCit)_2]^{2-}$ anion *(a)* and $[Ni(phen)_3]^{2+}$ cations of type A *(b)* and B *(c)* in structure 1, the one phen is disordered in two positions.

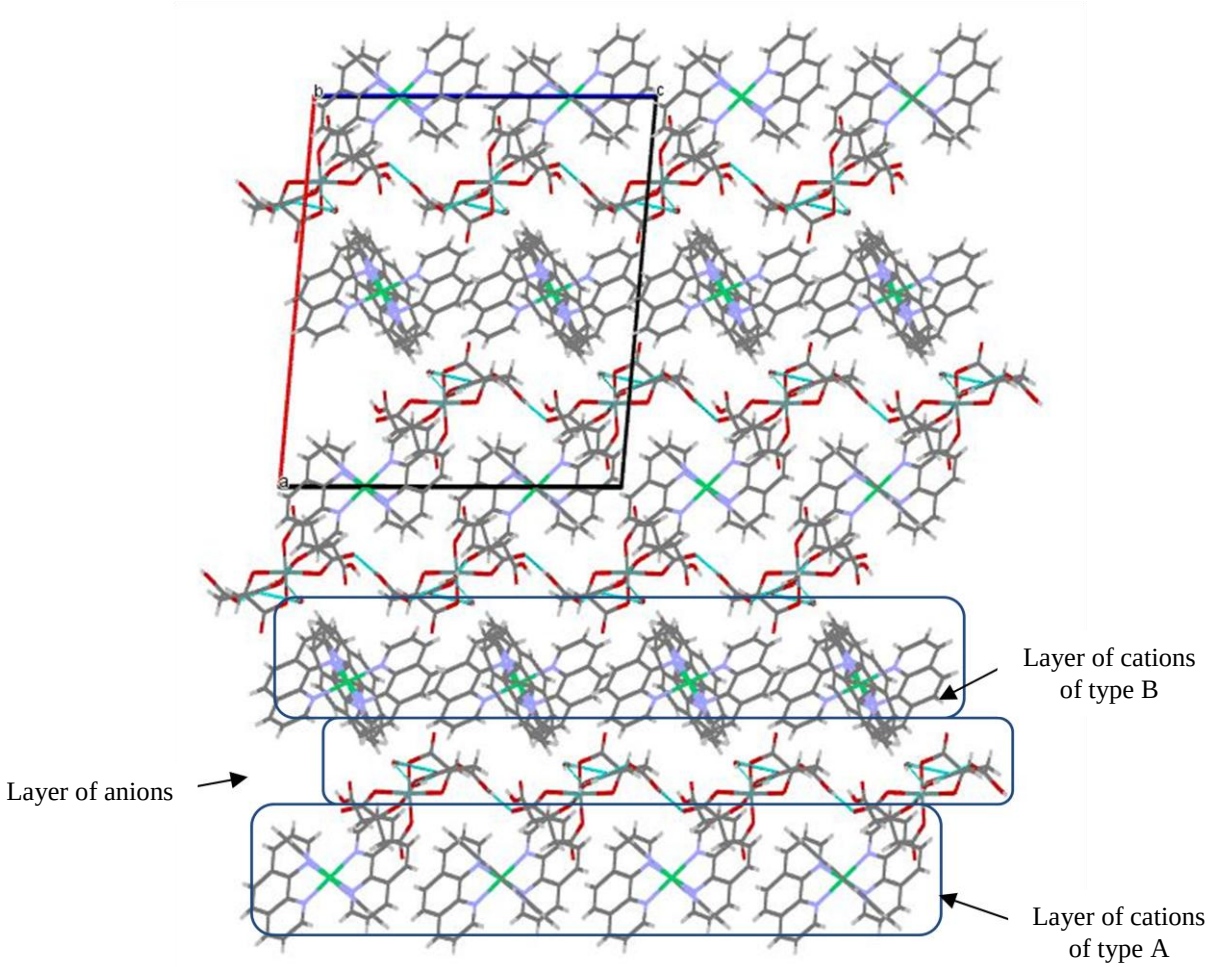

Figure 2. The crystal packing of $[Ni(phen)_3][Ge/Sn(HCit)_2]\cdot nH_2O$. View along the *b* crystallographic axis.

The absorption band at ~1340 cm^{-1} can be assigned to the ν(CN) heterocycle, the bands at ~1588, 1518 cm^{-1} - to the ν(C-C) phenanthroline ring vibrations. There are found deformation vibrations δ(C-H) of the aromatic rings: planar vibrations at 1041 cm^{-1}; non-planar vibrations at region 987-905 cm^{-1} [12].

The $[Ni(phen)_3][Ge/Sn(HCit)_2]\cdot nH_2O$ **1** and **2** were found to be complex salts that exist as hydrates in crystal phase. The bis(citrate)germanate $[Ge(HCit)_2]^{2-}$ in **1** and bis(citrate)stannate $[Sn(HCit)_2]^{2-}$ in **2** carries out the role of dianion while nickel $[Ni(phen)_3]^{2+}$ complexes are cations in both compounds. There are two parts of cations in the independent part of the unit cell in both structures. This is caused by the fact that Ni atoms are located in a special position on the 2-fold axis. Such a structure of compounds **1** and **2** is very similar to the previously described complexes [6].

The coordination polyhedrons of Ge/Sn atoms in **1** and **2** are distorted octahedrons, which are formed by two trident chelate $HCit^{3-}$ ligands. As a result, three pairs of different types oxygen atoms coordinate Ge/Sn atoms: hydroxyl (the O3 ad O10 atoms), α-carboxylate (the O1 and O8), β-carboxylate (the O4 and O11 atoms) (Figure 1*(a)*). The Ge-O bond lengths in **1** are not equivalent to the ones obtained previously in related structures [3,6]. The lengths of Ge1-O3 and Ge1-O10 hydroxyl bonds are shorter than the carboxylate bonds (Table 1). In the germanium complex Ge1-O1 coordinative bonds with one ligand are different: the bond with the α-carboxylate oxygen atom is slightly shorter than the bond with the β-carboxylate oxygen atom (Table 1). Similar coordinative bonds with another ligand are very close. It should be noted, that all coordinative bonds with carboxylate oxygen atoms are almost equal in the complex with the tin atom. The values of O—Ge/Sn—O bond angles in **1** and **2** varies within 81.9(2)–98.5(2)°.

The coordination of the Ge atom in **1** and the Sn atom in **2** by the organic ligands forms two five- and two six-membered metallocycles.

The Ge1-O4-C4-C3-C2-O3 and Ge1-O11-C10-C9-C8-O10 or Sn1-O4-C4-C3-C2-O3 and Sn1-O11-C10-C9-C8-O10 six-membered cycles adopt a half-chair conformation. Corresponding puckering parameters and atom deviations, and hydrogen bonds geometrical characteristics are given in Tables 2 and 3. Five-membered cycles in structures **1** and **2** adopt an envelope conformation. The O3 and O10 atoms in **1** and **2** deviate from the mean-square plane of the remaining atoms of the corresponding cycles by 0.56 Å, -0.58 Å and 0.63Å, -0.83Å, respectively.

Ni atoms are coordinated by three molecules of phenanthroline in cations of the structures **1** and **2**. The location of Ni atoms in a special position causes the fact that only 1.5 phenanthroline molecules are symmetrically independent (Figure 1*(b)*). One of the 1,10-phenanthroline molecules is disordered over two positions with equal populations due to symmetrical position relatively the 2-fold axis in the cation B of structure **1** (Figure 1*(c)*).

Table 1

Selected bond lengths (Å) and bond angles (°) in structures 1 and 2.

*Structure **1***			
Bond	*Bond length, Å*	*Bond*	*Bond length, Å*
Ge1—O1	1.909 (5)	Ni1—N2	2.075 (6)
Ge1—O3	1.808 (5)	Ni1—N3	2.072 (6)
Ge1—O4	1.940 (5)	Ni2—N4	2.108 (7)
Ge1—O8	1.925 (5)	Ni2—N5	2.084 (7)
Ge1—O10	1.824 (5)	Ni2—N6A	2.178 (11)
Ge1—O11	1.920 (6)	Ni2—N6B	2.03 (2)
Ni1—N1	2.111 (6)		
Bond angle	*Bond angle value, deg*	*Bond angle*	*Bond angle value, deg*
O1—Ge1—O4	88.6 (2)	N2—Ni1—N1	80.0 (2)
O1—Ge1—O8	89.8 (2)	N3—Ni1—N1^{1}	95.6 (2)
O3—Ge1—O1	86.7 (2)	N3—Ni1—N2^{1}	94.3 (2)
O3—Ge1—O4	92.6 (2)	N3—Ni1—N2	94.0 (2)
O3—Ge1—O10	98.5 (2)	N4^{2}—Ni2—N6A^{2}	98.9 (5)
O3—Ge1—O11	92.3 (2)	N4^{2}—Ni2—N6A	89.2 (5)
O8—Ge1—O4	83.8 (2)	N4—Ni2—N6A	98.9 (5)
O10—Ge1—O1	94.7 (2)	N5^{2}—Ni2—N4	93.2 (3)
O10—Ge1—O8	85.3 (2)	N5—Ni2—N4	79.0 (3)
O10—Ge1—O11	91.6 (2)	N5^{2}—Ni2—N5	90.7 (4)
O11—Ge1—O4	85.3 (2)	N5—Ni2—N6A	93.8 (4)
O11—Ge1—O8	90.9 (2)	N6A—Ni2—N6A^{2}	84.2 (8)
N1—Ni1—N1^{1}	90.5 (3)	N6B—Ni2—N4	90.8 (5)
N2—Ni1—N1^{1}	92.4 (2)		
*Structure **2***			
Bond	*Bond length, Å*	*Bond*	*Bond length, Å*
Sn1—O1	2.065 (4)	Ni1—N1	2.102 (5)
Sn1—O3	1.993 (4)	Ni1—N2	2.095 (5)
Sn1—O4	2.075 (4)	Ni1—N3	2.073 (3)
Sn1—O8	2.077 (3)	Ni2—N4	2.096 (5)
Sn1—O10	2.003 (4)	Ni2—N5	2.091 (4)
Sn1—O11	2.054 (4)	Ni2—N6	2.077 (4)
Bond angle	*Bond angle value, deg*	*Bond angle*	*Bond angle value, deg*
O1—Sn1—O4	87.23 (17)	N2—Ni1—N1^{3}	93.3 (2)
O1—Sn1—O8	92.87 (15)	N2—Ni1—N1	79.4 (2)
O3—Sn1—O1	81.97 (15)	N3—Ni1—N1^{3}	95.62 (19)
O3—Sn1—O4	89.46 (16)	N3—Ni1—N2	93.6 (2)
O3—Sn1—O11	95.07 (14)	N5^{2}—Ni2—N4	92.83 (17)
O4—Sn1—O8	87.30 (16)	N5—Ni2—N4	79.56 (17)
O10—Sn1—O1	97.40 (16)	N6—Ni2—N4	94.76 (17)
O10—Sn1—O8	81.02 (15)	N6—Ni2—N5	94.73 (17)
O10—Sn1—O11	88.45 (15)	N6—Ni2—N5^{2}	93.60 (17)
O11—Sn1—O4	87.40 (16)	N6—Ni2—N6^{2}	79.7 (2)
O11—Sn1—O8	89.78 (15)		

^{1} *-x+2, y, -z+3/2;* ^{2} *-x+1, y, -z+1/2,* ^{3} *-x, y, -z+1/2*

Table 2

The conformational characteristics of metalocycles in anions of structures 1 and 2.

Cyclic atoms	*Mean plane accuracy, Å*	*Atom/Deviations from the mean plane, Å*	*Puckering parameters [13]*		
			S	*θ, °*	*ψ, °*
*Structure **1***					
Ge1–O4–C4–C3–C2–O3	0.02	C2 -0.3 O3 0.61	0.93	49.66	25.41
Ge1–O11–C10–C9–C8–O10	0.02	C8 -0.29 O10 0.61	0.97	32.65	26.21
*Structure **2***					
Sn1–O4–C4–C3–C2–O3	0.03	C2 -0.4 O3 0.63	0.96	52.18	26.91
Sn2–O11–C10–C9–C8–O10	0.02	C8 -0.31 O10 0.62	1.0	29.38	28.34

Table 3

The hydrogen bonds geometrical characteristics for structures 1 and 2.

D—H···A	*H···A, Å*	*D···A, Å*	*D—H···A, °*
*Structure **1***			
O7—H7···O9[1]	1.79	2.600 (9)	171
C41—H41···O13	2.30	3.227 (13)	171
O15—H15A···O6	2.08	2.903 (10)	164
O15—H15B···O10	1.99	2.823 (8)	166
O16—H16A···O5	2.01	2.860 (10)	178
O16—H16B···O15[2]	2.02	2.815 (10)	155
*Structure **2***			
O13—H13···O17A	1.88	2.692 (10)	168
O13—H13···O17B	2.13	2.71 (3)	128
O15—H15A···O10	2.00	2.801 (7)	161
O16—H16A···O15	2.09	2.857 (9)	150
O17A—H17A···O5[3]	2.01	2.808 (11)	156
O17B—H17C···O16	2.10	2.90 (2)	157

[1] *x, -y+1, z+1/2;* [2] *x, y-1, z;* *x,* [3] *-y+2, z-1/2.*

The Ni coordination polyhedron is octahedron in all cations of the structures **1** and **2**. The Ni1-N bond lengths vary within the range of 2.073(6)-2.111(6) Å, and Ni2-N bonds have the lengths about of 2.077(4)-2.179(10) Å in structures **1** and **2**. The former bond lengths are well within the expected values, as revealed by a search in the CSD [13] for structures containing $[Ni(phen)_3]^{2+}$ cations (162 entries; range 2.04-2.19 Å). The N-Ni1-N bond angles vary within 80.0(2)-95.6(3)° in the cation of type A and within 79.0(3)-99.1(5)° in the cation of type B in structures **1** and **2** (Table 1).

In the crystal phase anions, cations, and water molecules of compounds **1** and **2** form alternate layers, which are parallel to the *bc* crystallographic plane (Figure 2). The layers can be divided into three types: 1) layers containing only anions; 2) layers containing cations of type A; 3) layers consisting of cations of type B. The anions within the layer are bound by the O—H···O intermolecular hydrogen bonds (as shown in Table 3).

Conclusions

Complexes of germanium(IV) and nickel(II) with citric acid and 1,10-phenanthroline were synthesized. The method of synthesis of tris(phenanthroline)nickel(II) bis(citrate)stannate using complex $[Ni(H_2O)_6][Sn(HCit)_2]\cdot 4H_2O$ as a starting compound was proposed for the first time. It was established, that $[Ge/Sn(HCit)_2]^{2-}$ anions with similar structure take part in the formation of obtained compounds. The coordination polyhedrons of the Ge/Sn are octahedral and are formed by three pairs of oxygen atoms of different types of two $HCit^{-3}$ ligands. The structure of these compounds is very similar to the structure of complexes $[Co(phen)_3][Ge(HCit)_2]\cdot 2H_2O$ and $[Fe(phen)_3][Ge(HCit)_2]\cdot 4H_2O$, that have been previously described by the authors. Changing of

metal from Co and Fe to Ni in the structure of cation does not influence the type and structure of formed bis(citrato)germanates.

References

1. Koenigsberger, L.C.; Koenigsberger, E.; May, P.M.; Hefter, G.T. Complexation of iron(III) and iron(II) by citrate. Implications for iron speciation in blood plasma. Journal of Inorganic Biochemistry, 2000, 78(3), pp. 175–184. DOI: https://doi.org/10.1016/S0162-0134(99)00222-6
2. Kluska, M. Some aspects of the analysis of biologically active organogermanium substances. Critical Reviews in Analytical Chemistry, 2008, 38(2), pp. 84–92. DOI: https://doi.org/10.1080/10408340701804459
3. Martsinko, E.E.; Minacheva, L.Kh.; Pesaroglo, A.G.; Seifullina, I.I.; Churakov, A.V.; Sergienko, V.S. Bis(citrato)germanates of bivalent 3d metals (Fe, Co, Ni, Cu, Zn): crystal and molecular structure of $[Fe(H_2O)_6][Ge(HCit)_2]\cdot 4H_2O$. Russian Journal of Inorganic Chemistry, 2011, 56(8), pp. 1243–1249. DOI: https://doi.org/10.1134/S0036023611080171
4. Martsinko, E.E.; Minacheva, L.Kh.; Chebanenko, E.A.; Seifullina, I.I.; Sergienko, V.S.; Churakov, A.V. The Conditions of formation of heterometallic complexes in the $GeCl_4$ ($SnCl_4$)–citric acid–$M(CH_3COO)_2$–H_2O systems. The crystal and molecular structures of $[M(H_2O)_6][Ge(HCit)_2]\cdot 4H_2O$ (M= Mg, Mn, Co, Cu, Zn) and $[M(H_2O)_6][Sn(HCit)_2]\cdot 4H_2O$ (M = Mg, Co, Ni). Russian Journal of Inorganic Chemistry, 2013, 58(5), pp. 515–522. DOI: https://doi.org/10.1134/S003602361305015X
5. Seifullina, I.I.; Martsinko, E.E.; Afanasenko, E.V. Design and synthesis of new homo- and heterometal coordination compounds of germanium(IV) for preparation of low toxic drugs with a wide therapeutic action. Odessa National University Herald. Chemistry, 2015, 20(4(56)), pp. 6–17. DOI: https://dx.doi.org/10.18524/2304-0947.2015.4(56).56690
6. Seifullina, I.I.; Martsinko, E.E.; Chebanenko, E.A.; Pirozhok, O.V.; Dyakonenko, V.V.; Shishkina, S.V. Synthesis, thermal stability, and structure of bis(citrato)germanates: $[Co(Phen)_3][Ge(HCit)_2]\cdot 2H_2O$, $[Fe(Phen)_3][Ge(HCit)_2]\cdot 4H_2O$ (H_4Cit= citric acid, phen= 1,10-phenanthroline). Russian Journal of Coordination Chemistry, 2017, 43(8), pp. 505–511. DOI: https://doi.org/10.1134/S1070328417080061
7. Seifullina, I.I.; Martsinko, E.E.; Chebanenko, E.A.; Pirozhok, O.V.; Dyakonenko, V.V.; Shishkina, S.V. Structure of bis(citrato)germanates with different types of cations: $(Hphen)_2[Ge(HCit)_2\cdot 3H_2O]$, $[CuCl(phen)_2]_2[Ge(HCit)_2\cdot 6H_2O]$, where H_4Cit is citric acid, phen is 1,10-phenanthroline. Journal of Structural Chemistry, 2017, 58(3), pp. 532–538. DOI: https://doi.org/10.1134/S0022476617030143
8. Shi, F.-N.; Cunha-Silva, L.; Hardie, M.J.; Trindade, T.; Paz, F.A.A.; Rocha, J. Heterodimetallic germanium(IV) complex structures with transition metals. Inorganic Chemistry, 2007, 46(16), pp. 6502–6515. DOI: 10.1021/ic700507j
9. Sheldrick, G.M. A short history of SHELX. Acta Crystallographica Section A, 2008, A64, pp. 112–122. DOI: https://doi.org/10.1107/S0108767307043930
10. CCDC, The Cambridge Crystallographic Data Centre, 12 Union Road, Cambridge, CB2 1EZ, UK, 44 1223 336408. E-mail: deposit@ccdc.cam.ac.uk https://www.ccdc.cam.ac.uk/
11. Bellamy, L.J. The Infra-Red Spectra of Complex Molecules. London: Chapman and Hall. 1975, 433 p. DOI: 10.1007/978-94-011-6017-9
12. Tarasevich, B.N. Infrared Spectra Of Basic Class Of Organic Compounds. Reference Materials. Moscow, 2012, 54 p. (in Russian). https://www.twirpx.com/file/1302520/
13. Zefirov, N.S.; Palyulin, V.A.; Dashevskaya, E.E. Stereochemical studies. XXXIV. Quantitative description of ring puckering via torsional angles. The case of six-membered rings. Journal of Physical Organic Chemistry, 1990, 3(3), pp. 147–158. DOI: https://doi.org/10.1002/poc.610030304

CHEMISTRY JOURNAL OF MOLDOVA. General, Industrial and Ecological Chemistry. 2018, 13(2), 63-68
ISSN (p) 1857-1727 ISSN (e) 2345-1688
http://cjm.asm.md
http://dx.doi.org/10.19261/cjm.2018.514

CHEMICAL COMPOSITION AND ANTIMICROBIAL ACTIVITY OF THE *LEVISTICUM OFFICINALE* W.D.J. KOCH ESSENTIAL OIL

Alexandru Ciocarlan [a,*], Ion Dragalin [a], Aculina Aricu [a], Lucian Lupascu [a], Nina Ciocarlan [b], Violeta Popescu [c]

[a]*Institute of Chemistry, 3, Academiei str., Chisinau MD 2028, Republic of Moldova*
[b]*Botanical Garden (Institute), 18, Padurii str., Chisinau MD-2002, Republic of Moldova*
[c]*Tiraspol State University, 5, Gh. Iablocikin str., Chisinau MD 2069, Republic of Moldova*
[*]*e-mail: algciocarlan@yahoo.com, phone: (+373 22) 739 769; fax: (+373 22) 739 775*

Abstract. The chemical composition of industrially obtained *Levisticum officinale* W.D.J. Koch (lovage) essential oil of Moldovan origin was analysed by means of chromatographic (GC-MS) and spectral (IR, ^{1}H and ^{13}C NMR) methods. According to gas chromatography-mass spectrometry analysis of the studied essential oil, thirty-two known and two unknown constituents were identified. The main components of *L. officinale* essential oil are monoterpenic hydrocarbons, which make up to 53.50% of the total number of components. *L. officinale* essential oil is also characterized by a high content of oxygenated monoterpenes (alcohols, cetones and esters), which reaches up to 33.60%. For the first time the presence of 6-butyl-cyclohepta-1,4-diene (0.56%) and 7-formyl-4-methyl-cumarine (0.15%) in lovage essential oil is reported. Antibacterial and antifungal activities of mentioned oil were evaluated *in vitro* on five strains of microorganisms. It was found that lovage volatile oil (*L. officinale*) exhibits high antibacterial and antifungal properties in the range of concentrations 0.015-0.030%.

Keywords: *Levisticum officinale*, essential oil, GC-MS analysis, antibacterial activity, antifungal activity.

Received: 11 September 2018/ Revised final: 10 October 2018/ Accepted: 11 October 2018

Introduction

Levisticum officinale W.D.J. Koch (Lovage) is a perennial, aromatic species belonging to *Apiaceae* family. It is native to Southwest Asia and Southern Europe [1,2], naturalized in many temperate regions and nowadays being cultivated throughout the world. All parts of the plant (seeds, leaves and roots) are strongly aromatic, being widely used in food, pharmaceutical, perfume and tobacco industries [3-5]. This plant has been used over the centuries as a traditional medicinal remedy that has spasmolytic, diuretic and carminative activities [6,7].

Many scientific studies showed antibacterial and antibiotic-potentiation [8,9], anti-inflammatory, antitumor, antioxidant [5,10,11], hepatoprotective [12], neuroprotective [13], spasmolytic and diuretic [14,15], nephroprotective and lytolytic [16] effects of *L. officinale*. These important therapeutic and flavouring properties are mainly attributed to the content of bioactive secondary metabolites, especially polyacetilenes, essential oil, polyphenols (flavonoids, phenolic acids), coumarins (furano- and pyranocoumarins), saponins and alkaloids [11,17-20]. The composition of the essential oil of *L. officinale* has been studied extensively and over 190 compounds were reported in its root, seed and leaf oil [6,9]. The main constituents of the essential oil are phthalides (butylidene-, dihydrobutyliden-, butyl- and propylidenephthalide; sedanonic anhydride; *cis*- and *trans*-ligustilide; senkyunolide; isosenkyunolide, validene-4,5-dihydrophthalide), terpenoids (α- and β-pinene, α- and β-phellandrenes, γ-terpinene, carvacrol, eugenol, and α-terpineol) and carboxylic acids (butyric, isovaleric, maleic, and angelic acids) [4,21-25].

The purpose of this paper is to establish the chemical composition and evaluate the antimicrobial activity of the essential oil of *L. officinale* cultivated industrially in climatic and soil conditions specific to Republic of Moldova.

Experimental

Materials

The sample of *L. officinale* essential oil was offered by the Moldovan-French company "*Molsalvia*" Pervomaysk village, Causeni district.

The essential oil (n^{20}_D= 1.4810) was obtained industrially by hydrodistillation of the aerial part of *L. officinale* collected in July of 2017.

Methods

The *GC-MS analysis* of the *L. officinale* essential oil was carried out on an Agilent Technologies 7890A system with 5975C Mass-Selective Detector (GC-MSD) equipped with split-splitless injector (split, 250°C, split ratio 1:50, 1 μL) and HP-5 ms capillary calibrated column (30 m x 0.25 mm x 0.25 μm); the carrier gas: helium 1.1 mL/min; oven: 70°C-2 min, 5°C/min-200°C-20/min-300°C/5 min; MSD in scan 30-300 amu, 15 min, 30-450 amu, solvent delay 3 min 40 s.

IR spectra were recorded on a Spectrum-100FT-IR spectrometer using the attenuated total reflection technique.

^1H and ^{13}C NMR spectra were acquired in $CDCl_3$ on a Bruker Avance DRX 400 spectrometer (400 MHz). All chemical shifts are quoted on the δ-scale in ppm and referred to residual $CHCl_3$ (δ_H at 7.26 ppm) and as $CDCl_3$ (δ_C at 77.00 ppm), respectively.

Antimicrobial activity assays

As test-microorganisms for the evaluation of the antimicrobial activity of lovage essential oil (*L. officinale*) were used the following: non-pathogenic Gram-positive and Gram-negative strains of *Bacillus subtilis* CNMN BB-01 and *Pseudomonas fluorescens* CNMN-PFB-01, respectively; phytopathogenic strains of *Xanthomonas campestris*, *Erwinia amylovora*, *Erwinia carotovora* and a fungus strain of *Candida utilis.*

For testing, the successive double dilution method was used. For this, at the initial stage, 1 mL of peptone broth for test bacteria and Sabouraud broth for test candida was introduced into a series of 10 tubes. Subsequently, 1 mL of the analysed preparation was dropped into the first test tube. Then, the obtained mixture was pipetted, after which 1 mL of it was transferred to the next tube, so the procedure was repeated until the tube no. 10 of the series. Thus, the concentration of the initial preparation decreased 2-fold in each subsequent tube.

At the same time, 24 hour test-microorganisms cultures were prepared.

Initially, suspensions of test microorganisms were prepared with optical densities of 2.0 for tested bacteria and 7.0 for fungus according to the McFarland index. Subsequently, 1 mL of the obtained microbial suspension was dropped in a tube containing 9 mL of sterile distilled water. The content of the tube was mixed, after which 1 mL was transferred to the tube no. 2 of the 5-tube series containing 9 mL of sterile distilled water.

From the 5-th tube of the series were taken 0.1 mL of the microbial suspension, which represent the seeded dose and added to each tube with titrated preparation. Subsequently, the tubes with titrated preparation and the seeded doses of the microorganisms were kept in the thermostat at 35°C for 24 hours. On the second day, a preliminary analysis of the results was made. The last tube from the series in which no visible growth of microorganisms has been detected is considered to be the minimal inhibitory concentration (MIC) of the preparation.

For the estimation of the minimal bactericidal and fungicidal concentrations (MBC, MFC), the contents of the test tubes with MIC and with higher concentrations are seeded on peptone and Sabouraud agar from Petri dishes with the use of the bacteriological loop. The seeded dishes are kept in the thermostat at 35°C for 24 hours. The concentration of the tested preparation that does not allow the growth of any colony of microorganisms is considered to be the minimal bactericidal and fungicidal concentrations of the preparation [26].

Results and discussion

Lovage chemical composition evaluation

According to gas chromatography-mass spectrometry analysis of studied essential oil thirty two known and two unknown constituents were identified (Figure 1).

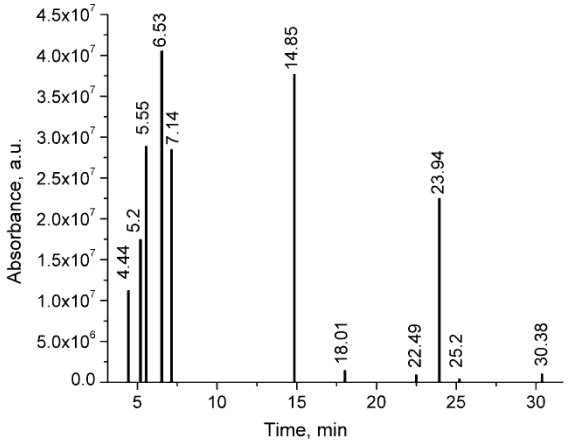

Figure 1. GC chromatogram of *L. officinale* essential oil.

It must be mentioned that the main components of *L. officinale* essential oil are monoterpenic hydrocarbons which make up to 53.50% of the total number of components (Table 1). Of these may be mentioned

β-phellandrene (22.39%), *β*-mircene (8.66%), *γ*-terpinene (6.84%), (*Z*)-*β*-ocimene (3.51%) and sabinene (3.39%) which are evidenced by a higher content.

As well, *L. officinale* essential oil is characterized by a high content of oxygenated monoterpenes (alcohols, cetones and esters) which reaches up to 33.60%. Of these, should be mentioned *α*-terpinyl acetate (30.99%), *α*-terpineol (1.11%) and geranyl acetate (0.55%). From the sesquiterpenoid series only germacrene D (0.29%) was identified.

It is significant the presence of some phtalides like (*Z*)-3-buthylidene phtalide **29** (RT= 22.428, 0.23%), (*Z*)-ligustillide **31** (RT= 23.942, 11.19%) and (*E*)-ligustillide **32** (RT= 25.201, 0.20%) (Figure 2).

For the first time, the presence of 6-butyl-cyclohepta-1,4-diene **18** (0.56%) and 7-formyl-4-methyl-cumarine **30** (0.15%) in lovage essential oil is reported (Figure 3).

The molecular mass of all identified compounds was confirmed by mass-spectrometry analysis.

Table 1

Phytochemical composition of *L. officinale* essential oil of Moldovan origin.

No.	*RT* (min)*	*Component*	*%*	***No.***	*RT* (min)*	*Component*	*%*
1	4.294	*α*-Thujene	0.578	***18***	9.641	6-Butyl-cyclohepta-1,4-diene	0.557
2	4.442	*α*-Pinene	1.998	***19***	10.187	Terpinen-4-ol	0.278
3	4.739	Camfene	0.240	***20***	10.460	Cryptone	0.130
4	5.209	Sabinene	3.396	***21***	10.533	*α*-Terpineol	1.111
5	5.298	*β*-Pinene	0.588	***22***	12.248	Linalyl acetate	0.107
6	5.550	*β*-Mircene	8.657	***23***	13.040	Bornyl acetate	0.085
7	5.866	*α*-Phellandrene	2.693	***24***	13.985	(*E*)-Sabynil acetate	0.044
8	6.001	*δ*-3-Carene	0.043	***25***	14.859	*α*-Terpinyl acetate	30.992
9	6.141	*α*-Terpinene	0.204	***26***	15.085	Perillyl alcohol	0.147
10	6.339	*p*-Cymene	1.455	***27***	15.520	Geranyl acetate	0.545
11	6.536	*β*-Phellandrene	22.393	***28***	18.010	Germacrene D	0.292
12	6.608	(*Z*)-*β*-Ocimene	3.506	***29***	22.428	(*Z*)-3-Buthylidene phtalide	0.232
13	6.836	(*E*)-*β*-Ocimene	0.204	***30***	23.484	7-Formyl-4-methyl-cumarine	0.146
14	7.149	*γ*-Terpinene	6.841	***31***	23.942	(*Z*)-Ligustillide	11.188
15	7.858	(+)-4-Carene	0.699	***32***	25.201	(*E*)-Ligustillide	0.202
16	8.134	Linalool	0.107	***33***	30.385	$[M]^+$ 258 m/z	0.142
17	8.780	(*E*)-4-Thujanol	0.050	***34***	30.471	[M]+ 286 m/z	0.084

**RT - retention time.*

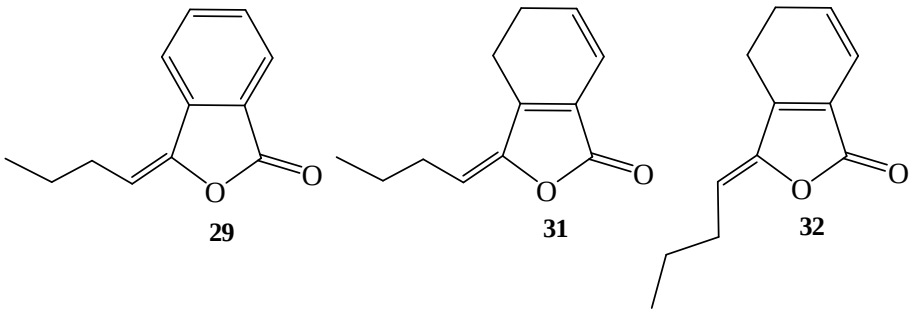

29 **31** **32**

Figure 2. The structure of (*Z*)-3-buthylidene phtalide *29*, (*Z*)-ligustillide *31* and (*E*)-ligustillide *32*.

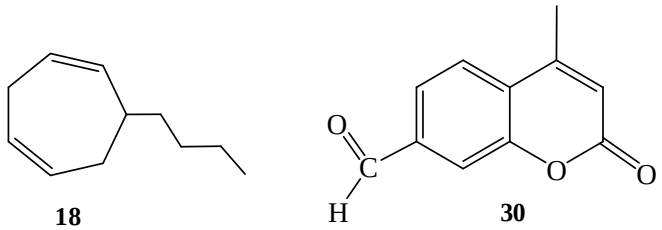

18 **30**

Figure 3. The structure of 6-butyl-cyclohepta-1,4-diene *18* and 7-formyl-4-methyl-cumarine *30*.

The presence of constituents mentioned above is confirmed by spectral analysis. Thereof, in IR spectra of *L. officinale* essential oil there are absorption peaks of exocyclic and trisubstituted double bonds from identified terpenic molecules at 3011, 1670, 1636, 1366 and 876 cm^{-1}. Peaks representing ester groups (acetates) are localized at 1730 and 1256 cm^{-1} and that from 1772 cm^{-1} confirm the presence of unsaturated lactones.

The ^{1}H NMR spectrum can be divided in 2 zones. The first one includes singlet signals of methyl groups localized in strong field: *gem*-dimethyls at 0.86-0.99 ppm, methyl groups attached to hydroxylated carbon atoms at 1.38-1.41 ppm. Singlets of the methyl groups adjacent to double bonds are visible at 1.58-1.69 ppm, and that of methyl groups from acetates are localized at 1.93 ppm. Protons of exocyclic methylene groups and those adjacent to double bonds are visible in the weaker field as doublets or broad singlets from 4.69 ppm to 6.12 ppm.

The ^{13}C NMR spectra are in accordance with proton spectra. The signal of primary carbon atoms ($-CH_3$) are localized from 19.41 ppm to 42.54 ppm, of tertiary hidroxylated carbon atoms (≥C-OH) at 84.69 ppm, of secondary exocyclic carbons ($=CH_2$) at 109.83 ppm, of tertiary unsaturated carbon atoms (-CH=CH- or >C=CH) at 120.3 ppm. The signal of quaternary carbon atoms (>C=O and lactonic) are visible at 170.28 ppm.

Antimicrobial activity evaluation

Lovage volatile oil (*L. officinale*) exhibits high antibacterial and antifungal properties in the range of concentrations 0.015-0.030% (Table 2). It can be mentioned that the antimicrobial properties of the lovage extract are due to the high content of *β*-phellandrene (RT= 6.536, 22.39%), *α*-terpinyl acetate (RT= 14.859, 30.99%) and (*Z*)–ligustillide (RT= 23.942, 11.19%). The above-mentioned compounds exhibit pronounced antimicrobial properties through mechanisms that include: breaking of the cell wall and cytoplasmic membrane, reduction of the cytoplasm around the nucleus, disturbance of the lipid fraction of the plasma membrane resulting in the alteration of its permeability and the leakage of the intracellular content [27-29].

Table 2

The antimicrobial activity *(MBC, MFC) of the oil extracted from the *Levisticum officinale* plants.**

Test-microorganisms	*Concentration (%)*							
	0.25	*0.12*	*0.06*	*0.03*	*0.015*	*0.007*	*0.0035*	*0.0017*
Bacillus subtilis CNMN BB-01 (4.8×10^8 CFU/mL)	-	-	-	-	+	+	+	+
Pseudomonas fluorescens CNMN-PFB-01 (4.8×10^8 CFU /mL)	-	-	-	-	+	+	+	+
Xanthomonas campestris (4.8×10^8 CFU /mL)	-	-	-	-	-	+	+	+
Erwinia amylovora (4.8×10^8 CFU /mL)	-	-	-	-	+	+	+	+
Erwinia carotovora (4.8×10^8 CFU /mL)	-	-	-	-	-	+	+	+
Candida utilis (3.0×10^7 CFU /mL)	-	-	-	-	+	+	+	+

* *MBC- minimal bactericidal concentration;*
MFC- minimal fungicidal concentration.

Conclusions

The qualitative (IR, ^{1}H and ^{13}C NMR) and quantitative (GC-MS) analyses of industrially obtained *Levisticum offcinale* essential oil of Moldovan origin were performed for the first time. As a result, thirty-two constituents, most of them, belonging to monoterpens, their derivatives and sesquiterpenoids with the total content of 87.30% were identified, together with some specific for the mentioned species butyl phtalides (11.62%). The *in vitro* tests have shown that the minimal bactericidal and fungicidal concentrations of oil extracted from *L. officinale* against *B. subtilis*, *P. fluorescens*, *X. campestris*, *E. amylovora*, *E. carotovora* and *C. utilis* are quite low 0.015-0.03%, which denotes its high antibacterial and antifungal activity.

Acknowledgements

The authors are grateful to the Institute of Genetics, Physiology and Plant Protection and the National Collection of Non-Pathogenic Microorganisms of the Institute of Microbiology and Biotechnology for the offering of the microbial strains for testing.

References

1. Downie, S.R.; Plunkett, G.M.; Watson, M.F.; Spalik, K.; Katz-Downie, D.S.; Valiejo-Roman, C.M.; Terentieva, E.I.; Troitsky, A.V.; Lee, B.-Y.; Lahham, J.; El-Oqlah, A. Tribes and clades within *Apiaceae* subfamily *Apioideae*: the contribution of molecular data. Edinburgh Journal of Botany, 2001, 58(2), pp. 301-330. DOI: https://doi.org/10.1017/S0960428601000658
2. Tutin, T.G.; Heywood, V.H.; Burges, N.A.; Moore, D.M.; Valentine, D.H.; Walters, S.M.; Webb, D.A. Flora Europaea. Cambridge: University Press, 1968, 2, 486 p. https://www.cambridge.org/
3. Bylaitė, E.; Venskutonis, R.P.; Roozen, J.P. Influence of harvesting time on the composition of volatile components in different anatomical parts of lovage (*Levisticum officinale* Koch). Journal of Agricultural and Food Chemistry, 1998, 46(9), pp. 3735-3740. DOI: http://dx.doi.org/10.1021/jf9800559
4. Preedy, V.R. Essential oils in food preservation, flavor and safety. Elsevier: Oxford, 2016, pp. 539-549. DOI: https://doi.org/10.1016/C2012-0-06581-7
5. Kemzūraitė, A.; Venskutonis, P.R.; Navikienė, D. Processing of lovage into high-value components using supercritical CO_2 and pressurized liquid extraction. Chemical Engineering & Technology, 2014, 37(11), pp. 1854-1860. DOI: https://doi.org/10.1002/ceat.201300735
6. Moradalizadeh, M.; Akhgar, M.R.; Rajaei, P.; Faghihi-Zarandi A. Chemical composition of the essential oils of *Levisticum officinale* growing wild in Iran. Chemistry of Natural Compounds, 2012, 47(6), pp. 1007-1009. DOI: https://doi.org/10.1007/s10600-012-0130-7
7. Peter, K.V. Handbook of Herbs and Spices. Woodhead Publishing Ltd.: Cambridge, 2006, vol. 3, 568 p. https://www.elsevier.com/books/handbook-of-herbs-and-spices/peter/978-1-84569-017-5
8. Ebrahimi, A.; Eshraghi, A.; Mahzoonieh, M.R.; Lotfalian, S. Antibacterial and antibiotic-potentiation activities of *Levisticum officinale L.* extracts on pathogenic bacteria. International Journal of Infection, 2017, 4(2), e38768. DOI: 10.5812/iji.38768
9. Mirjalili, M.H.; Salehi, P.; Sonboli, A.; Hadian, J.; Ebrahimi, S.N.; Yousefzadi, M. The composition and antibacterial activity of the essential oil of *Levisticum officinale* Koch flowers and fruits at different developmental stages. Journal of the Serbian Chemical Society, 2010, 75(12), pp. 1661-1669. DOI: 10.2298/JSC100524126M
10. Abd El-Hamid, S.R.; Abeer, Y.I.; Hendawy, S.F. Anti-inflammatory, antioxidant, anti-tumor and physiological studies on *Levisticum officinale*-Koch plant. Planta Medica, 2009, 75(09), PE62. DOI: 10.1055/s-0029-1234623
11. Popa, C.V.; Lungu, L.; Savoiu, M.; Bradu, C.; Dinoiu, V.; Danet, A.F. Total antioxidant activity and phenols and flavonoids content of several plant extracts. International Journal of Food Properties, 2012, 15(3), pp. 691-701. DOI: https://doi.org/10.1080/10942912.2010.498545
12. Afarnegan, H.; Shahraki, A.; Shahraki, J. The hepatoprotective effects of aquatic extract of *Levisticum officinale* against paraquat hepatocyte toxicity. Pakistan Journal of Pharmaceutical Sciences, 2017, 30(6), pp. 2363-2369. http://www.pjps.pk/?page_id=258&type=1
13. Mahmoudzehi, S.; Dorrazehi, G.M.; Jamalzehi, S.; Khabbaz, A.H.H.; Ghorbani, F.; Hooti, A.; Dadkani, A.G.; Souran, M.M. The neuroprotective effects of alcoholic extract of *Levisticum officinale* on alpha motoneurons degeneration after sciatic nerve compression in male rats. International Journal of Medical Research & Health Sciences, 2016, 5(9s), pp. 647-653. https://www.ijmrhs.com/archive/ijmrhs-vol-5-issue-9-specialissue-2016.html
14. Yarnell, E. Botanical medicines for the urinary tract. World Journal of Urology, 2002, 20(5), pp. 285-293. DOI: https://doi.org/10.1007/s00345-002-0293-0
15. Segebrecht, S.; Schilcher, H. Ligustilide: guiding component for preparations of *Levisticum officinale* roots. Planta Medica, 1989, 55(6), pp. 572-573. DOI: 10.1055/s-2006-962102
16. Naber, K.G. Efficacy and safety of the phytotherapeutic drug Canephron® N in prevention and treatment of urogenital and gestational disease: review of clinical experience in Eastern Europe and Central Asia. Research and Reports in Urology, 2013, 5, pp. 39-46. DOI: https://doi.org/10.2147/RRU.S39288.
17. Schinkovitz, A.; Stavri, M.; Gibbons, S.; Bucar, F. Antimycobacterial polyacetylenes from *Levisticum officinale*. Phytotherapy Research, 2008, 22(5), pp. 681–684. DOI: https://doi.org/10.1002/ptr.2408
18. Christensen, L.P.; Brandt, K. Bioactive polyacetylenes in food plants of the *Apiaceae* family: occurrence, bioactivity and analysis. Journal of Pharmaceutical and Biomedical Analysis, 2006, 41(3), pp. 683-693. DOI: https://doi.org/10.1016/j.jpba.2006.01.057
19. Ceska, O.; Chaudhary, S.K.; Warrington, P.J.; Ashwood-Smith, M.J. Photoactive furocoumarins in fruits of some *Umbellifers*. Phytochemistry, 1986, 26(1), pp. 165–169. DOI: https://doi.org/10.1016/S0031-9422(00)81503-4
20. Najda, A.; Wolski, T.; Dyduch, J.; Baj, T. Determination of quantitative composition of polyphenolic compounds occur in anatomically different parts of *Levisticum officinale* Koch. Electronic Journal of Polish Agricultural Universities, Series Horticulture, 2003, 6(1), 02. http://www.ejpau.media.pl/volume6/issue1/horticulture/art-02.html

21. Gijbels, M.J.M.; Scheffer, J.J.C.; Svendsen, A.B. Phthalides in the essential oil from roots of *Levisticum officinale*. Planta Medica, 1982, 44(4), pp. 207-211. DOI: 10.1055/s-2007-971448
22. Raal, A.; Arak, E.; Orav, A.; Kailas, T.; Müürisepp, M. Composition of the essential oil of *Levisticum officinale* W.D.J. Koch from some European countries. Journal of Essential Oil Research, 2008, 20(4), pp. 318-322. DOI: https://doi.org/10.1080/10412905.2008.9700022
23. Hogg, C.L.; Svoboda, K.P.; Hampson, J.B.; Brocklehurst, S. Investigation into the composition and bioactivity of essential oil from lovage (*Levisticum officinale* W.D.J. Koch). International Journal of Aromatherapy, 2001, 11(3), pp. 144-151. DOI: https://doi.org/10.1016/S0962-4562(01)80050-3
24. Szebeni-Galambosi, Zs.; Galambosi, B.; Holm, Y. Growth, yield and essential oil of lovage grown in Finland. Journal of Essential Oil Research, 1992, 4(4), pp. 375-380. DOI: https://doi.org/10.1080/10412905.1992.9698088
25. Santos, P.A.G.; Figueiredo, A.C.; Oliveira, M.M.; Barroso, J.G.; Pedro, L.G.; Deans, S.G.; Scheffer, J.J.C. Growth and essential oil composition of hairy root cultures of *Levisticum officinale* W.D.J. Koch (Lovage). Plant Science, 2005, 168(4), pp. 1089-1096. DOI: https://doi.org/10.1016/j.plantsci.2004.12.009
26. Method of serial dilutions in broth. Saint-Petersburg Pasteur Institute. http://www.dntpasteur.ru/metodic2_4_2_2.php (in Russian).
27. Li, L.; Shi, C.; Yin, Z.; Jia, R.; Peng, L.; Kang, S.; Li, Z. Antibacterial activity of *α*-terpineol may induce morphostructural alterations in *Escherichia coli*. Brazilian Journal of Microbiology, 2014, 45(4), pp. 1409-1413. DOI: http://dx.doi.org/10.1590/S1517-838220140 00400035
28. Ait-Ouazzou, A.; Cherrat, L.; Espina, L., Lorán, S.; Rota, C.; Pagán, R. The antimicrobial activity of hydrophobic essential oil constituents acting alone or in combined processes of food preservation. Innovative Food Science & Emerging Technologies, 2011, 12(3), pp. 320-329. DOI: https://doi.org/10.1016/j.ifset.2011.04.004
29. Trombetta, D.; Castelli, F.; Sarpietro. M.G.; Venuti, V.; Cristani, M.; Daniele, C.; Saija, A.; Mazzanti, G.; Bisignano. G. Mechanisms of antibacterial action of three monoterpenes. Antimicrobial Agents and Chemotherapy, 2005, 49(6), pp. 2474-2478. DOI: 10.1128/AAC.49.6.2474-2478.2005

CHEMISTRY JOURNAL OF MOLDOVA. General, Industrial and Ecological Chemistry. 2018, 13(2), 69-73
ISSN (p) 1857-1727 ISSN (e) 2345-1688
http://cjm.asm.md
http://dx.doi.org/10.19261/cjm.2018.494

ADSORPTION OF STRONTIUM IONS FROM AQUEOUS SOLUTIONS ON NUT SHELLS ACTIVATED CARBONS

Gheorghe Duca, Mihai Ciobanu, Tudor Lupascu, Igor Povar *

Institute of Chemistry, 3, Academiei str., Chisinau MD 2028, Republic of Moldova
**e-mail: ipovar@yahoo.ca; phone: (+373) 22 73 97 36*

Abstract. The adsorption of strontium ions from aqueous solutions on nut shells activated carbons (samples CAN-7 and CAN-8) at different temperatures has been studied. The isotherm of adsorption of strontium ions from aqueous solutions on activated carbon CAN-7 has two inflection points at relatively small and high equilibrium concentrations. As the temperature increases, the adsorption values decrease, which indicates that the adsorption process is exothermic.

Keywords: activated carbon, adsorption heat, entropy, exothermic process, strontium ion.

Received: 30 May 2018/ Revised final: 02 July 2018/ Accepted: 02 July 2018

Introduction

It is known that the carbon adsorbents obtained from olive stones have an enhanced adsorption capacity to Pb^{2+}, and those obtained from almond shells have a competitive adsorbent capacity [1-2]. The adsorption capacity depends on the metal used, being in the following order: $Tl^{+} > Sr^{2+} > Co^{2+} > Cs^{+}$ [1-2]. Rivera-Utrilla, J. and Ferro-Garcia, M.A. stated that with increasing activation time, the adsorption of cobalt ions from solutions increases [2]. The activated carbon made from almond shells with a specific surface area of 1820 m^2/g has an enhanced adsorbent capacity to cobalt ions. In another publication the adsorption of zinc, cadmium and copper ions on activated carbon, obtained from almond shells, olive kernels and peach kernels, has been studied, which showed that the obtained activated carbons had on their surface basic acidic functional groups and high values of specific surfaces [3]. The nature of the raw material for the activated carbons production has an important role in the adsorption process of heavy metal cations from aqueous solutions. It is stated that the adsorption of Zn^{2+} and Cd^{2+} ions on these adsorbents decreases with increasing temperature (exothermic effect), while the adsorption of copper ions on the same adsorbents increases (endothermic effect) [3]. Another research team studied the adsorption of strontium ions from aqueous solutions on various adsorbents obtained from the chemically treated almond green shells [4]. The adsorbent capacity of this adsorbent was investigated in two ways: different chemical treatment and different adsorbent content and different concentration of Sr^{2+} ions in the solution. The optimal dose of adsorbent for the maximum Sr^{2+} ion adsorption was 0.3 g at 102 mg/L of solution. Removal of Sr^{2+} ions from aqueous solutions on activated carbon obtained from almond hull was studied as well [5]. The obtained experimental results demonstrate a good fitting of the points (R^2= 0.9806) into linear coordinates of the Langmuir model. Probably, the activated carbon prepared from almond shells, according to the technology presented herein, has homogeneous adsorption centres. In the paper [6], the study of the adsorption of strontium ions on activated carbon demonstrated the endothermicity of the adsorption process, the isotherm of adsorption being described by the Freundlich model.

The purpose of this paper is to present the study of the adsorption of strontium ions from aqueous solutions on two samples of activated carbons obtained from nut shells by chemical activation with phosphoric acid (CAN-7) and water vapour activation (CAN-8). Previously, this process has been studied in order to assess the possibility of using CAN-7 activated carbon for the removal of strontium ions from groundwater (Hirjauca water, Calarasi district, Republic of Moldova [7]).

Experimental

Materials

Two samples of activated carbons from nut shells were used for studies: *(i)* CAN-7, obtained by chemical activation with phosphoric acid (at 460°C) and *(ii)* CAN-8, prepared by the

physico-chemical method of activation with water vapours (at 960°C). Activated carbon fractions of 0.8-1.0 mm were used for adsorption studies.

Strontium nitrate of reagent grade was used for the adsorption studies.

Methods

The adsorption isotherms of strontium ions on activated carbon were determined at various concentrations of strontium ions in solution, a constant solid/liquid ratio and different temperatures (25-65°C). The equilibrium concentration of strontium ions in solutions was determined on the AAS-1 spectrophotometer.

The *differential isosteric adsorption heat (Q)* at different values of the specific adsorption *a* was calculated based on the Clausius–Clapeyron equation (Eq.(1)).

$$Q = R\left(\frac{\partial lnC}{\partial \frac{1}{T}}\right)_a = 2.303\ R\left(\frac{\partial lnC}{\partial \frac{1}{T}}\right)_a \qquad (1)$$

The value $\partial \log C / \partial \frac{1}{T}$ was determined as the angle of inclination of the adsorption isostere at the axis 1/T.

The *standard adsorption entropy* (ΔS^0) of strontium ions on activated carbon was determined by Eq.(2) [7].

$$\Delta S^0 = -\frac{Q^0}{T} + R\ lnK_2 \qquad (2)$$

where, ΔS^0 is the standard variation of entropy;

Q^0 means the standard isosteric heat of adsorption;

K_2 is the equilibrium adsorption constant.

Results and discussion

The structure parameters of activated carbons obtained from nut shells by various activation methods are shown in Table 1. The parameters W_0, E_0 and X_0 were determined on the basis of the benzene vapour adsorption isotherm using the Dubinin–Radushkevich equation. The specific surface area (S_{sp}) of the activated carbon CAN-8 is 708 m^2/g. If we compare the structure parameters of these two activated carbons, then we find that the activated carbon CAN-8 has a much smaller share of very small pores (X_0= 0.44 nm), while on CAN-7 sample X_0= 2.18 nm, where X_0 is the half-width of micropores.

Figure 1 shows the adsorption isotherm of strontium ions from aqueous solutions on the activated carbon CAN-7. As shown in Figure 1, the presented isotherm has inflection points even at higher values of the equilibrium concentrations. The isotherm of adsorption of strontium ions in the coordinates of $log(C_{ads}/C_e)$ *vs.* $f(C_e)$ is shown in Figure 2. The $logK_{ads}$ value was graphically obtained by extrapolating the curve $log(C_{ads}/C_e)= f(C_e)$ to $C_e= 0$.

Table 1

Structure parameters of activated carbons determined from benzene sorption-desorption isotherms, by Dubinin–Radushkevich equation*.

Sample	W_0, cm^3/g	E_0, *kJ/mol*	X_0, *nm*	S_{me}, m^2/g	V_{me}, cm^3/g	S_{sp}, m^2/g
CAN-7	0.24	15.72	2.18	210	0.24	725
CAN-8	0.35	22.77	0.44	166	0.23	708

**W_0- micropore volume;*
E_0- adsorption energy in micropores;
X_0- half width of micropore;
S_{me}- surface of mesopores;
V_{me}- mesopores volume;
S_{sp}- specific surface area.

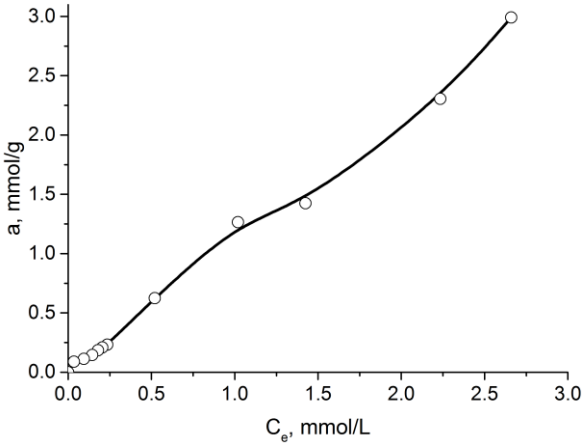

Figure 1. Adsorption isotherm of strontium ions from aqueous solutions on the activated carbon CAN-7.

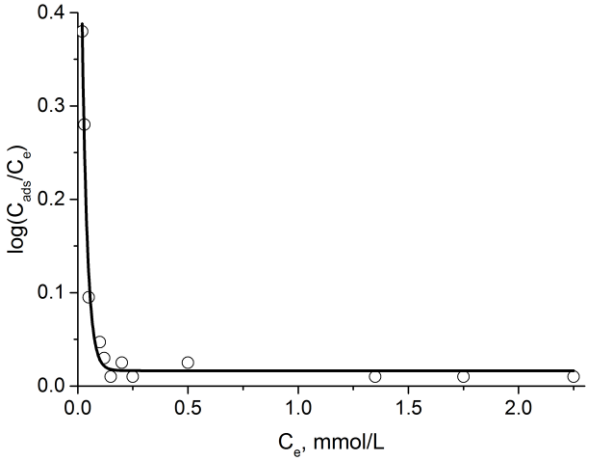

Figure 2. The isotherm of adsorption of strontium ions from aqueous solutions on the activated carbon CAN-7, in the coordinates of $log(C_{ads}/C_e)$ *vs.* C_e, at t= 25°C.

The calculation of the adsorption equilibrium constant for strontium ions has been done based on the concept presented in paper [5], from which it follows that the adsorption equilibrium constant equals to 2 and, respectively, the ΔG_0 value is 0.5 kJ/mol ($\Delta G_0 = RTlnK_{ads}$). According to the data presented in the paper [7] for the carbonic adsorbent - water interface ΔG_0 for H_2O is equal to 2.3 kJ/mol. The adsorbent with a lower standard molar differential free energy of adsorption (ΔG_0) less than the solvent (water) cannot displace it from the surface of the adsorbent (from its pores), however strontium ions are adsorbed at relatively high equilibrium concentrations, the value of adsorption of these ions being considerable (Figure 1). This phenomenon is explained by the fact that at low equilibrium concentrations strontium ions interact with the water molecules in the porous structure of activated carbon CAN-7 forming the $Sr(OH)^+$ ions. The formation and diffusion processes of $Sr(OH)^+$ in the microporous structure of carbonic adsorbent were reported earlier [6].

At relatively higher equilibrium concentrations, the water molecules will not be displaced by strontium ions that are bound to activated carbon by the interaction with carboxylic groups (-COOH) and also with phosphate and polyphosphate groups (P=O, C-O-P).

Figures 3 and 4 show the adsorption isotherms of strontium ions from aqueous solutions on the CAN-7 and CAN-8 activated carbons, respectively, at different temperatures. From the data presented, it is seen that with the increase in temperature, the adsorption values on the both CAN-7 and CAN-8 activated carbon samples are diminishing, but just the shape of adsorption isotherms of strontium ions on the CAN-8 activated carbon at low equilibrium concentrations differs from that on the CAN-7 activated carbon. At somewhat higher equilibrium concentrations, we also distinguish a difference in the shape of strontium ion adsorption isotherms on the CAN-8 activated carbon sample compared to that of the CAN-7 activated carbon.

Figures 5 and 6 show the adsorption isosteres of strontium ions from aqueous solutions on the CAN-7 and CAN-8 activated carbons at different specific adsorption values.

The differential isosteric adsorption heats Q at different values of the specific adsorption a were calculated based on the Clausius–Clapeyron equation (Eq.(1)). Figures 7 and 8 show the values of isosteric adsorption heat (Q_{is}) as function of a, assuming the linearity of the correlation up to $a = 0$. Thus, one can determine the standard Q^0 adsorption heat by extrapolation.

The data presented in Figures 7 and 8 show that the standard adsorption heat values of strontium ions on the CAN-7 and CAN-8 activated carbons are different. The Q^0 value of CAN-7 is higher than that of the CAN-8 activated carbon, equal to 8.6 kJ/mol and 6.8 kJ/mol, respectively.

In order to evaluate the degree of mobility of strontium ions in the adsorbent layer, having determined the values of standard heat adsorption Q^0 of strontium ions on activated carbon, Eq.(2) has been used. The value of standard adsorption entropy (ΔS^0) of strontium ions on the CAN-7 activated carbon is equal to 0.023 kJ/mol·grad at T= 298.15 K. This absolute value is small, indicating that the mobility of strontium ions in the adsorbent layer is high. Most likely, in this case a located adsorption does not take place.

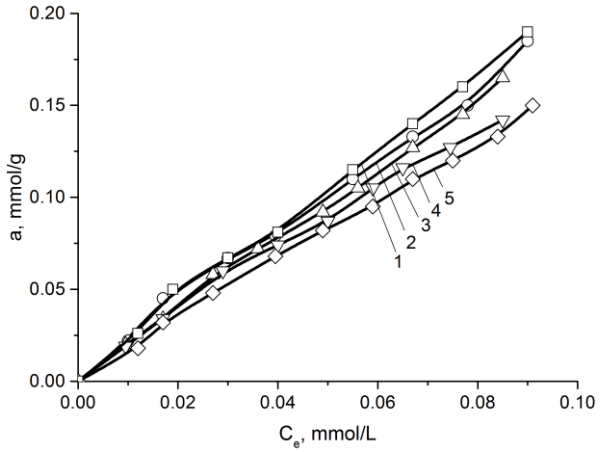

Figure 3. Adsorption isotherms of strontium ions from aqueous solutions on activated carbon CAN-7, at different temperatures: *(1)*- 25°C, *(2)*- 35°C, *(3)*- 45°C, *(4)*- 55°C, *(5)*- 65°C.

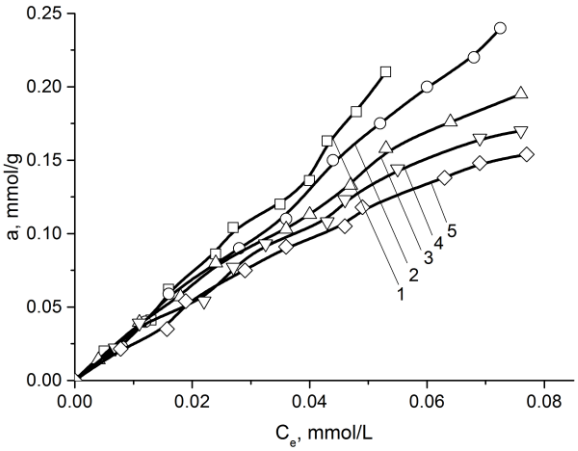

Figure 4. Adsorption isotherms of strontium ions from aqueous solutions on the activated carbon CAN-8, at different temperatures: *(1)*- 25°C, *(2)*- 35°C, *(3)*- 45°C, *(4)*- 55°C, *(5)*- 65°C.

Figures 9 and 10 show the adsorption isotherms of strontium ions in coordinates of $log(C_{ads}/C_e)$ *vs.* (C_e) on the activated carbons CAN-7 and CAN-8, at 35°C, 45°C and 55°C. The values of $logK_{ads}$ were plotted as a result of the extrapolation of curves $log(C_{ads}/C_e)= f(C_e)$ to $C_e=0$. From the data presented in Figures 9 and 10, we note that these values do not differ significantly. Thus, the interaction of $Sr(OH)^+$ ion with the functional polar groups on the surface of the activated carbons CAN-7 and CAN-8, being however relatively low, based on the obtained data, determines the adsorption process of strontium ions at low equilibrium concentrations.

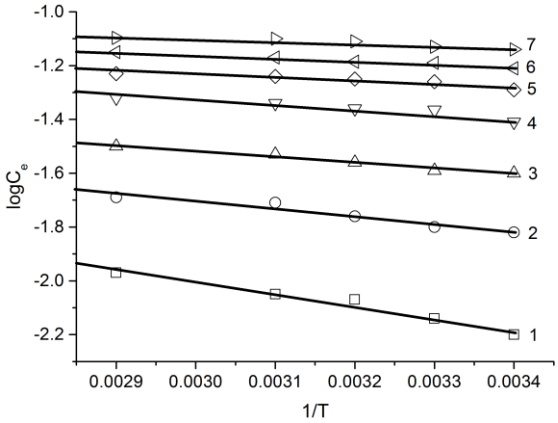

Figure 5. Isosteres of strontium ion adsorption from aqueous solutions on activated carbon CAN-7, at specific adsorption values: *(1)*- 0.02 mmol/g, *(2)*- 0.04 mmol/g, *(3)*- 0.06 mmol/g, *(4)*- 0.08 mmol/g, *(5)*- 0.1 mmol/g, *(6)*- 0.12 mmol/g, *(7)*- 0.14 mmol/g.

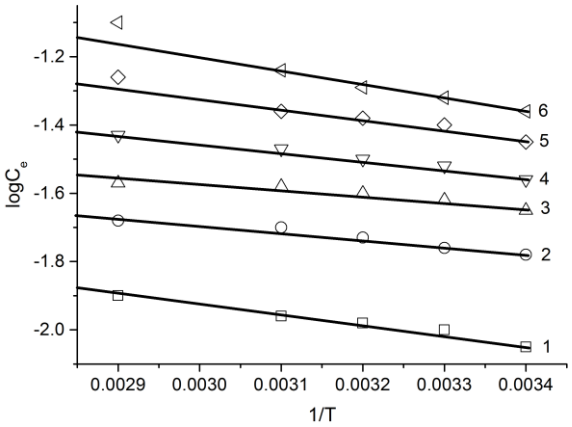

Figure 6. Isosteres of strontium ion adsorption from aqueous solutions on activated carbon CAN-8, at specific adsorption values: *(1)*- 0.025 mmol/g, *(2)*- 0.05 mmol/g, *(3)*- 0.075 mmol/g, *(4)*- 0.1 mmol/g, *(5)*- 0.125 mmol/g, *(6)*- 0.15 mmol/g.

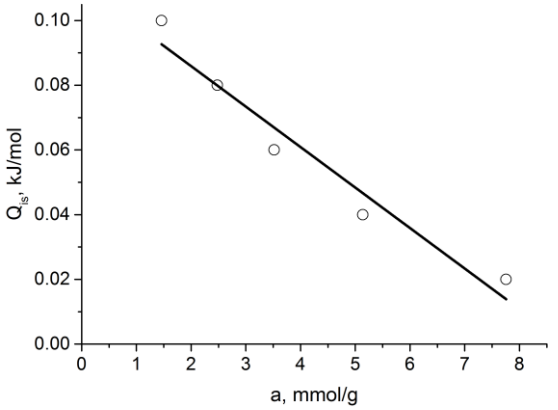

Figure 7. Correlation of the adsorption isosteric heat (Q_{is}) of strontium ions on the activated carbon CAN-7 and the specific adsorption *a*.

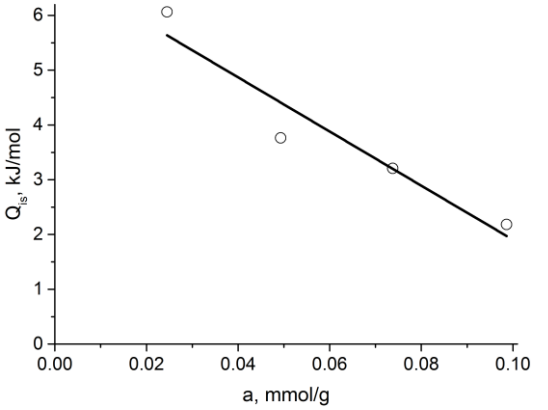

Figure 8. Correlation of the adsorption isosteric heat (Q_{is}) of strontium ions on the activated carbon CAN-8 and the specific adsorption *a*.

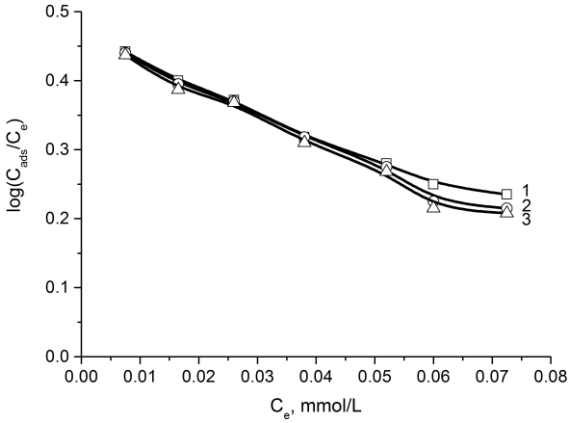

Figure 9. Adsorption isotherms of strontium ions from aqueous solutions on the activated carbon CAN-7 in the coordinates of $log(C_{ads}/C_e)$ *vs.* C_e, at *(1)*- 35°C, *(2)*- 45°C and *(3)*- 55°C.

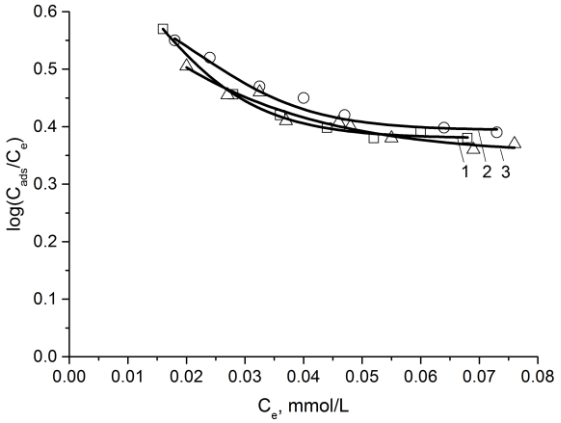

Figure 10. Adsorption isotherms of strontium ions from aqueous solutions on activated carbon CAN-8 in the coordinates of $log(C_{ads}/C_e)$ *vs.* C_e, at *(1)*- 35°C, *(2)*- 45°C and *(3)*- 55°C.

Conclusions

The isotherm of adsorption of strontium ions from aqueous solutions on the activated carbon CAN-7 has two inflection points, even at relatively low concentrations of equilibrium concentrations.

As the temperature rises, the adsorption values decrease, indicating that the adsorption process is exothermic. The values of standard heats of adsorption of strontium ions on the activated carbons CAN-7 and CAN-8 are different. The Q^0 value of activated carbon CAN-7 is higher than that for the sample CAN-8, equal to 8.6 kJ/mol and 6.8 kJ/mol, respectively.

The absolute value of the standard entropy variation of adsorption for strontium ions on the activated carbon CAN-7 is small, which is related to the high mobility of strontium ions in the adsorbent, consequently, the adsorption may be of non-located type.

Acknowledgements

The research has been partially supported by the Horizon 2020 Programme (Marie Skłodowska-Curie Research and Innovation Staff Exchange) of the European Commission, project NanoMed No. 691123.

References

1. Rivera-Utrilla, J.; Ferro-Garcia, M.A.; Mingorance, M.D.; Bautista-Toledo, I. Adsorption of lead on activated carbons from olive stones. Journal of Chemical Technology & Biotechnology, 1986, 36(2), pp. 47-52. DOI: https://doi.org/10.1002/jctb.280360202
2. Rivera-Utrilla, J.; Ferro-Garcia, M.A. Study of cobalt adsorption from aqueous solution on activated carbons from almond shells. Carbon, 1987, 25(5), pp. 645-652. DOI: https://doi.org/10.1016/0008-6223(87)90218-1
3. Ferro-Garcia, M.A.; Rivera-Utrilla, J.; Rodriguez-Gordillo, J.; Bautista-Toledo, I. Adsorption of zinc, cadmium, and copper on activated carbons obtained from agricultural by – products. Carbon, 1988, 26(3), pp. 363-373. DOI: https://doi.org/10.1016/0008-6223(88)90228-X
4. Ahmadpour, A.; Zabihi, M.; Tahmasbi, M.; Rohani Bastami, T. Effect of adsorbents and chemical treatments on the removal of strontium from aqueous solutions. Journal of Hazardous Materials, 2010, 182(1-3), pp. 552-556. DOI: https://doi.org/10.1016/j.jhazmat.2010.06.067
5. Liyaghati- Delshad, M.; Moradi, R. Removal of Sr^{2+} from aqueous solutions by adsorbent activated carbon of almond shell. International Research Journal of Applied and Basic Sciences, 2014, 8(11), pp. 1950-1958. http://www.irjabs.com/en/archive.php?rid=100
6. Kaçan, E.; Kütahyali, C. Adsorption of strontium from aqueous solutions using activated carbon produced from textile sewage sludges. Journal of Analytical and Applied Pyrolysis, 2012, 97, pp. 149-157. DOI: https://doi.org/10.1016/j.jaap.2012.06.006
7. Ciobanu, M.; Botan, V.; Lupascu, T.; Mitina, T.; Rusu, M. Adsorption of strontium ions from water on modified activated carbons. Chemistry Journal of Moldova, 2016, 11(2), pp. 26-33. DOI: https://doi.org/10.19261/cjm.2016.11(2).01
8. Koganovskii, A.M.; Levcenco, T.M. Change in free energy at displacing water from the surface of activated carbon by benzene adsorbed from aqueous solutions. Colloid Journal, 1966, 28(2), pp. 225-228. (in Russian). http://www.maik.ru/ru/journal/kolzhur/
9. Qadeer, R.; Hanif, J.; Saleem, M.; Afzal, M. Selective adsorption of strontium on activated charcoal from electrolytic aqueous solution. Collection of Czechoslovak Chemical Communications, 1992, 57(10), pp. 2065-2072. DOI: https://doi.org/10.1135/cccc19922065
10. Koganovskii, A.M.; Levcenco, T.M.; Kiricenco, V.A. Adsorption of Dissolved Substances. Naukova Dumka: Kiev, 1977, 222 p. (in Russian). http://www.ndumka.kiev.ua/

CHEMISTRY JOURNAL OF MOLDOVA. General, Industrial and Ecological Chemistry. 2018, 13(2), 82-88
ISSN (p) 1857-1727 ISSN (e) 2345-1688
http://cjm.asm.md
http://dx.doi.org/10.19261/cjm.2018.522

EFFECT OF THE NATURE OF SURFACTANT ON THE REACTIVITY OF *C,N*-DIPHENYLNITRONE TOWARDS ACRYLONITRILE IN DIFFERENT MICROEMULSION SYSTEMS

Kahina Hamza [a,b*], Abdelkader Touati [a], Ahmed Ait-Yahia [a,b], Michel Baltas [c], Christiane André Barres [c], Saâd Moulay [d]

[a]*The Laboratory for Research on Bioactive Products and the Valorization of Biomass, Ecole Normale Supérieure, 92, Vieux-Kouba str., Algiers, Algeria*
[b]*Faculty of Sciences, Saâd Dahlab University of Blida, 270, Soumâa Road str., Blida 09000, Algeria*
[c]*Laboratory of Synthesis and Physico-Chemistry of Molecules of Biological Interest, Paul Sabatier University, 118, Narbonne Road str., Toulouse 31062, France*
[d]*Faculty of Technology, Saâd Dahlab University of Blida, 270, Soumâa Road str., Blida 09000, Algeria*
**e-mail: kahina_hamza@yahoo.fr; phone: (+213) 21 297 511; fax: (+213) 21 282 067*

Abstract. The reactivity of the 1,3-dipolar cycloadditions of *C,N*-diphenylnitrone with acrylonitrile in different microemulsion systems has been investigated. The effect of the nature of surfactant (cationic, anionic), a component of water- and oil-borne microemulsions, on the rate of this reaction have been studied. The electrostatically attractive character of cetyltrimethylammonium bromide, a cationic surfactant, would bring the reactants closer to each other; hence, a rate enhancement would ensue, particularly within the water-rich zone. Besides, the fact that acrylonitrile played a dual role, as a component of the microemulsion and a dipolarphile in the cycloaddition reaction, made the work-up advantageously sound. Additionally, the increase in reagents molar ratio was found to promote higher reactivity.

Keywords: acrylonitrile, cycloaddition, isoxazolidine, microemulsion, nitrone.

Received: 09 October 2018/ Revised final: 27 November 2018/ Accepted: 27 November 2018

Introduction

Microemulsion is a dispersed state of one-in-the-other mixture of two immiscible liquids in the form of microdroplets [1-3]. As per the nature of substrate added to a microemulsion, three solubilisation sites for this substrate are plausible: the micellar core, the interface created between the polar heads, and the dispersing medium [4,5]. A myriad of reports, endorsed the fact that microemulsions are favourable media for organic reactions, which are usually hampered in conventional ones. Such macroscopically isotropic and microscopically structured media allow the reactants to draw near each other, to concentrate, and to induce their organization, hence, a better reactivity coupled with a better regio- and stereoselectvity [6-11].

Heterocyclic chemistry remains indubitably a weighty chapter of organic chemistry. Its role and benefits increasingly gain a giant foothold in several industries, including pharmaceuticals, dyes, plastics, and agrochemicals [12-14]. One of our ongoing researches is synthesis of isoxazolidines and study of their biological activities. Apart from this biological property, they are known for the anti-inflammatory activity and others [15-19]. The common procedure to make them has been through the 1,3-dipolar cycloaddition of nitrones with alkenes [20,21]. This reaction is also known as the Huisgen cycloaddition or Huisgen reaction that proceeds by concerted mechanism. Generally, 5-substituted isoxazolidines are obtained starting from mono-substituted and 1, 1-disubstituted alkenes. The formation of 4-substituted products is observed only for strong electron-withdrawing groups [22]. This cycloaddition has been extensively studied both computationally [23-26] and experimentally [27-28], in a variety of media: aqueous media [29-31], solid state [22,32-34], ionic liquids [35-38], emulsions and microemulsions [39,40].

In the present paper, we wish to report the results of the effects of the type of the microemulsion (water- and oil-borne ones, O/W and W/O) and the electrical charge of the polar head of the surfactant (cationic, anionic), a basic constituent of the microemulsion, on the reaction rate of 1,3-dipolar cycloaddition of

C,N-diphenylnitrone (DPN) with acrylonitrile (ACN) when run in the microemulsion medium. Scheme 1 recalls the mechanism illustrating the two possible sites of attack, giving rise to two pairs of isoxazolidine isomers, (3R, 4R; 3R, 4S) and (3R, 5R; 3R, 5S).

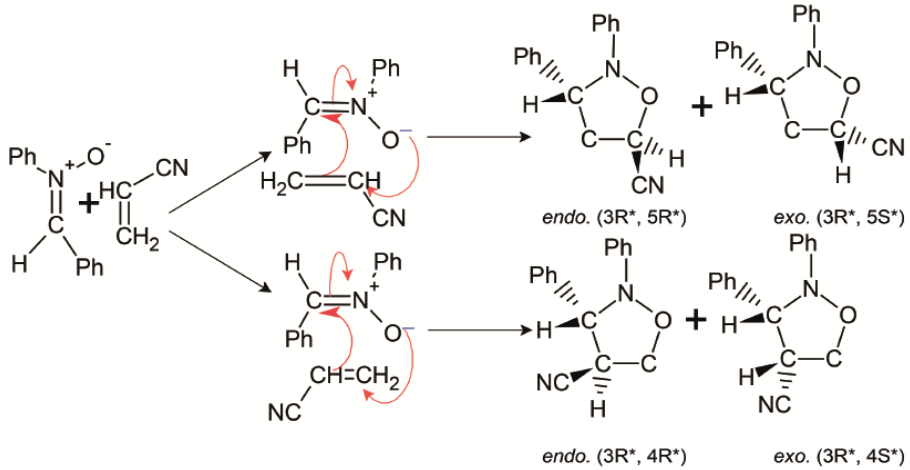

Scheme 1. Mechanism of 1,3-dipolar cycloaddition between DPN and ACN.

Experimental

Chemicals and equipment

Chemicals and solvents (purity > 95%) were purchased from either Fluka or Prolabo. *C,N*-Diphenylnitrone was prepared as previously described [41]. Acrylonitrile was purified by distillation before use. UV-visible spectra were recorded on a Shimadzu 160 double beam spectrophotometer.

Pseudo-ternary phase diagrams

Establishment of pseudo-ternary phase diagrams was deemed to be an inevitable step for confining the existent domains of the studied microemulsions. For a matter of comparison herein dealt with, sodium dodecylsulphate (SDS) and cetyltrimethylammonium bromide (CTAB) were chosen as anionic and cationic surfactants, respectively. *n*-Butanol was used as co-surfactant in this study and the mixture surfactant/ co-surfactant was thus taken as a pseudo-component of the microemulsion. The choice for *n*-butanol as co-surfactant was not arbitrary; but was based on its chemical inertness towards ACN and its ability to take part in the stability of the microemulsion. Based on our previous work [41] and others [4], the [surfactant]/[co-surfactant] weight ratio was set to ½, allowing a broad domain of microemulsion existence. The cycloaddition was first examined with toluene as an oily constituent of the microemulsion to provide an insight into the course and outcome of the reaction under these conditions. Then, toluene was substituted by ACN, acting as oily constituent of the microemulsion and dipolarphile in the proposed cycloaddition. Accordingly, the following four phase diagrams were drawn to represent four pseudo-ternary systems:

System I: Water/(SDS/*n*-Butanol=1/2)/Toluene.
System II: Water/(CTAB/*n*-Butanol=1/2)/Toluene.
System III: Water/(SDS/*n*-Butanol=1/2)/ACN.
System IV: Water/(CTAB/*n*-Butanol=1/2)/ACN.

To realize the pseudo-ternary phase diagrams, demixion curves that delimit the existence domain of microemulsions ought to be established as follows:

Downward demixion curve

1. Titration of *water/oil* binary mixtures of different compositions (from water-rich compositions to oil-rich ones) at 25°C, with a solution made of 75% of water and 25% of surfactant and *n*-butanol (*surfactant*/*n-butanol*= ½) until a transparency occurred.
2. Titration of pseudo-binary mixtures of *oil/*(*surfactant/n-butanol= ½)* with pure water until a cloudy appearance was observed.
3. Titration of pseudo-binary mixtures of *water/*(*surfactant/n-butanol= ½)* with oil until a cloudy appearance was observed.

Upward demixion curve

1. Titration of pseudo-binary mixtures of *oil/*(*surfactant/n-butanol= ½)* with pure water until a transparency occurred.
2. Titration of pseudo-binary mixtures of *water/*(*surfactant/n-butanol= ½)* with oil until a cloudy appearance was observed.

The employed microemulsions were selected from the drawn phase diagrams, one water-borne micromemulsion W/O (**A**) and one

oil-borne one O/W (**B**). The microemulsions were made according to the data shown in Table 1.

Table 1

Composition (wt.%) of the microemulsions.

Microemulsion	*Water*	*SDS or CTAB*	*n-Butanol*	*Toluene or ACN*
A	50	12.5	25	12.5
B	20	12.5	25	42.5

1,3-Dipolar cycloaddition in microemulsion

In a 25 mL flask, 0.294 g (1.5 mmoles) of DPN was dissolved in 3 mL of microemulsion, followed by addition of the required amount of ACN. The mixture was vigorously stirred at 25°C. The follow-up of the reaction was through UV-visible analysis at a given reaction time. To do so, a 5 µL sample of the mixture was diluted with 4 mL of ethanol and the unreacted DPN was quantified by measuring the UV-visible absorbance at λ_{max}= 313 nm of the diluted sample [11].

Calibration curve

A mother solution DPN/microemulsion was prepared by dissolving 0.294 g of DPN in 3 mL of microemulsion. Aliquots of 1, 2, 3, 4, 6, 8, 10 and 12 µL were then sampled and diluted in 8 mL of ethanol. Absorbance of each diluted sample was measured at λ_{max}= 313 nm and the curve *Abs= f(C)* was drawn.

Results and discussion

Figure 1 present the phase diagrams delineating the areas of the existence of microemulsions. It can be noticed the vast domains of the existence of microemulsion for the four systems *I-IV* in the vicinity of water- and oil-rich sides. However, the choice was focused on surfactant-rich ones as per the superposition of the four diagrams.

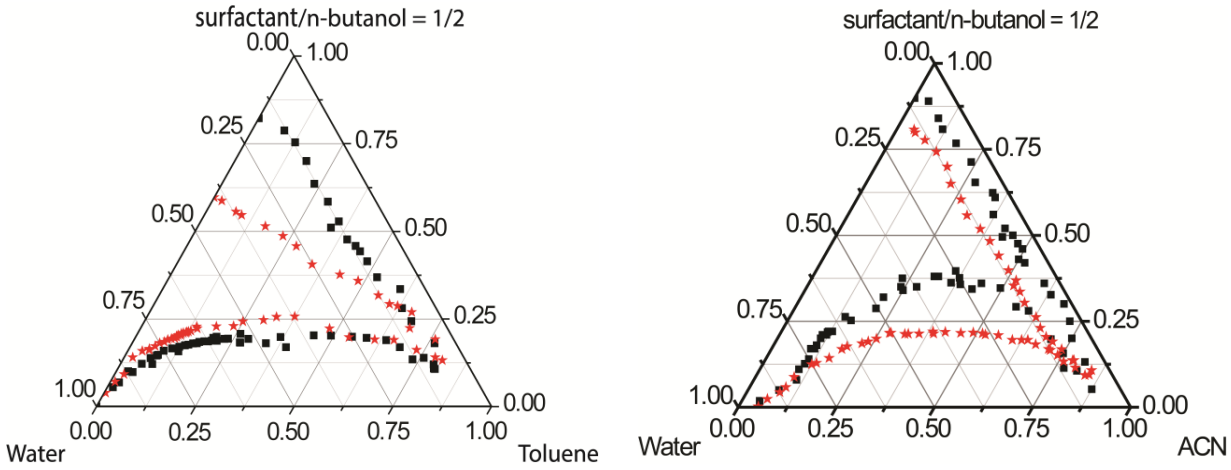

(a) ***(b)***

Figure 1. Pseudo-ternary phase diagrams for:
(a) ★ water/(SDS/*n*-butanol)= ½)/toluene; ■ water/(CTAB/*n*-butanol)= ½)/toluene,
(*b*) ★ water/(SDS/*n*-butanol)= ½)/ACN; ■ water/(CTAB/*n*-butanol)= ½)/ACN.

The kinetics of the cycloaddition reaction was monitored by UV-visible analysis of the residual DPN. It is worth mentioning that whatever the location of the dissolved substrate within the microemulsion, either in its interior or at the interface of microaggregates, would not distort the overall interpretation of the spectra. The evolution of the intensity of the absorbance band of DPN with reaction time for microemulsion **B** of system *I* is illustrated in Figure 2. The increasingly fading of the absorbance band at 313 nm and the rising one at 238 nm, a characteristic band of the isoxazolidine, was an evidence of the success of the cycloaddtion in microemulsion medium.

The appearance of an isosbestic point at 253 nm proves the existence of equilibrium between the two species without intermediates. From this analysis, the rate constants *k* of the cycloaddition in different microemulsions were computed and are gathered in Table 2.

Needless is to recall that the microenvironment of the reactants affects their reactivity. Hence, reaction outcome in oil-borne microemulsion will differ from that in water-borne one, as confirmed by many reports [42-46]. In the present work, isoxazolidines were synthesized in both O/W and W/O microemulsions, **A** and **B**. The latter one consists of water microdroplets dispersed in toluene,

separated by a film made of surfactant and co-surfactant; DPN and ACN ended up in an environment similar to conventional medium, with slight nitrone content at the water-toluene interface as illustrated in Figure 3*(b)*. On the contrary, the former microemulsion one consists of oil microdroplets dispersed in water, separated by a film made of surfactant and co-surfactant. Both organic substrates, DPN and ACN, tended to move towards the interface where to react. While the formed isoxazolidine migrated to the hydrophobic core of the microemulsion, the reactants tended to concentrate once again at the mentioned interface, promoting a reaction rate enhancement (Figure 3*(a)*).

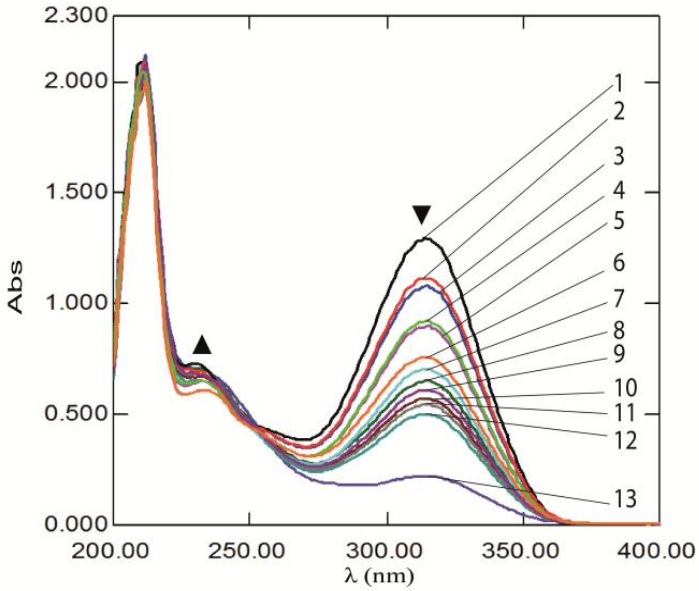

Figure 2. UV-visible spectra evolution with reaction time, for DPN-microemulsion *I*B, at 25°C, in ethanol.

Table 2

Rate constants of 1,3-dipolar cycloaddition between DPN and ACN for different DPN/ACN molar ratios in microemulsion systems at 25°C.

Run	*1*	*2*	*3*	*4*	*5*	*6*	*7*	*8*
Microemulsion	(*I***B**)	(*I***A**)	(*II***B**)	(*II***A**)	(*III***B**)	(*III***A**)	(*IV***B**)	(*IV***A**)
Surfactant	SDS	SDS	CTAB	CTAB	SDS	SDS	CTAB	CTAB
Oil	toluene	toluene	toluene	toluene	ACN	ACN	ACN	ACN
DPN/ACN	1/20	1/20	1/20	1/20	1/80	1/24	1/80	1/24
$k\times10^3$ ($M\cdot s^{-1}$)	1.2	1.3	1.9	2.3	4.4	2.1	7.4	3.2

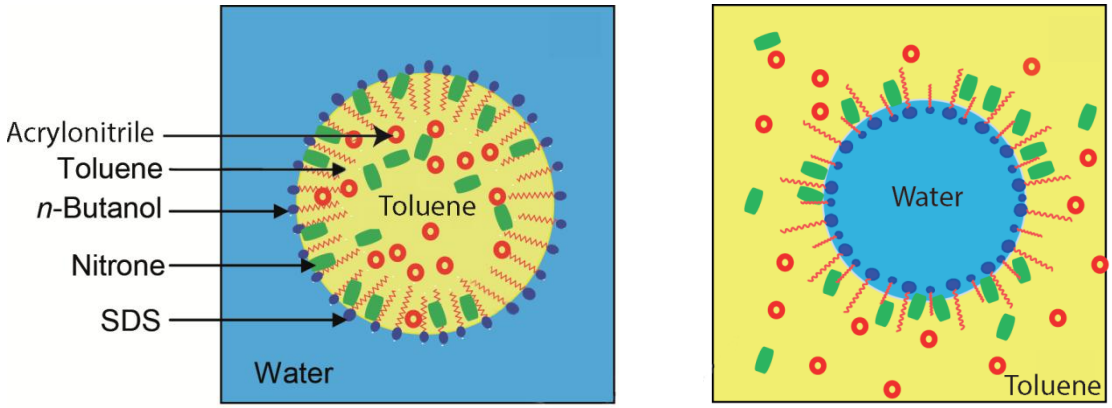

(a) ***(b)***

Figure 3. Illustration of location sites of DPN and ACN in: *(a)* a direct microemulsion, *I*A; *(b)* a reverse microemulsion, *I*B.

The results shown in Table 2 for runs 1 and 2 suggest that the rate constant of the cycloaddition remained nearly unchanged on going from oil-rich zone to water-rich one. Reversing the shape of the micelles in water-borne microemulsion **A** and re-concentrating the reactants in the microdroplets did not improve the reaction rate.

The type of charge of the surface active agent may affect the microemulsion characteristics, thus, the reaction course. The double layer, comprised of the polar heads of surfactant and its counterions, created a local electrical field, giving rise to another kind of interfacial environment which influenced the position of the reactants. In fact, the ensued repulsive electrostatic interactions would have allowed the reactants to stand either close to the interface or far from it. Moreover, this created field may have either reduced the stability of the reactants, provoking an acceleration of the reaction, or enhanced their stability, inducing a reaction rate drop.

A rate acceleration can be noted when the kinetic results for the microemulsions *I***A** and *II***A** (SDS as surfactant) were compared with those for *I***B** and *II***B** (CTAB as surfactant) (Table 2); the rate constant increased from 1.2×10^{-3} $M\cdot s^{-1}$ to 1.9×10^{-3} $M\cdot s^{-1}$ in the case of oil-borne microemulsions (**B**) and from 1.3×10^{-3} $M\cdot s^{-1}$ to 2.3×10^{-3} $M\cdot s^{-1}$ in the case of water-borne ones (**A**). These results are in agreement with those reported by Chatterjee, A. *et al.* [47]. Their report indicates that excellent yields of the 1,3-dipolar cycloaddition reactions between *C*-aryl-*N*-phenyl nitrones and alkenes were observed when run in microemulsion with CTAB as surfactant, as compared with microemulsion consisting of SDS surfactant.

On the other hand, the effect of microemulsion as medium for organic reactions was supported by the work of Engberts, J. *et al.* [48]. In their investigation, they observed that the reaction rates of 1,3-dipolar cycloaddition between benzonitrile oxide and *N*-ethylmaleimide at 25°C were 35 and 150 times greater in AOT/isooctane/water microemulsion than in water and isooctane, respectively. The rationale of this rate improvement was the increase of reactants concentrations at the interface and the destabilization of benzonitrile oxide by the electrical field induced by the anionic polar heads of AOT surfactant. This reaction was also studied in SDS- and CTAB-based micellar media and the result was a reactivity decline as compared to the reaction outcome in water [39]. The relatively better reactivity in water was reasoned as due to the undisturbed '*solvated state*' of benzonitrile oxide, hence becoming more stable and less reactive. However, the reactivity depression that occurred in microemulsion was explained as due to '*solvation power lowering*', ensuring higher reactivity.

In the light of the above results, an explanation for the difference in chemical reactivity of DPN towards ACN when CTAB and SDS were used (Figure 4), lies on the electrostatic force exerted by the dodecylsulphate ion on the negative charge of the nitrone molecule; the latter species will end up in the aqueous superficial layer, full of cationic counterions (Na^+), to become more stable by solvation. A chemical reactivity reduction ensues regardless the type of microemulsion used (O/W or W/O) (Figure 4*(a)*).

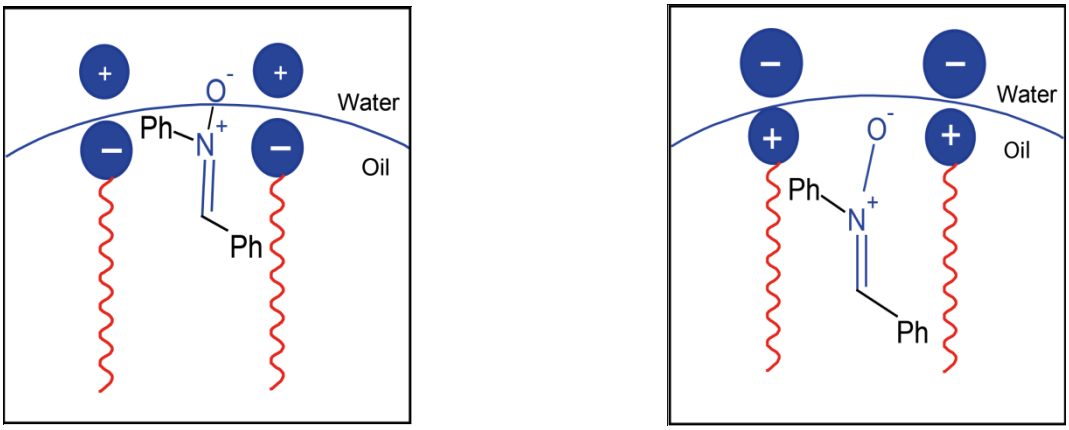

(a) ***(b)***

Figure 4. Positioning of DPN molecule at the W/O interface in the presence of surfactant: *(a)* SDS, *(b)* CTAB.

In the case of the positively charged polar heads of CTAB, attractive electrostatic forces stimulated the migration of DPN molecules towards the interface zone. The high concentration of anionic counterions (Br^-) within the superficial layer that is close to the interface, would keep DPN molecules far from the aqueous environment, impeding their solvation. In this fashion, the interface, acting as a microreactor, would allow nitrone molecules to concentrate near ACN ones, and therefore the reactivity increases (Figure 4*(b)*).

It is worthwhile to point out to the positive role of the cationic surfactants in the microemulsion as far as the cycloaddition course was important. So, as observed for systems *III* and *IV*, the increase in DPN/ACN molar ratio was found to promote higher reactivity. For example, the rate constant rose from 1.9×10^{-3} $M\cdot s^{-1}$ to 7.4×10^{-3} $M\cdot s^{-1}$, on going from microemulsion *II***B** to microemulsion *IV***B**.

Conclusions

The use of oil-borne microemulsions (O/W) in the synthesis of isoxazolidine is in tune with green chemistry. The dual employment of ACN, as microemulsion component and reactant, makes the water-borne microemulsions (W/O) environmentally-friendly by excluding the use of another organic component.

SDS-based W/O or O/W microemulsions with an ACN/DPN molar ratio of 20 showed no difference of chemical reactivity. On the contrary, the O/W CTAB-based microemulsions allowed higher reactivity.

Another important issue is the impact of solvation (hydration) of reactants on the course of the cycloaddition reaction in microemulsion. The negative charge of the counterion of a cationic surfactant will contribute to hydration lowering of nitrone, favouring its increased reactivity.

References

1. Paul, B.K.; Moulik, S.P. Microemulsions: an overview. Journal of Dispersion Science and Technology, 1997, 18(4), pp. 301-367. DOI: https://doi.org/10.1080/01932699708943740
2. Hloucha, M. Microemulsion. Ullmann's Encyclopedia of Industrial Chemistry, 2014, pp. 1-16. DOI: https://doi.org/10.1002/14356007.q16_q02
3. Bellocq, A.M.; Biais, J.; Bothorel, P.; Clin, B.; Fourche, G.; Lalanne, P.; Lemaire, B.; Lemanceau, B.; Roux, D. Microemulsions. Advances in Colloid and Interface Science, 1984, 20(3-4), pp. 167-272. DOI: https://doi.org/10.1016/0001-8686(84)80005-6
4. Lattes, A. Structure-chemical reactivity relationship and photochemical in microemulsions. Journal of Physical Chemistry, 1987, 84, pp. 1061-1073. (in French). DOI: https://doi.org/10.1051/jcp/1987841061
5. Hellweg, T. Phase structures of microemulsions. Current Opinion in Colloid & Interface Science, 2002, 7(1-2), pp. 50-56. DOI: https://doi.org/10.1016/S1359-0294(02)00004-3
6. Ghosh, P.; Kar, B.; Bardhan, S.; Kundu, K.; Saha, S.K.; Paul, B.K.; Das, S. Microemulsion mediated organic synthesis and the possible reaction site. Journal of Surface Science and Technology, 2016, 32(1-2), pp. 8-16. DOI: https://doi.org/10.18311/jsst/2016/6596
7. Holmberg, K. Organic reactions in microemulsions. European Journal of Organic Chemistry, 2007, 0(5), pp. 731-742. DOI: https://doi.org/10.1002/ejoc.200600741
8. Malik, M.A.; Wani, M.Y.; Hashim, M.A. Microemulsion method: a novel route to synthesize organic and inorganic nanomaterials: 1st nano update. Arabian Journal of Chemistry, 2012, 5(4), pp. 397-417. DOI: https://doi.org/10.1016/j.arabjc.2010.09.027
9. Wituła, T. Organic Reactions in Organized Media. Ph.D. Thesis, Chalmers University of Technology, Göteborg, Sweden, 2007, 63 p.
10. Holmberg, K. Organic reactions in microemulsions. Current Opinion in Colloid & Interface Science, 2003, 8(2), pp. 187-196. DOI: https://doi.org/10.1016/S1359-0294(03)00017-7
11. Schomäcker, R.; Holmberg, K. Microemulsions: Background, New Concepts, Applications, Perspectives. John Wiley and Sons: Oxford, 2009, pp. 148-179. DOI: https://doi.org/10.1002/9781444305524.ch5
12. Belen'kii, L.I.; Evdokimenkova, Y.B. Chapter Four - The Literature of heterocyclic chemistry, Part XVI, 2016. Advances in Heterocyclic Chemistry, 2018, 126, pp. 173-254. DOI: https://doi.org/10.1016/bs.aihch.2018.02.003
13. Cordero, F.M.; Giomi, D.; Lascialfari, L. Five – Membered Ring Systems with O & N Atoms. Progress in Heterocyclic Chemistry, 2014, 26, pp. 319-348. DOI: https://doi.org/10.1016/B978-0-08-100017-5.00011-X
14. Cordero, F.M.; Giomi, D.; Lascialfari, L. Five – Membered Ring Systems with *O* and *N* Atoms. Progress in Heterocyclic Chemistry, 2016, 28, pp. 361-390. DOI: https://doi.org/10.1016/B978-0-08-100755-6.00011-9
15. Loh, B.; Vozzolo, L.; Mok, B.J.; Lee, C.C.; Fitzmaurice, R.J.; Caddick, S.; Fassati, A. Inhibition of HIV-1 replication by isoxazolidine and isoxazole sulfonamides. Chemical Biology & Drug Design, 2010, 75(5), pp. 461-474. DOI: https://doi.org/10.1111/j.1747-0285.2010.00956.x
16. Berthet, M.; Cheviet, T.; Dujardin, G.; Parrot, I.; Martinez, J. Isoxazolidine: a privileged scaffold for organic and medicinal chemistry. Chemical Reviews, 2016, 116(24), pp. 15235-15283.

DOI: 10.1021/acs.chemrev.6b00543
17. Chiacchio, M.A.; Giofrè, S.V; Romeo, R.; Romeo, G.; Chiacchio, U. Isoxazolidines as biologically active compounds. Current Organic Synthesis, 2016, 13(5), pp. 726-749. DOI: 10.2174/1570179412666150914195807
18. Chakraborty, B.; Samanta, A.; Sharma, C.D.; Khatun, N. Synthesis of some novel class of isoxazoline and isoxazolidine derivatives in ionic liquid *via* 1,3-dipolar cycloaddition reaction of dihydropyran derived nitrones and their antimicrobial activities. Indian Journal of Chemistry, 2014, 53B(02), pp. 218-226. http://nopr.niscair.res.in/handle/123456789/26506
19. Ghannay, S.; Bakari, S.; Msaddek, M.; Vidal, S.; Kadri, A.; Aouadi, K. Design, synthesis, molecular properties and *in vitro* antioxidant and antibacterial potential of novel enantiopure isoxazolidine derivatives. Arabian Journal of Chemistry, 2018. DOI: https://doi.org/10.1016/j.arabjc.2018.03.013
20. Huisgen, R. 1,3-dipolar cycloadditions. Past and future. Angewandte Chemie International Edition, 1963, 2(10), pp. 565-598. DOI: https://doi.org/10.1002/anie.196305651
21. Loska, R. Recent advances in cycloaddition reactions of heterocyclic N-oxides. Heterocyclic N-Oxides, 2017, 53, pp. 85-110. DOI: https://doi.org/10.1007/7081_2017_2
22. Rück-Braun, K.; Freysoldt, T.H.E.; Wierschem, F. 1,3-Dipolar cycloaddition on solid supports: nitrone approach towards isoxazolidines and isoxazolines and subsequent transformations. Chemical Society Reviews, 2005, 34(6), pp. 507-516. DOI: 10.1039/B311200B
23. Domingo, L.R.; Ríos-Gutiérrez, M.; Adjieufack, A.I.; Ndassa, I.M.; Nouhou, C.N.; Mbadcam, J.K. Molecular Electron Density Theory Study of *Fused* Regioselectivity in the Intramolecular [3+2] Cycloaddition Reaction of Cyclic Nitrones. Chemistry Select, 2018, 3(19), pp. 5412-5420. DOI: https://doi.org/10.1002/slct.201800224
24. Ríos-Gutiérrez, M.; Darù, A.; Tejero, T.; Domingo, L.R.; Merino, P. A molecular electron density theory study of the [3+2] cycloaddition reaction of nitrones with ketenes. Organic & Biomolecular Chemistry, 2017, 15(7), pp. 1618-1627. DOI: 10.1039/C6OB02768G
25. Merino, P.; Tejero, T.; Chiacchio, U.; Romeo, G.; Rescifina, A. A DFT study on the 1,3-dipolar cycloaddition reactions of C-(hetaryl) nitrones with methyl acrylate and vinyl acetate. Tetrahedron, 2007, 63(6), pp. 1448-1458. DOI: https://doi.org/10.1016/j.tet.2006.11.073
26. Yahia, W.; Khorief Nacereddine, A.; Liacha, M.; Djerourou, A. A quantum-chemical DFT study of the mechanism and regioselectivity of the 1,3-dipolar cycloaddition reaction of nitrile oxide with electron-rich ethylenes. International Journal of Quantum Chemistry, 2018, 118(11), 11 p. DOI: https://doi.org/10.1002/qua.25540
27. Zhang, W. 1,3-Dipolar cycloaddition-based synthesis of diverse heterocyclic scaffolds. Chemistry Letters, 2013, 42(7), pp. 676-681. DOI: https://doi.org/10.1246/cl.130504
28. Hellel, D.; Chafaa, F.; Khorief Nacereddine, A.; Djerourou, A.; Vrancken, E. Regio- and stereoselective synthesis of novel isoxazolidine heterocycles by 1,3-dipolar cycloaddition between *C*-phenyl-N-methylnitrone and substituted alkenes. Experimental and DFT investigation of selectivity and mechanism. Royal Society of Chemistry Advances, 2017, 7(48), pp. 30128-30141. DOI: 10.1039/C7RA00258K
29. Moulay, S.; Touati, A. Cycloaddition reactions in aqueous systems: A two-decade trend endeavor. Comptes Rendus Chimie, 2010, 13(12), pp. 1474-1511. DOI: https://doi.org/10.1016/j.crci.2010.05.025
30. Coutouli-Argyropoulou, E.; Sarridis, P.; Gkizis, P. Water as the medium of choice for the 1,3-dipolar cycloaddition reactions of hydrophobic nitrones. Green Chemistry, 2009, 11(11), pp. 1906-1914. DOI: 10.1039/B916765J
31. Chakraborty, B.; Sharma, P.K. Green synthesis of nitrone and isoxazolidines: one pot convenient cycloaddition reactions in water. RASAYAN Journal of Chemistry, 2010, 3(3), pp. 454-460. http://rasayanjournal.co.in/vol-3_issue-3.html
32. Franzén, R.G. Recent advances in the preparation of heterocycles on solid support: a review of the literature. Journal of Combinatorial Chemistry, 2000, 2(3), pp. 195-214. DOI: 10.1021/cc000002f
33. Feliu, L.; Vera-Luque, P.; Albericio, F.; Alvarez, M. Advances in solid-phase cycloadditions for heterocyclic synthesis. Journal of Combinatorial Chemistry, 2007, 9(4), pp. 521-565. DOI: 10.1021/cc070019z
34. Harju, K.; Yli-Kauhaluoma, J. Recent advances in 1,3-dipolar cycloaddition reactions on solid supports. Molecular Diversity, 2005, 9(1-3), pp. 187-207. DOI: https://doi.org/10.1007/s11030-005-1339-1
35. Johari, N.L.S.; Poad, S.N.M.; Hassan, N.H.; Hassan, N.I. Synthesis of isoxazolidine *via* 1,3-dipolar cycloaddition of *N*-4-tert-benzylidene nitrone and maleimide in imidazolium-based ionic liquids. Malaysian Journal of Analytical Sciences, 2016, 20(6), pp. 1241-1246. DOI: http://dx.doi.org/10.17576/mjas-2016-2006-02
36. Hazra, A.; Bharitkar, Y.P.; Maity, A.; Mondal, S.; Mondal, N.B. Synthesis of tetracyclic pyrrolidine/ isoxazolidine fused pyrano[3,2-*h*]quinolines *via* intramolecular 1,3-dipolar cycloaddition in ionic liquid. Tetrahedron Letters, 2013, 54(32), pp. 4339-4342. DOI: https://doi.org/10.1016/j.tetlet.2013.06.029
37. Kaur, N. Green synthesis of three-to five-membered *O*-heterocycles using ionic liquids. Synthetic Communications, 2018, 48(13), pp. 1588-1613. DOI: https://doi.org/10.1080/00397911.2018.1458243

CHEMISTRY JOURNAL OF MOLDOVA. General, Industrial and Ecological Chemistry. 2018, 13(2), 89-92
ISSN (p) 1857-1727 ISSN (e) 2345-1688
http://cjm.asm.md
http://dx.doi.org/10.19261/cjm.2018.487

HYGROSCOPIC PROPERTIES OF ENOXIL-SILICA COMPOSITES

Oksana Stavinskaya [a*], Iryna Laguta [a], Olga Kazakova [a], Pavlo Kuzema [a], Tudor Lupascu [b]

[a]*Chuiko Institute of Surface Chemistry of National Academy of Sciences of Ukraine, 17, General Naumov str., Kiev 03164, Ukraine*
[b]*Institute of Chemistry, 3, Academiei str., Chisinau MD 2028, Republic of Moldova*
[*]*e-mail: icvmtt34@gmail.com*

Abstract. Enoxil-silica composites with various Enoxil-to-silica ratios were prepared by mechanical mixing of the biologically active Enoxil and fumed silica powders. The hygroscopic properties of the composites were studied by the gravimetric method. It has been shown that the use of Enoxil in composites with silica may significantly reduce the Enoxil ability to absorb water from the gas phase and, therefore, improve its storage stability. The strongest hygroscopicity reduction is observed for the composites with Enoxil-to-silica ratio of (0.15÷0.35):1, which corresponds to an approximate monolayer distribution of the Enoxil biomolecules on the silica surface.

Keywords: Enoxil, biomolecule, fumed silica, composite, hygroscopicity.

Received: 17 April 2018/ Revised final: 30 May 2018/ Accepted: 31 May 2018

Introduction

Enoxil is a biologically active powder with high antioxidant and antimicrobial properties [1,2]. Enoxil production procedure includes extraction of biologically active substances from grape seeds and subsequent oxidation of the extracted compounds (mainly proanthocyanidins, the representatives of flavonoids) with hydrogen peroxide [3]. Enoxil is a mixture of monomeric catechin/epicatechin molecules and their derivatives; mass-spectrometric studies revealed that the main components of Enoxil are gallic acid, catechin, epicatechin and catechingallate [2]. All these compounds have three or more reactive hydroxyl groups in the phenolic rings of the molecules. These are the groups that are mainly responsible for chemical and biological activity of flavonoids [4,5] and that provide Enoxil with high antioxidant/antimicrobial properties.

Due to a large amount of hydrophylic groups, Enoxil possesses enhanced hygroscopicity and requires to be kept under special conditions. The hygroscopicity of medicinal powders, dry extracts and other pharmaceutical medications may be reduced using auxiliary agents, in particular, silica [6,7]. The results of our previous study [8] show that adsorption of Enoxil on the silica surface or even simple mechanical mixing of Enoxil and silica powders leads to a marked decrease in the integral hygroscopicity of the composite, while bioactive molecules in such composites were found to retain their antioxidant properties during prolonged storage at ambient conditions. The decrease in hygroscopicity seems to be due to the involvement of hydroxyl groups of Enoxil molecules into an interaction with silanol groups of silica surface and should depend on the contents of Enoxil and silica in the mixture.

The aim of this work was to prepare Enoxil-silica composites with various Enoxil-to-silica ratios and to examine the effect of this ratio on the composites water absorption.

Experimental

To prepare Enoxil-silica composites, fumed silica with specific surface area of 280 m^2/g (A-300, Kalush, Ukraine) was mechanically mixed with Enoxil powder (produced at the Institute of Chemistry, Academy of Sciences of Moldova [3]) in a ball mill, the processing time was 5 min. The Enoxil-to-silica ratio in the composites was within the range (0.08÷0.90):1.

The *hygroscopicity* of the Enoxil and Enoxil-silica composites was determined gravimetrically as the sample mass (*m*) change after water absorption from the gas phase. Samples of certain mass were placed into weighing bottles, which then were placed into a desiccator with distilled water and held there at a temperature of 20÷22°C for 1÷365 days. The presented results are the average of three independent experiments, the data scattering corresponds to a 95% confidence interval. In order to evaluate the effect of the Enoxil-to-silica

ratio on the hygroscopicity of the composite, the data on the water absorption were presented in the following manner. For each composite and each period of time that the sample was held in the desiccator, we calculated the amount of water, $m(H_2O)_{cal}/m$(composite) that would be absorbed by a sample consisting of appropriate amounts of silica and Enoxil, provided that the components of the composite do not effect the water absorption of each other. To do this, we used the determined in the same experiment values of water absorption for pure Enoxil, $m(H_2O)_{abs}/m$(Enoxil), and pure silica, $m(H_2O)_{abs}/m$(silica), as well as the data on the amount of the components in the composite. The obtained $m(H_2O)_{cal}/m$(composite) value was compared with the actual water absorption value, $m(H_2O)_{abs}/m$(composite), measured for the given composite. The difference was divided by the calculated water absorption value, $m(H_2O)_{cal}/m$(composite), and expressed as a percentage. The obtained value Δ (Eq.(1)) characterizes the degree of reduction (when negative values) or the increase (when positive values) of the hygroscopicity of the composite in comparison with the sum of its components. It is equal to zero when the components do not affect the hygroscopicity of each other.

$$\Delta = \frac{m(H_2O)_{abs}/m(comp.) - m(H_2O)_{cal}/m(comp.)}{m(H_2O)_{cal}/m(comp.)} \cdot 100\% \quad (1)$$

Quantum chemical calculations were carried out using semiempirical PM3 method (GAMESS, current version [9]) to find the optimal configuration for the adsorbed biomolecules on the surface of silica particle modelled by clusters of 36 $SiO_{4/2}$ tetrahedrons with 24 silanol groups.

Results and discussion

Figure 1 shows the water absorption data for the pure Enoxil, pure silica and for the composites with the Enoxil-to-silica ratio of (0.08÷0.90):1. As one can see from Figure 1, pure Enoxil rapidly absorbs water from the gas phase; after 12 months in the desiccator, the increase in the weight of the initial Enoxil, $m(H_2O)_{abs}/m$(Enoxil), reached more than 1000%, while Enoxil became liquid, *i.e.*, it was in a dissolved state. The initial silica is also characterized by considerable hygroscopicity, the water absorption reached the value of $m(H_2O)_{abs}/m$(silica)= 260%. All composites have less water absorption per unit mass, $m(H_2O)_{abs}/m$(composite), than the initial Enoxil. Upon this, the hygroscopicity of the composites does not change monotonically with the change in the Enoxil-to-silica ratio, and for the samples with the ratio of 0.15:1 and 0.23:1 (Figure 1, curves 4 and 5), the water absorption per unit mass is less than that for both pure Enoxil and pure silica (Figure 1, curves 1 and 2). Figures 2 and 3 give the Δ values *versus* Enoxil-to-silica ratio for the holding time in the desiccator of 1, 14, 30, 92, 141, and 365 days.

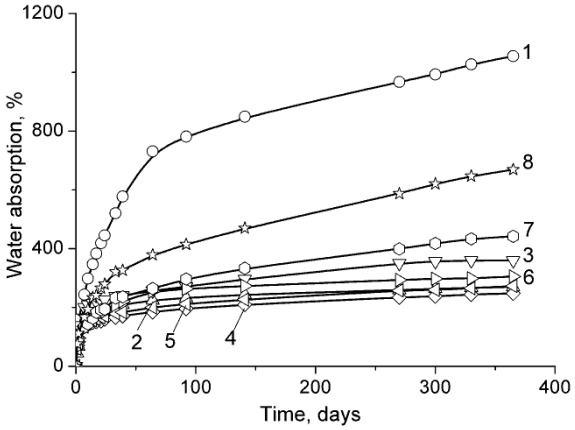

Figure 1. Absorption of water by Enoxil *(1)*, silica *(2)* and composites with the Enoxil-to-silica ratio of 0.08:1 *(3)*, 0.15:1 *(4)*, 0.23:1 *(5)*, 0.35:1 *(6)*, 0.55:1 *(7)*, 0.90:1 *(8)*.

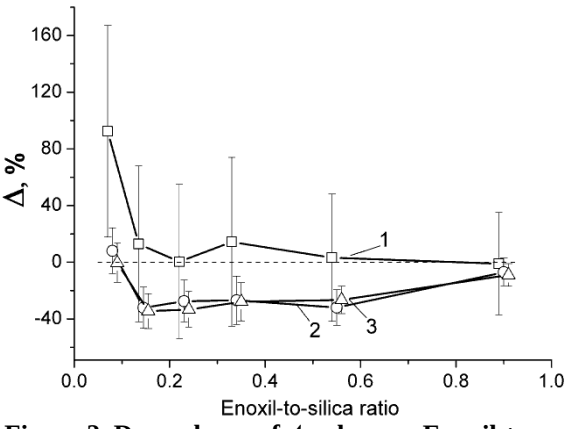

Figure 2. Dependence of Δ values on Enoxil-to-silica ratio for the holding time in the desiccator of 1 *(1)*, 14 *(2)* and 30 *(3)* days.

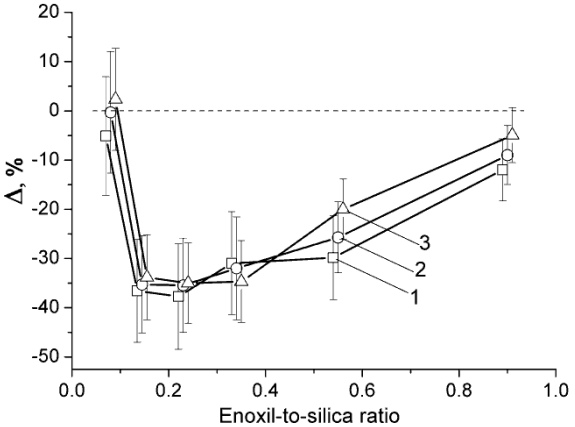

Figure 3. Dependence of Δ values on Enoxil-to-silica ratio for the holding time in the desiccator of 92 *(1)*, 141 *(2)* and 365 *(3)* days.

As it was mentioned above, the Δ values characterize the changes in hygroscopicity of the composites in comparison with the sum of their components. Figures 2-3 show that for the samples with the ratio of (0.15÷0.90):1 and a holding time in the desiccator of 14 days or more, the Δ values are negative. It means that the composites absorb less water than individual components of the composite. As we noted earlier [8], this effect can be related to the interaction of hydroxyl groups of Enoxil and silanol groups of silica with each other and, therefore, to their exclusion from the interaction with water molecules. The interaction of surface groups of silica with hydroxyl groups of the biomolecules was confirmed by IR spectroscopic studies. As it was shown earlier [8], the intensity of the band at 3750 cm^{-1} (corresponding to isolated silanol groups of silica) in the Enoxil-silica composites spectra decreased in comparison with the initial silica spectrum, which indicates the involvement of silanol groups in an interaction with Enoxil. The decrease in the intensity of the band was observed not only in the case of Enoxil adsorption on the silica surface, but also for the mechanical mixture of Enoxil and silica powders prepared by grinding the components in a ball mill.

Apparently, in such a mixture Enoxil is in the form of small crystals or associates, bound, nevertheless, to the silica surface. The growth of powder dispersity during the grinding process should lead, on the one hand, to an increase in the hygroscopicity due to the increase of the surface area of the crystallites/associates and, on the other hand, to a reduction in water absorption due to an increase in the number of bonds between the crystals/associates and the silica surface groups. As it was noted in previous work [8], the first factor appears to play a major role in the initial stage of powders/composites exposure to water, which is reflected in the enhancement of the composites hygroscopicity (Figure 2, curve 1). Over time, the hygroscopicity of the composites decreases in comparison with the sum of hygroscopicities of the composite components. It can be assumed that after the absorption of certain amounts of water, crystallites are further dispersed and dissolved in the absorbed water, followed by the redistribution of biomolecules on the silica surface to form an adsorbed layer. Indeed, as can be inferred from the data in Figure 1, after 14 days of maintaining the samples in the desiccator, the amount of water absorbed by the composites is 1.5-2.5 times greater than the total mass of the composites and 5-15 times greater than the mass of Enoxil in the composites. According to our previous studies on Enoxil solubility, such an amount of water is several times higher than the amount needed to completely dissolve Enoxil and, therefore, it is sufficient to induce Enoxil dissolution and adsorption of the dissolved biomolecules on the silica surface.

The most significant decrease in the hygroscopicity is observed for the composites with the Enoxil-to-silica ratio of (0.15÷0.35):1 (Figures 2, 3). As it is shown below, this range of ratios corresponds to an approximate monolayer distribution of biomolecules on the silica surface. The results of quantum-chemical calculations make it possible to estimate the equilibrium configuration of the main Enoxil biomolecules in the adsorption layer on the silica surface (examples of such equilibrium configurations are given in Figure 4) as well as to evaluate the surface area, occupied by one molecule.

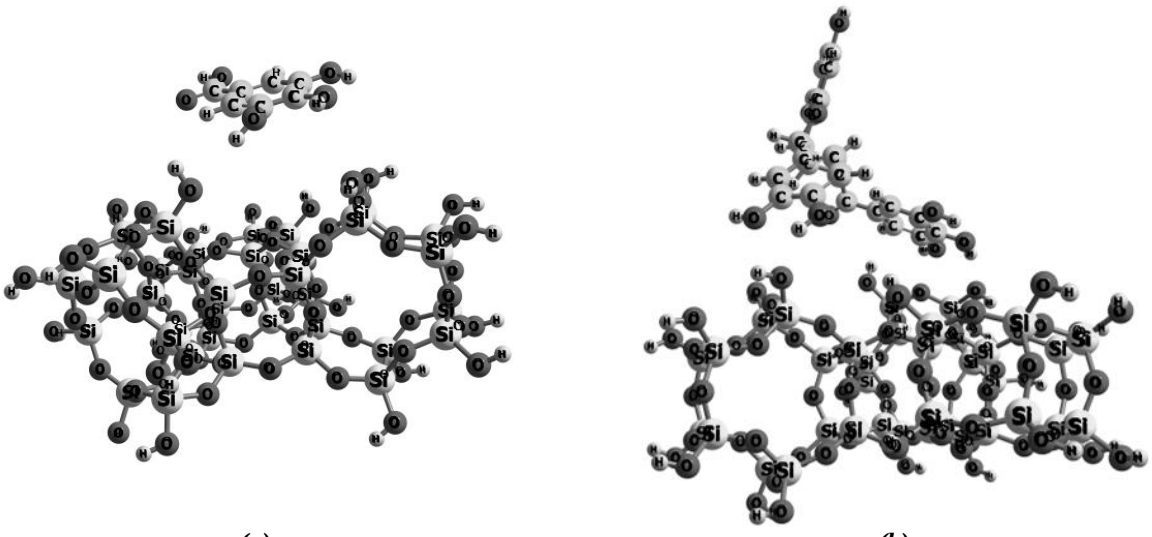

(a) ***(b)***

Figure 4. Equilibrium configuration for the smallest (gallic acid, *(a)*) and the largest (epicatechingallate, *(b)*) Enoxil biomolecules on the silica surface.

The obtained data show that this parameter for various molecules of Enoxil (gallic acid, catechin, epicatechin, catechingallate) ranges between 0.4 and 0.7 nm^2. Taking into account the silica surface area, 280 m^2/g, the maximum amount of the smallest (gallic acid, molar mass 170 g/mole) and the largest (epicatechingallate, molar mass 442 g/mole) molecules, there should be around 0.20 and 0.31 g, respectively, on the surface of 1 g of silica.

With a monolayer distribution of Enoxil on the surface of silica, the largest number of hydroxyl groups of Enoxil biomolecules appears to be involved in interaction with surface silanol groups, as well as in lateral interactions with neighbouring Enoxil molecules. According to the results of quantum chemical calculations, bioactive molecules of Enoxil interact with the silica surface involving on the average 2 hydroxyl groups [8]. The molecules of gallic acid, catechin/epicatechin and catechingallate contain 3, 5 and 7 hydroxyl groups, respectively, *i.e*. from 1 to 5 hydroxyl groups remain free and can interact with water (or with neighbouring Enoxil molecules). The maximum reduction in the hygroscopicity of the composite compared to the sum of the components is about 40%, which approximately corresponds to excluding of about two-fifths of the groups of Enoxil molecules from the interaction with water.

Conclusions

The obtained results indicate that the use of Enoxil in the composition with fumed silica can lead to a significant decrease in the Enoxil ability to absorb water from the gas phase and to improve its storage stability.

The hygroscopicity of the Enoxil-silica composites depends on the components ratio, the greatest effect of hygroscopicity reduction (35-40%) is achieved for the samples with the Enoxil-to-silica ratio of (0.15÷0.35):1, which corresponds to an approximate monolayer distribution of biomolecules on the silica surface.

References

1. Lupascu, L.; Rudic, V.; Cotos, V.; Lupascu, T. Antimicrobial activity of the autochthonous compound Enoxil. Journal of Biomedical Science and Engineering, 2010, 3(8), pp. 758-762. DOI: 10.4236/jbise.2010.38101
2. Duca, Gh.; Lupascu, T.; Vlad, P.; Kulcițki, V.; Nastas, R. Studies on the water solubilization processes of oenotannins and their physico-chemical properties. Chemistry Journal of Moldova, 2006, 1(1), pp. 60-64. DOI: https://dx.doi.org/10.19261/cjm.2006.01(1).01
3. Lupascu, T.; Lupascu, L. The obtaining procedure of the water soluble enotannins. MD Patent, 2006, No. 3125. (in Romanian).
4. Pandey, K.B.; Rizvi, S.I. Plant polyphenols as dietary antioxidants in human health and disease. Oxidative Medicine and Cellular Longevity, 2009, 2(5), pp. 270-278. DOI: https://doi.org/10.4161/oxim.2.5.9498
5. Men'shchikova, E.B.; Lankin, V.Z.; Kandalintseva, N.V. Phenolic Antioxidants in Biology and Medicine. Structure, properties, mechanisms of action. Saarbrücken: Lap Lambert Academic Publishing, 2012, 496 p. (in Russian). https://www.twirpx.com/file/2051208/
6. Gallo, L.; Llabot, J.M.; Allemandi, D.; Bucalá, V.; Piña, J. Influence of spray-drying operating conditions on *Rhamnus purshiana* (Cáscara sagrada) extract powder physical properties. Powder Technology, 2011, 208(1), pp. 205-214. DOI: https://doi.org/10.1016/j.powtec.2010.12.021
7. Gallo, L.; Ramírez-Rigo, M.V.; Piña, J.; Palma, S.; Allemandi, D.; Bucalá, V. *Valeriana officinalis* dry plant extract for direct compression: preparation and characterization. Scientia Pharmaceutica, 2012, 80(4), pp. 1013-1026. DOI: https://doi.org/10.3797/scipharm.1206-05
8. Kuzema, P.O.; Laguta, I.V.; Stavinskaya, O.N.; Kazakova, O.A.; Borysenko, M.V.; Lupascu, T. Preparation and characterization of silica-Enoxil nanobiocomposites. Nanoscale Research Letters, 2016, 11(68), 7 p. DOI: https://doi.org/10.1186/s11671-016-1287-y
9. Schmidt, M.W.; Baldridge, K.K.; Boatz, J.A.; Elbert, S.T.; Gordon, M.S.; Jensen, J.J.; Koseki, S.; Matsunaga, N.; Nguyen, K.A.; Su, S.; Windus, T.L.; Dupuis, M.; Montgomery, J.A. Jr. General atomic and molecular electronic structure system. Journal of Computational Chemistry, 1993, 14(11), pp. 1347-1363. DOI: https://doi.org/10.1002/jcc.540141112